Editor Dr. Philippe Peylin
Geophysical Model Development

Dr. Tea Thum
Hans-Knöll-Straße 10
07745 Jena

Dear Dr. Philippe Peylin,

we are now submitting the new version of the manuscript gmd-2019-49, “A new model of the coupled carbon, nitrogen, and phosphorus cycles in the terrestrial biosphere (QUINCY v1.0; revision 1996)” by Thum et al.

In this new version we have taken into account the constructive and helpful comments given by the three reviewers. We have included a more detailed introduction of the novel concepts of the model in the model description, providing case studies (S1-S3) to illustrate some of the newly introduced processes. We also provide more detail on the model-based causes for the simulated trends across a climatic gradient as a means to test the nutrient responses to different climates (S6-S8). In addition, we have completely revised the parameter sensitivity section and revised the model description in the SI.

We have addressed the open-access problem of the code by removing the requirement for active collaboration with our group such that we can now make the scientific code of the model available via a GPLv3 license. However, the software infrastructure remains subject to a MPI-software license agreement. The code is now available for registered users via a git repository: https://git.bgc-jena.mpg.de/quincy/quincy-model-releases

To comply with the requirement to make an anonymous code review for the reviewers possible, we have deposited the code also here:

https://oc.bgc-jena.mpg.de/index.php/s/2QAGC1VI24LdJ4C

Password: QUINCY4GMDreview2019

We hope that you will consider taking this manuscript to publication.

On behalf of the authors,

Tea Thum

Below are the answers to the reviewer comments, followed by the difflatex-files for the main manuscript and the supplement. Due to difficulties in producing the difflatex-files, the Table 2 and 3 are not showing, even though those have been changed completely.

Answer to the Anonymous Reviewer #1

The reviewer comments are in bold, and the replies in regular font.

Thum et al describes a new terrestrial biosphere model, called QUINCHY, and presents a first evaluation of the carbon, nitrogen and phosphorous cycle against site-level data. Although the quality of what has been presented is good, I'm concerned about what has not been presented in the manuscript and its supplement: (1) the benefit(s) of starting a new terrestrial biosphere model, (2) the impact of the "consistent model formulation" (as called by the authors), (3) a clear overview of what makes QUINCHY stands out among the existing terrestrial biosphere models, (4) an evaluation of the energy and water balance, and (5) the target/criteria used to decide that the model's performance is "acceptable".

We thank the reviewer for the feedback on the quality of the paper and for pointing out things that need some improvement in this manuscript.

(1) The authors remind the readers that "Many process-based models of the terrestrial biosphere have been gradually extended from considering carbon-water interactions to also including nitrogen, and later, phosphorus dynamics." and state that "This evolutionary model development has hindered full integration of these biogeochemical cycles and the feedbacks amongst them". Although I fully agree with the first part of their assessment, models like CLM (10.5194/bg-11-1667-2014), CABLE (10.5194/bgd-6-9891-2009; 10.5194/gmd-2017-265), ORCHIDEE (10.5194/gmd-10-3745-2017) and JSBACH (10.5194/bg-9-3547-2012) show that the second part of the statement needs to be toned down unless the authors can provide evidence in support of their claim. The current presentation contains no elements that demonstrate that the technical and/or scientific performance of QUINCHY was only possible due to the fact that the group started their model developments from scratch. Most of the groups that maintain and develop a terrestrial biosphere model that has a history that goes back to over a decade are likely to have considered a rewrite of their model at one point. Most of these groups, however, decided to continue with "evolutionary developments". If this evolutionary approach really hinders scientific progress (as the authors seem to claim), this is an important message but it should be supported by evidence.

We agree with the reviewer that the statement can be read to say that science itself would be hindered due to evolutionary model development, for which there is likely no citable evidence. We have therefore clarified this statement in the revised manuscript. In particular, we have toned down the abstract (p. 1, lines 3-6):

"*Here, we present a new terrestrial ecosystem model, QUINCY (QUantifying Interactions between terrestrial Nutrient CYcles and the climate system), which has been designed from scratch to allow for a seamless integration of the fully coupled carbon, nitrogen, and phosphorus cycles with each other and with processes affecting the energy and water balance in terrestrial ecosystems*."

Without referencing the evolutionary approach at this level. We do not mean to suggest that evolutionary development of models necessarily results in inconsistent or inferior model results, but rather to justify our own choice for developing a new model to reduce the caveats of being prisoner to a structure dictated by the needs of the water and carbon cycle only calculations. In the introduction, we motivate our approach stating (p. 2, lines 26-30):

"*One important obstacle to such an approach is the gradual development of terrestrial biosphere models, which implies that new features, such as processes describing the dynamics of the N or P cycle, have been added to existing, carbon-cycle only land surface model formulations. This evolutionary approach can result in a situation where assumptions that were made in earlier versions of the model are incompatible with the new assumptions, or that the old model structure cannot appropriately accommodate new structures, therefore limiting the ability to take new ecophysiological understanding into account.*"

And further in (p. 3, lines 18-23) of the Introduction:

"*The QUINCY model contains entirely newly written code, although certain process representations are adapted from literature and previous models, including but not limited to OCN (Zaehle and Friend, 2010) and JSBACH3 (Roeckner et al., 2003). This new code approach allows for an appropriate separation of model infrastructure (e.g. memory allocation etc.) and scientific code, a better integration of model components, and thereby to include an internally consistent representation of ecosystem processes and in particular nutrient effects on plant photosynthesis, growth and soil organic matter turnover through the inclusion of a common set of underlying hypotheses.*"

We would like to point out that adding nutrient dynamics to a model introduces dependencies between model compartments that are typically less tightly connected in carbon only land surface type models, e.g. through the dependence of soil organic matter decomposition on nutrient availability, and therefore directly on plant nutrient uptake and productivity. These additional dependencies are sometimes in conflict with the pre-existing model structure, such that including nutrient cycles either requires substantial code restructuring, or scientific compromises in the extent of nutrient effects represented by the model (e.g. the need to

assume that certain processes have priority over others, because they are calculated sequentially in the model). It is this complication and limitation that we were referring to when we wrote that evolutionary model development prevents full integration of nutrient dynamics, because taking account of all the interactions between nutrient dynamics and carbon and water cycles suggests that a fresh implementation has advantages and allows for a full and consistent representation of nutrient effects.

(2) It is mentioned several times that QUINCHY has "a consistent representation of element cycling in terrestrial ecosystems". It remained unclear to me what is meant by this. Towards the end of the manuscript I was under the impression that "consistent" referred to the fact that all processes in QUINCHY are calculated at the same half-hourly time step. Although I can appreciate that such an approach makes the code easier to read and maintain, I'm less sure this approach can be claimed to be "consistent" because the time step of the model itself is still arbitrary (1800 seconds) when compared to the actual time step of the processes. Moreover, the idea to use different time steps for different processes has been justified by a more efficient use of limited computer resources. This far most terrestrial biosphere models favored speed above accuracy for the calculation of the non-linear processes. The QUINCHY group choose to trade computer time for an expected increase in accuracy. Can you demonstrate that there was an increase in accuracy? Based on your experience and findings can you recommend other groups to make the same choice? Will you maintain this "consistency" in the near future when adding landscape-level processes to the model such as plant biogeography and disturbances?

We agree that in the previous version of the manuscript, the word "consistent" has been used too loosely. With consistent representation we were referring to the representation of nutrient feedbacks with a common set of hypotheses on how plant growth (through the nutrient effects on photosynthesis or respiration), short to long-term labile carbon and nutrient storage as well as the interaction between plant N uptake and soil organic matter decomposition are considered. Such consistency is not necessarily maintained in other models, in which for instance, nitrogen limitation operates on different timescales to affect soil processes or plant growth (e.g. Xu-Ri et al. 2008), or in which N affects photosynthesis (e.g. CLM5, which employs the FUN model, with the intrinsic assumption of constant leaf C:N, while the model actually simulates flexible C:N). In the revised manuscript we now write (p. 3, lines 21-23):

"t*o include an internally consistent representation of ecosystem processes and in particular nutrient effects on plant photosynthesis, growth and soil organic matter turnover through the inclusion of a common set of underlying hypotheses.*"

While we have the same timestep for all model processes, our intention was not to state that this was the only reason for "consistency". In fact, some processes respond on different timescales, through time-averaging of driving variables and therefore their influence on the ecosystem state is smoothed. We demonstrate the effect of these lagged responses at the

example of the control of nutrient uptake in Figure S2. We do not imply that the half-hourly timestep is strictly required for this type of biosphere model, but we do expect that there are benefits from using such an approach, for instance, because it avoids the need for latent pools, in which carbon and other elements need to be stored temporarily to link processes on short-time scale (such as photosynthesis and respiration), with that operating at longer-time scales (vegetation growth and dynamics). This physical consistency of pools and fluxes reduces the need for numerical fixes to maintain mass balance, which are one key obstacle in biosphere models operating on different time-steps, and such an approach is strictly necessary for the accurate calculation of changes in isotopic composition of the biosphere. We expect to maintain this time-scale consistency also in future model versions, but remain open to simplify model structure, if we can prove that the simplification does not entail any relevant loss in calculation accuracy.

Given the modular design of QUINCY, we will be able to test the importance of the detailed versus lumped representation of processes when scaled to larger scale. This is something that will hopefully be valuable also to the other groups in the community.

(3) The authors claim that QUINCHY is a new model. Although I have no doubt that this assessment is correct from a technical point of view, it is less clear whether this is also true from a scientific point of view. It would be interesting to present the family tree of QUINCHY as it seems to be strongly inspired by O-CN (10.1029/2009GB003521). When thinking about weighting models in the IPCC context (10.1038/s41558-018-0355-y), would you argue that QUINCHY is independent or do you expect similarities with for example ORCHIDEE (10.5194/gmd-10-3745-2017) in which the C and N-cycle seems to be very similar to the one used in QUINCHY. If I understood the model legacies correctly, O-CN partly relied on ORCHIDEE and subsequent versions of ORCHIDEE (10.5194/gmd-10-3745-2017 and 10.5194/gmd-2018-261) relied on O-CN. Given that QUINCHY adopted many approaches from O-CN is it fair to assume that both models are likely to have some similar behavior? As a reader it is not clear at all what makes QUINCHY unique. After reading the current manuscript and its supplement, I expect that prospective model user will still have no idea when they should choose QUINCHY over CABLE, CLM, ORCHIDEE, JULES, JSBACH,. . .

While it is true that the QUINCY model has some commonality with the O-CN model (e.g. the photosynthesis scheme), the two models differ in fundamental aspects (e.g. the representation of labile pool dynamics and the competition of plants and soil organisms for nutrients, representation of vertical soil profiles, which affect the response of soil processes to perturbations). We have revised the manuscript's model description and the SI be clearer about which aspects of QUINCY derive from O-CN, and which are new (see also our response to reviewer #3). Given these differences, we do expect that the QUINCY model results can be considered as independent from O-CN. We would like to highlight that there are a number of important differences between the ORCHIDEE and O-CN models (in terms of the

photosynthesis and allocation schemes and the representation of stand-level vegetation dynamics), such that these models should also be considered as independent.

We have highlighted in the manuscript the processes that are considered novel. In this manuscript, we provide a model description and first evaluation to lay the groundwork for future studies evaluating the novel aspects and features of this model, and only together with these studies (which as reviewer #3 points out merit a scientific paper on their own) it will be possible for the wider community to decide as to whether the QUINCY model is an interesting and valid contribution to the ensemble of terrestrial biosphere models.

(4) Although the SI presents the formalisms used to simulate the water and energy budgets, these processes are not at all discussed in the manuscript. The whole point of having a terrestrial biosphere model (especially when it will be coupled to a general circulation model which is the case for QUINCHY) is that the terrestrial biosphere model links carbon, nutrients, water and energy cycles in a quantitative way. In my opinion, the most telling evaluation targets for a terrestrial biosphere model are those showing the skill of the model in jointly reproducing two or more cycles. Such analyses has not been presented.

We agree that it is important to show two or more cycles jointly, which is why we show the model behaviour with different biogeochemical coupling, ie. the carbon only version alongside the carbon and nitrogen as well as the carbon, nitrogen and phosphorus versions, and provide metrics of carbon, nitrogen and phosphorus cycles at selected sites. We choose to not show a detailed evaluation of the water and energy cycles in this paper, as these processes are not the main target of the model development, and the representation of these cycles will very likely be replaced after the coupling with ICON. Nevertheless, to address this concern, we have added an evaluation of the simulated latent heat fluxes to the FLUXNET analysis already presented in Figure S5.

(5) The evaluation is sound but routine meaning that no clear effort was made to go beyond the typical "acceptable performance" where "acceptable" remains undefined and "performance" is limited to a RMSE or a correlation. I do realize that this represents a common modus operandi in the community but the tools and data exist to do better. Hence, there is no excuse for a leading journal as GMD not to raise the bar by insisting on more ambitious evaluation practices. Could you, for example, set quantitative targets, i.e., reproducing 95% of the seasonal cycles in addition to 50% of the residuals data structure (i.e. observations minus the seasonal cycle)? Or using a simple purely climate driven statistical model as the reference to beat? Subsequently, quantify whether these targets were met or not. The statistical methods for such an approach are available and have even been proposed for spatially explicit analysis (see SI of 10.1038/nature02771). Furthermore, the study somewhat overlooks the concerns of the community who wants to learn about the performance of QUINCHY who presents itself as "the new kid in town". From a community point of view it would make sense

to run the model through the ilamb benchmarks (10.1029/2018MS001354) and compare QUINCHY's performance relative to what is considered state of the art within the community (in addition to the evaluation shown by the authors).

In this paper our aim is to introduce the model and present its functionality and in the revised version of the paper we will aim to better illustrate the underlying novel processes so that the high level model evaluation can be better understood. We agree with the reviewer that the model evaluation is very important, but we chose to follow eviewers #2 and #3, who requested more emphasis on illustrating the new model characteristics because this is what is novel in this study. While this is a more qualitative way to look into the model's behaviour than rigorous numerical benchmarking, we believe that this is nonetheless helpful to judge model performance. We note that many of the suggested benchmarks apply to global evaluation, which will be important for future studies.

We have added a sentence mentioning the importance of proper benchmarking exercises to be done in (p. 16, lines 14-15) in the conclusions: "*This integration will also allow more comprehensive and rigorous benchmarking against a wider variety of data products.*"

Answer to the Anonymous Referee #2

The reviewer comments are in bold, and the replies in regular font.

This manuscript describes a new model of biogeochemical and biogeophysical cycles. The motivation for the model is to build (from the bottom-up) a comprehensive model of these cycles that incorporates the latest ecophysiological understanding, rather than bolting new processes onto an old/existing TBM. This is an ambitious (and worthwhile) task, and the new model has some exciting aspects and functionality compared to the present generation of models. The authors highlight the major/novel advances in QUINCY as: source/sink dynamics enabled through fast and slow non-structural carbohydrate pools; including N and P limitation in initial model development; lagged responses to instantaneous variations in climate; explicitly resolved vertical soil processes affecting litter and soil organic matter; and novel diagnostics to enable model Evaluation.

We thank the reviewer for this assessment and for the recognition of this work's importance.

After reading the manuscript, I still have some questions about how the model performs, and the results section could better highlight these core processes and developments and their emergent behaviors in the model. I think the manuscript would benefit from re-organizing the results around these 5 themes. I'm sure each of these could warrant a whole study on their own, so I'm only suggesting some simple plots to exhibit the model behavior in these areas. This is already done for the nutrient limita-

tion (although further displaying the process-level results mentioned on Page 11 Lines 13-16 would be informative) and an example using isotopes. It seems to fully document the model, the other major advances included in QUINCY should be illustrated. For example, when does down-regulation of photosynthesis due to sink-limitation occur (Also as mentioned in the SI Page 8 Line 9-12: under what conditions are severe C deficit likely to occur to down-regulate respiration?)? What is the impact of the temperature acclimation on photosynthesis and respiration (some plots of GPP and Ra vs average temperature)?

We thank the reviewer for these suggestions that have helped to illustrate the characteristics of the model better. The re-organizing of the results section along the five mentioned topics seems challenging, because we do not have evaluation data for all the aspects mentioned by the reviewer. We therefore prefer to keep it this way, as it is currently organized by evaluation data source and we find this order logical and easy to follow.

We have followed the suggestion by adding a number of conceptual plots (Figures S1-S4) illustrating the effect of sink limitation, the effect of lagged responses, and the effect of explicitly considering vertical soil structure to the description of the model in the Methods Section. We did not include a presentation of the effect of down-regulation of maintenance respiration under severe labile C stress, because all of the ecosystems simulated in this study were in climate zones, where such a deficit did not occur. Specifically, we write in the Methods and Results sections:

i) sink limitation now shown in Figure S1, as described in p. 5, lines 10-12:

"*In addition, photosynthesis can become downregulated due to sink limitation, if nutrient or water availability or low temperatures limit growth and cause accumulation of photosynthates in the labile pool (Hartmann et al., 2018, see Fig. S1 for an example)*."

ii) Lagged environmental responses, now shown in Figure S2, as described in p. 5, lines 15-18 :

"*Rather than relying on instantaneous plant demand, the response of plant nutrient uptake to plant demand is modelled as a lagged response (of a few days) to balance short-term fluctuations in photosynthesis and soil nutrient availability and to represent memory effects in the plant's control of its nutrient uptake (SI Sect. 1, Fig. S2)*."

iii) Effect of vertically layered soil, now shown in Figure S3, as described in p. 7, lines 10-14:

"*As an example of the benefit of QUINCY's modular approach, Fig. S3 shows that the explicit representation of the vertical soil profile, compared to a zero-dimensional, lumped soil approach, has little effect on the seasonal course of heterotrophic respiration. However, it does affect the simulated nutrient dynamics because of the explicit separation of a nutrient*

immobilisation in the litter dominated layers from the gross-mineralisation dominated soil layers with a proportionally higher content of soil organic matter."

iv) The effect of temperature acclimation of Jmax on GPP, now shown in Figure S7, as described in page 11 lines 15-17:

"*While the acclimation of photosynthesis to growth temperature does matter at the diurnal time-scale particularly on cloudy days (Figure S7), the positive and negative effects cancel each other out at the long-term annual mean, and therefore plays no role in the simulated GPP-MAT relationship.*"

v) The effect of temperature acclimation of respiration on GPP and Ra, now shown in Figure S8, as described in page 11, lines 17-19 as:

"*Despite a notable decline of maintenance respiration in higher temperatures due to the acclimation of respiration to growth temperature (see Figure S8), the spatial trend in simulated CUE is predominantly driven by MAT (Fig. S10).*"

Also I can see the benefit of the uncertainty analysis but it is hard to put these results into context when most of the variables or the parameter values shown in Figure 8 are not otherwise discussed in the text.

We have completely rewritten the text describing the sensitivity analysis to be more focussed on the relevant of individual processes and parameters, adding a supplementary table S1 giving details on how specific simulated model quantities respond to parameter variations, as well as Figure S12, which illustrates the co-variation of simulated model quantities with each other. To further clarify the presentation of the results, we have added color coding to the variable names in Table 3, which links them to certain processes and the rank-transformed partial correlation coefficients to the table.

Specific Comments

Page 4, Line 26: Are the leaf chlorophyll and N concentrations updated variables in the model?

Yes, these are state variables. This is presented in the SI section M2.1. We have expanded the model description in the new version of the manuscript and will also clarify this point in the main manuscript part, and not only in SI. Now this point is clarified in the main text on p 5 l 5-8 as:

"*Photosynthetic parameters, including chlorophyll content, further are assumed to depend on leaf N concentration (Friend et al., 1997). As foliar mass and N concentrations both respond to soil N availability (Vicca et al., 2012; Hyvönen et al., 2007; Meyerholt and Zaehle, 2015), this*

causes canopy photosynthesis to be directly affected by soil N availability in addition to meteorological variables."

Page 8, Line 24-25: It's not clear to me how the short-term uptake is not affected, if the mid-day GPP values are lower with nutrient limitation? This is also mentioned on Page 11 Lines 16-17.

We have rephrased this sentence to say (p. 9 | 24-27): "*In other words, the effect of diurnal and seasonal variability in soil nutrient availability is buffered through the labile and reserve storage pools in the vegetation, such that it affects vegetation gross carbon uptake only via slow processes such as foliar nutrient and allocation changes, but has no effect on variability at the daily to weekly time-scale.*"

And (p. 13 | 35-37)

"*However, short-term diurnal or sub-seasonal shortage of soil nitrogen or phosphorus does not directly and instantaneously affect simulated productivity because of the buffering introduced through the labile and reserve storage.*"

Page 8, Line 25-26: Which experiments do these rˆ2 values refer to?

The r2 -values here refer to C and CN(P) experiment values (CN and CNP experiments have identical r2 values) and what improvements took place between these two. We have made this part of the text clearer.

The modified text reads now (p. 9, 31-33): "*There is little overall effect of the nutrient cycles on the correlation between half-hourly simulated and observed GPP at FI-Hyy (all versions: r2=0.76), FR-Hes (all versions:r2=0.63), and BR-Ma2 (all versions:r2=0.67), and only a minor reduction for AU-Tum (r2=0.70 versus 0.65 for C and CN(P), respectively)*."

Page 9, Lines 19-24: It's interesting that the P cycle is not having an impact on the tropical sites, as would be expected. What is the reason for this?

We have explained the causes for this in the discussion section, now in p. 14 l. 16-20. The reasons include efficient recycling of the P in the litter layer, as well as unknown initial soil concentration of plant available P and uncertainties in the rate of P weathering. As these were already mentioned in the older version of the manuscript, not in the Results section to where the reviewer is referencing here, but in the Discussion section, we rather leave it the way it was earlier in the revised version.

Table 2: This is a lot of information which is difficult for the reader to evaluate what it means in terms of model performance. I'm not sure it's all necessary to include here. Do each of these stocks and fluxes have corresponding representation in Figure 1? It

could be possible to show these results graphically, reproducing Fig. 1 for each site but to add the observed values when they are available.

Taking into consideration also the comments from Reviewer #3 to this table, we have changed it so that it shows the observed and modelled values for GPP, TER and leaf C:N -values for these sites. The reason we showed the whole CNP budgets in the old version of the table was to highlight that the model is giving realistic and reasonable values for all parts of the nutrient cycles. However, now with the added plots that were suggested by the reviewers, we believe that this will be shown through those.

Table 2 has been modified along with its discussion in the Results section in p. 10 | lines 9-16:

"*Table 2 summarises the observed and simulated GPP, total ecosystem respiration (TER) and foliar C:N with the CNP version of the model for these four FLUXNET sites, calculated for the time period of the flux observations (Table A1). The annual GPP from the CO2 flux observations is in line with the modelled values for FI-Hyy and FR-Hes, while productivity at BR-Ma2 is somewhat overestimated, and strongly underestimated at AU-Tum. The TER is somewhat overestimated for FI-Hyy and FR-Hes, and strong overestimation occurs at BR-Ma2. At AU-Tum the TER is underestimated. Simulated foliar C:N was within the observational range reported in the La Thuille database (NOA, 2007) for all four sites. Observations for nutrient availability and fluxes are not consistently available across these sites.*"

SI

Equation 1: Could you provide examples of where these lag effects occur later in the set of model equations?

These lag effects take place e.g. in the response of photosynthesis, respiration and nutrient uptake to their driving variables, but also in labile pool dynamics and phenological processes. We have explained this better in the SI text, and added the equations, where these lag effects occur, to the Table 1.

Equation 6: What is the reason for using Tair to model leaf photosynthesis instead of leaf or canopy temperature?

At the moment, QUINCY does not calculate leaf or canopy temperature in the model, but only the bulk surface temperature (as do other land surface model such as ORCHIDEE and JSBACH). We will separate the canopy and soil energy balance in a future version of the model.

Now we mention this explicitly in the SI p 4 l 13-14 as: "*Note that the current version of QUINCY does not include a representation of canopy temperature and we are therefore using air temperature for all aboveground processes.* "

Page 4 Line 8: Should this be "excessive soil moisture stress constraints"?

Yes, thank you, this has been corrected.

Equation 46: Is there an equation for S somewhere that I have missed?

We have now clarified that S is updated according to this equation starting from a set initial value in p. 14 | 23.

Answer to the Anonymous Reviewer #3

The reviewer comments are in bold, and the replies in regular font.

We would like to thank the reviewer for their in-depth and detailed comments. We largely agree with the suggestions and respond to each in turn below.

This paper presents a novel model (named QUINCY) for the coupled cycling of carbon, water, N, and P in terrestrial ecosystems. This is a substantial contribution to a relatively small set of available models with a comparable scope: possible global applications [although only site-scale simulations are presented here], mechanistic representation of processes that determine the response of the terrestrial biosphere to global environmental change, applicability within a Earth System Modelling framework. The model is evaluated with respect to GPP and NEE data from FLUXNET, NPP/GPP ratios from paired FLUXNET and forest inventory data, and foliar d13C - a proxy for leaf-level water use efficiency.

The main innovation of the present model lies in the coupled representation of N, P, and C cylces; and in the model's entirely (?, please clarify) newly written code, that is designed in a modular way (p. 3, l.19) and allows for an appropriate design of the basic model structure to accommodate the new modelling capacities of simulating interactive carbon and N/P cycling as opposed to adding respective processes onto a "first-generation" C-only model. Parts of the model, however, are process parametrisations that are implemented as such in other Dynamic Global Vegetation Models (see also comments below).

The model is entirely newly written code. This is now mentioned in p. 3 | 18-23: "*The QUINCY model contains entirely newly written code, although certain process representations are adapted from literature and previous models, including but not limited to OCN (Zaehle and Friend, 2010) and JSBACH3 (Roeckner et al., 2003). This new code approach allows for an appropriate separation of model infrastructure (e.g. memory allocation etc.) and scientific code, a better integration of model components, and thereby to include a consistent representation of*

ecosystem processes and nutrient feedbacks through the inclusion of a common set of underlying hypotheses."

The model is designed in a modular way, with more detailed in the revised version given in the SI Section M1.2.

We have improved the model description in the main text and the SI to make more clear where concepts have been borrowed from other models.

It is highly challenging for a reviewer to assess whether the present model is appropriate and accurate in simulating all key processes that determine the coupled C, N, P, and water cycling. Especially given the immensity of the number of equations and paremeters implemented in the model (see SI). Therefore, I'm trying to evaluate how far the present paper got me to being convinced that this model works.
In summary, I am convinced that this model is a highly valuable contribution and that its description should eventually be published in GMD. I am less convinced that the model works (practically and off-the-shelf) and can be used by the wider community, since the code is not made fully publicly accessible ("The source code is available online, but its access is restricted to registered users and the fair-use policy stated on https://www.bgc-jena.mpg.de/bgi/index.php/Projects/ QUINCYModel. Readers interested in running the model should contact the corresponding authors for a username and password."). Therefore, I could not apply the model myself and my assessment is merely based on the descriptions in the text. I am always disappointed to see model code not being made fully open access along publications in GMD (an open-access journal!). In that sense, and very strictly speaking, what is the purpose of a publication in GMD? Shouldn't such a model description just remain an internal technical document then? I leave it to the editors to handle this and will evaluate the further aspects of the paper assuming that the editors support non-open access code in GMD.

We are grateful for this assessment, and apologise for the lack of code accessibility. We would like to point out that we have made the code available to editors and reviewers of this manuscript by sharing access details to a complete tar-ball on the institute's servers. The QUINCY model code will be available under a GNU public license (GPL v3) upon publication of this manuscript. The access to the code will be restricted to registered users, because the scientific code of QUINCY model relies on technical infrastructure (e.g. memory and tile handling) provided by software developed by the MPI for Meteorology in Hamburg, which is subject to acceptance of the institutional MPI-ESM software licence.

Below, I'm listing a few MAJOR points that I would like to see addressed in a re-submission, followed by a number of MINOR points that I hope would improve the manuscript.

1 MAJOR

1. Evaluation. It is a practically impossible task to comprehensively evaluate a model that simulates virtually every important process that operates in a terrestrial ecosystem (and is typically represented in comparable models). I also consider that a complete and detailed description of the model itself may be the main part of a GMD paper, and that the evaluation with data may be secondary and addressed by further studies. However, as the paper is designed now, the "meat" is in the SI (all equations and parameter values), while the main text provides a rather brief description of basic model concepts and approaches in intuitively accessible language, and provides a rather brief evaluation against a small set of observational data and and overview of the model sensitivity. I think this is generally a good form of presentation.

Thank you for this assessment.

However, the evaluation becomes a central point of the paper and the evaluation presented here is relatively slim. The key challenge is to identify what we learn from including N and P cycling and limitation in a vegetation model and to identify key phenomena that can only be explained with including nutrient cycling (What are the key phenomena that can only be explained with including nutrient cycling?).

The reviewer is correct that the main purpose of nutrient enabled biosphere models is to address the key scientific challenge noted above, and it is our intention to study exactly this challenge using QUINCY in the future. However, in the manuscript we presented the structure and provided essential background information that any model is required to meet even before the question of nutrient cycling is addressed. Of course, performing a sequence of dedicated model experiments is an important task. However, we believe that introducing the model, adding the necessary assessment of the overall model performance in transient but not manipulation setting and providing a sensitivity study is already providing a lot of material for a reader to digest and consequently that that we would overload readers by adding a complete set of nutrient fertilisation benchmarks, each with their own uncertainty and requirement for detailed discussion. We have therefore opted to present some key features, so as to provide a background for a number of in-depth studies evaluating the nutrient cycling effect in QUINCY at site and global scales.

We have followed the reviewer's suggestions to add more "meat" to the manuscript by better introducing the novel concepts of the model in the model description, providing case studies (new figures S1-S3) to illustrate some of the newly introduced processes, we provide more detail on the model-based causes for the simulated trends across a climatic gradient as a means to test the nutrient responses to different climates (new figures S6-8). In addition, we have completely revised the parameter sensitivity section, providing a better narrative as to why certain parameters matter (adding a supplementary table), how this relates to variability in the

model output (adding a supplementary figure to illustrate the co-variation between the model output parameters).

I was intrigued by the evaluation of carbon use efficiency, CUE (Fig. 6c) but would have liked to understand more about why the model captures the overall magnitude of observed values, but does not explain the substantial variability in observations within vegetation types (e.g. NE forests).

The QUINCY model is driven by meteorology, soil texture and atmospheric deposition of nutrients, but does not consider other factors that might contribute to within-PFT variability of CUE, such as site fertility not related to N and P availability, soil pH, site history, and species-level effects on CUE. Such discrepancies have been previously recorded for other similar models.

Some of these points have been addressed in the fifth paragraph in the previous version. However, soil pH was not mentioned there, and we have now added it in p. 15 | 12-13: "*Finally, the intra-PFT variation of observed CUE likely depends on other site-specific factors that affect site fertility, which are currently not adequately represented in the model, such as the effects of soil pH, site history, and species-level variability.*"

I would also have like to see how foliar stoichiometry, C allocation, the root:shoot ratio, soil respiration, or N fixation change across climatic and N (and P)-deposition gradients and how it (broadly) compares to observations. These processes have been identified previously as key mechanisms that determine the coupled C and nutrient cycling (Medlyn et al., 2015). I was less convinced that the diurnal and seasonal GPP evaluation (Fig. 3) provides much insight in that respect. I suspect that the model can easily be tuned to match the magnitude of observed fluxes for each model setup (C, CN, CNP), and it is stated in the text that nutrient limitations do not affect diurnal and seasonal C dynamics (p. 11, l. 16).

While our model has not been tuned to any specific site, we agree with the reviewer that the evaluation based only on diurnal and seasonal GPP does not provide the necessary mechanistic insights. However, providing such an evaluation is still an important component of any biosphere model evaluation, given the challenges involved in coupling several biogeochemical cycles together.

To respond to the concerns raised, we have included a series of explanatory figures (S5, S6, S9-11) showing the changes of GPP, NPP, CUE, simulated foliar C:N stoichiometry, and N fixation across climatic and N/P deposition gradients, which are used to cast light into the simulated results, in p. 11 | 12-30:

"*Underlying these results are the emergent sensitivities of ecosystem processes to the model drivers. Fig. S5 and S6 show that the large-scale gradients of simulated GPP and NPP are*

largely controlled by mean annual temperature (MAT), with an additional clear effect of mean annual precipitation. For temperate and boreal forests, also N deposition is positively related to GPP and NPP. While the acclimation of photosynthesis to growth temperature does matter at the diurnal time-scale particularly on cloudy days (Figure S7), the positive and negative effects cancel each other out at the long-term annual mean, and therefore plays no role in the simulated GPP-MAT relationship. Despite a notable decline of maintenance respiration in higher temperatures due to the acclimation of respiration to growth temperature (see Figure S8), the spatial trend in simulated CUE is predominantly driven by MAT (Fig. S9). Trends apparent in the CUE response to MAP and N deposition as small and likely confounded by the MAT response. However, the general tendency of PFT-specific foliar C:N to decline with increasing N deposition (Fig. S10), something that is expected to happen based on observational evidence Hyvönen et al. (2007); Meyerholt and Zaehle (2015), suggest that the linearly increasing maintenance respiration rates per unit tissue drives whole-plant maintenance respiration up stronger than the saturating effect of increased leaf N on GPP, therefore reducing CUE with increasing N availability, counter to expectations (Vicca et al., 2012). The root to shoot ratio did not show strong dependency to any of these environmental variables (data now shown), probably contributing to the lack of a decline in CUE with declining N availability. Generally, PFT-wise foliar stoichiometry appears to be more strongly influenced by N deposition than MAT or MAP. This result occurs despite a clear dependency of the simulated biological N fixation on temperature and precipitation (Fig. S12), where the simulated range and response to climate drivers is consistent with the available evidence suggesting the highest N fixation in hot and moist environments (Fig. S11 Cleveland et al., 1999, 2013). In addition, in agreement with recent evidence, enhanced atmospheric N input suppresses simulated N fixation."

Additionally, we include a series of more conceptual figures (S1-S3, S7, S8) to illustrate the role of photosynthetic sink limitation as well as the role of temperature acclimation, as suggested by reviewer #2.

We have furthermore clarified the nutrient limitation like to clarify that long-term N and P availability does affect the daily and seasonal maximum GPP, but short-term variation in nutrient availabilities do not affect the shape of the diurnal or seasonal cycles, because of the lagged effect response of plant growth to nutrient uptake, p. 13 | 35-37:

"*However, short-term diurnal or sub-seasonal shortage of soil nitrogen or phosphorus does not directly and instantaneously affect simulated productivity because of the buffering introduced through the labile and reserve storage.*"

An explicit representation of chlorophyll (Chl) was included in the model in order to provide a useful diagnostic (with readily available Chl data), but no evaluation was shown.

We would like to highlight that the explicit representation of chlorophyll was not simply because it provides an additional observational constraint, but also because it allows for a more realistic

simulation of the photosynthetic light-response, as described by Kull & Kruijt 1998. While some chlorophyll data are available, largely from remote sensing products but also from site-level observations, these data are not straightforward to use in model comparison given the scaling problems involved in comparing model and observations. We will therefore make this a subject of a separate study which will further explore the assumptions and implications of the canopy representation within QUINCY.

We have updated the introduction to make clear that the evaluation of chlorophyll is not subject of this paper, p. 3 | l. 33 & p. 4 | 1-6:

"..., *the leaf chlorophyll content is explicitly modelled from the leaf N to improve the simulated light response of photosynthesis throughout the canopy (Kull and Kruijt, 1998), but this will allow for novel ways to compare the simulation results with in situ and remotely sensed observations in the future*."

2. Sensitivity analysis. I am most interested to learn about which parameters the modelled variables X are most sensitive to, and not primarily about how much X varies when several variables are varied at the same time (which is shown now in Fig. 8 if I understand this correctly). Could the results of the sensitivity analysis be shown differently? Also, in my interpretation, the sensitivity analysis primarily reflects the choice of the range over which the model parameters are chosen to vary. Therefore, the conclusion on p. 10, l. 18 that "the model output (Fig. 8) is well constrained and centred around the results of the standard parameterisation" is mainly an implication of this choice. If the range over which the parameter values were sampled was larger, then the range of simulated variables would be larger ("less well constrained"). However, I agree with the authors that non-linear, interactive effects could lead to asymmetric simulated distribution. Anyway, I think this sensitivity analysis as presented now does not provide very useful information. Providing information about the sensitivity of modelled variables w.r.t. A selection of the most important parameters, and to clearly show which variables are most important in a figure, would be more useful.

We thank the reviewer for pointing out that the model sensitivity analysis has not been explored in a satisfactory manner, a point which has also been raised by reviewer #2. Fig. 8 is meant to illustrate the stability of model state variables, while Table 3 shows parameters ranked in order of importance. We agree that, as it stood, this table was hard to interpret. The Table has been revised to clearly show which parameter is linked to each process (e.g. photosynthesis, growth, soil biogeochemistry) and the implications of the ranking is now better discussed in the text, which has been completely revised. Instead of adding a large number of plots showing the correlation of output quantities to parameters, which given the large number of variables and parameters to consider would be hard to interpret, we have added Table S1, which details the correlation coefficients for a number of output variables.

We would like to point out that we did not intend to quantify the overall model uncertainty, but to test the overall stability of the model and its sensitivity to its parameters, given the large number of sometimes badly constrained parameters and non-linear equations. Defining realistic bounds for many of these parameters is a challenge, and 10% is large for some, but certainly too narrow for others. It is correct that a larger variation in parameter values would lead to a larger variation in model variables. However, we do believe that an assessment of the 10% deviation already gives a clear indication of whether a parameter is highly important or less, and that by using latin-hypercube sampling rather than an OAT approach, we can robustly assess model stability.

3. Model description - several points here:
• In the main text should provide an intuitively understandable description of the model, a characterisation of its behaviour, and a clear identification of the most important assumptions and choices made for model structure. This is done on p. 3 l. 1-18, however I would have liked to see this description more comprehensive and better referenced to the existing literature. In particular, I encourage the authors to make some of the central assumptions underlying
the model more explicit, e.g. the following - if I'm correct:
– A "sink limitation term" (function of temperature, soil moisture, and nutrient availability) is included on Vcmax and Jmax, Eqs. 7d.
– Using air temperature for photosynthetic rates
– Canopy N determines photosynthetic rates. This implies that photosynthetic capacity (A for saturating light conditions) is strongly controlled by N availability, and not by climate.
– Biochemical (acting on Vcmax and Jmax) and stomatal limitations by low soil moisture considered
– Acclimating basal respiration following Atkin et al., 2014
– Resource uptake respiration depending on the form of N uptake (NO3 or NH4)
– Root respiration scales with temperature but not with N or P uptake Capacity.

Response: This is true, however, as noted in the manuscript, root N uptake costs are explicitly accounted for.

– Strict space constraint in forest stands by prescribing a maximum foliar projective cover. Constrains the number and size of individuals.

Response: There is a space constraint, but it is less strict than implied by the reviewer, because it depends on the actual foliar projective cover, which is a dynamic property depending on the number and size of individuals, but also their allocation strategy and realised individual leaf area index per unit crown area (see Sitch et al. 2003).

– SOM turnover is N limited.

Response: Because of the stoichiometric parameterisation, the decomposition of SOM is not N limited, but the decomposition of litter is N (and P) limited. This is a basic functionality inherited from the Century model approach

– Labile pool dynamics determined by sources and sinks, sink limitation on growth by temperature and soil moisture

Response: Sink limitation also occurs because of nutrient limitation.

– P just limits (imposing a “cap") growth (unlike N which also regulates the photosynthetic capacity)

These are indeed some of the main new assumptions in QUINCY, and we once again thank the reviewer for the in-depth analysis of the paper. We have followed this suggestions and have extended the model description to emphasise these points as well as further references where needed. Please see revised Section 2.1 for details.

• Model structure (and complexity): The model contains a very large number of parameters and it remains unclear how the parameters can be constrained from observations, or whether they are relatively well known from independent measurements. E.g., the fraction of C allocated to fruit production (Eq. 29) seems enormously complex. Is the complexity chosen here always necessary?

We agree with the reviewer that although we did try to keep the model simple, it does contain a large number of poorly observable parameters describing scaling or response functions. This fact was the motivation to include a hierarchical parameter sensitivity study to test whether any of the poorly unconstrained parameters will have a strong influence on key model predictions. The fact that it does not, does not imply that these parameters are a sign of superfluous complexity, as they may well have an impact on particular time-scales or responses to environmental drivers. For instance, the complexity of the fruit allocation equation results from the new concept of this model (compared to other dynamic global vegetation models) that fruit production matters for the re-establishment of new individuals (requiring that there is a minimum allocation to fruits), in combination with the representation of daily allocation, which prevents the application of the typical constant allocation to fruits, as this would result in a disproportional allocation of reserves to fruits at the beginning of the growing season, and therefore a delayed development of foliage. Another reason for using sometimes complex equations is that we decided to avoid latent model complexity by for instance not allowing for hidden biogeochemical pools to buffer short-term flux variability, as commonly done in other models, we were forced to implement scaling equations to accommodate these short-term flux variations. The structure of any single equation can be debated, and alternative models might be applied with similar outcome.

Some of the processes and parameters introduced can potentially be constrained by additional data (e.g. the labile and reserve dynamics can be constrained in principle by measurements of non-structural hydrocarbons, and carbon isotope tracer studies), and we plan to use the QUINCY model to use these additional data sources in future studies. As the reviewer has pointed out, many of these evaluations require a scientific paper on their own. We agree with the reviewers concern that not all parameters of this model (or in any other terrestrial biosphere model) are constrained by observations, which introduces uncertainty in the model outcome. This fact calls for the need to perform parameter ensemble simulations wherever possible to ascertain the robustness of the model finding.

Equations are presented mostly without reference to justify the choice of the model structure. It is unclear whether the structures of equations used to describe the many processes are adopted from other references, are grounded in fundamental laws that are sort of standard representations, or whether they are designed here for the first time. If so, it may require some additional words on the motivation. For example, the photosynthesis scheme in SI Sec. 2: Is it adopted from Kull Kruijt (1998) or what parts of what's implemented here are new? Reference for N retranslocation upon heartwood formation (Sec. 3.5)? Many of the parameters are "shape parameters" of the functions used, and the systems dynamics may not be very sensitive to these.

In the revised version, we have added references where they were missing to explain the usage of previously published equations. We have furthermore clarified in the introduction of the supplementary material (p. 1 | 7-8) that:

"*Where no explicit reference to other studies is given, the equations have been developed in this study*."

It is indeed correct that the overall system dynamics in general may not be very sensitive to many of the shape parameters, however, this is not universally the case, and specific threshold values for e.g. the onset of sink limitation on photosynthesis, or the downregulation of nutrient uptake given the labile nutrient constraint, can have important effects on seasonal fluxes, even if they do not have a major contribution to the overall uncertainty in stoichiometry or productivity. The parameter sensitivity study demonstrates that the model's predictions are not strongly affected by such threshold values. However, it would be wrong to conclude that the shape of the response functions does not matter for the model predictions. A full analysis of the effect of these response functions is beyond the scope of this paper, but could be the subject of future studies focussing on the interactions of specific processes.

It would be useful to identify the most important feedbacks and discuss how these may shape the system dynamics in response to manipulations of temperature, CO2, N-input, etc.

It is certainly the purpose of the QUINCY model to provide such an assessment. However, this discussion is out of scope for this particular manuscript in which we document the model and its performance against a range of benchmarks. We have added a set of conceptual and explanatory figures to the SI to elucidate better the underlying processes and their climate and N deposition response. We feel that a discussion of the important feedbacks without providing a substantial evaluation against ecosystem manipulation experiments would be text-book style and not appropriate for a journal article, and as we have argued in our responses, adding a sufficiently detailed and sound assessment of the model against manipulation experiments is beyond the scope of our paper.

• Motivation and description of advantages of this new model:
– Merit of model is described as "decoupling of photosynthesis and growth" (p. 11, l. 6). This is unclear.

We extended the presentation of this decoupling by more clearly motivating that it is well known that photosynthesis and growth are independently controlled (Körner, 2006; Fatichi et al., 2013), and added a supplementary figure S1 to demonstrate the effect of this decoupling (p. 5 | 10-12):

"*In addition, photosynthesis can become downregulated due to sink limitation, if nutrient or water availability or low temperatures limit growth and cause accumulation of photosynthates in the labile pool (Fatichi et al., 2013; Hartmann et al., 2018, see Fig. S1 for an example)*."

We also write in the discussion section now more clearly (p. 13 | 23-25):

"t*hat there is an explicit decoupling of the growth processes from C-supply due to photosynthesis by accounting for temperature, moisture and nutrient constraints in the formation of new tissue, as opposed to the simpler treatment of these dynamics in Zaehle and Friend (2010)*,"

The present model structure allows testing whether this de-coupling has important implications for the simulation of long-term biogeochemical cycling, which we will do in a future study. What this approach already now allows to simulate is the ability of the model to temporally decouple carbon from nutrient uptake, and therefore allows for a more realistic simulation of seasonal cycles without having to rely on the heuristic representation of reserve generation under nutrient stress as commonly employed in other biogeochemical models.

– The model is described as "modular" (p. 3, l. 19), but then, the model description refers to specific model representations, not alternative ones within the same model. It remains unclear, what "modular" means in this sense.

We have clarified the nature of modularity now in the introduction (p. 3 | 30-32):

"*We have formulated this model in a modular structure to facilitate the consistent testing of multiple hypotheses for one particular process, and to reduce the scope of the model (e.g.*

separately simulating canopy dynamics, vegetation dynamics, or soil biogeochemistry) to study the impact of particular processes (see SI for details)."

And supplementary material (Section M1.2, p. 3 | 2-14):

"*The code structure of QUINCY has been designed in a modular way, with two intentions.*

Modularity regarding the scope of the model The model can be run configured as a canopy flux scheme (simplified representation of LAI dynamics given the phenology subroutines, full consideration of soil hydrology, surface energy, canopy radiation and photosynthesis), a stand-alone vegetation model (all of the canopy flux schemes, but with LAI dependent on vegetation growth and dynamics, however without biogeochemical soil feedbacks), a stand-alone soil biogeochemical model (driven by pre-calculated soil moisture and temperature as well as atmospheric and plant litter inputs), a configuration of any of the former without considering soil moisture constraints, and the fully coupled canopy, vegetation and soil model as applied here. This approach allows for testing the implications of particular processes at reduced model complexity.

Modularity regarding the ability to test different hypothesis regarding specific process representations that the subroutine structure of the model facilitates the testing of alternative process hypotheses. These include alternative assumptions about temperature acclimation, the vertical structure of the soil (bulk or one-dimensional with flexible numbers of layers), as well as submodules to be tested in future studies."

We did not present the modular structure of QUINCY in the first version of the manuscript in detail, as it was meant to demonstrate the performance of the standard version of QUINCY, against which future studies relying on the modularity can be compared. In the revised manuscript we will take advantage of this structure to showcase for instance the effect of photosynthetic and respiration acclimation and the vertical soil discretisation.

2 MINOR

We thank the reviewer for the in-depth analysis of our paper and for reading the entire model description in such detail. We address all the minor comments below.

2.1 Main text

• p. 2, l. 3: "induce" instead of "provide"

Thank you, this has been changed.

• p. 3, l. 17 "nutrient uptake" instead of "root uptake"

Thank you, this has been changed.

• p. 4, l. 16: From what sources were these inputs prescribed? In particular: What is the source for rooting depth?

The sources of these inputs are described in Section 2.3.1 (we have added a reference to that section here). The source for the rooting depth was unfortunately missing from these descriptions, we thank the reviewer for noting this. We obtain the rooting depth from Jackson et al. (1996). This has been now added to p. 8 | 8.

• p. 4, l. 31: Description of plant nutrient uptake

We have broadened this section 2.1.1 on vegetation processes (p. 5 | 12-18):

"*Plant nutrient uptake is assumed linearly dependent on fine root biomass density for each soil layer, and follows a Michealis-Menten parameterisation to simulate the effects of soil soluble* NH_4*,* NO_3*, and* PO_4 *concentrations (SI Sect. 4.5, Zaehle and Friend, 2010). As in Zaehle and Friend (2010), plant internal nutrient demand can up- or downregulate uptake, but rather than relying on instantaneous plant demand, the response of plant nutrient uptake to plant demand is modelled as a lagged response (of a few days) to balance short-term fluctuations in photosynthesis and soil nutrient availability and to represent memory effects in the plant's control of its nutrient uptake (Fig. S2)*."

• p. 4, l. 22: turnover at two time scales: What is the motivation and the effect of this fast nutrient turnover and resorption/remobilisation to/from the labile pool?

The fast nutrient turnover is based on the observation that the Rubisco and other photosynthetic molecules break-down at a faster rate than the lifetime of a leaf, leading to seasonal variations in foliar nutrient concentrations, as the reflux of nutrients into the leaf are based on the current availability of nutrients for leaf growth as discussed in Zaehle & Friend 2010.

We have now added further explanation of this to the text in p. 6 | 9-13:

"*Tissue turnover is considered at two time-scales: (i) the rapid breakdown of enzymes (N) and associated RNA (P) from tissue, and their ensuing replacement from the labile N and P pools (recycling; at the time scale of days, Zaehle and Friend, 2010), which allows for seasonal changes in tissue nutrient concentrations; and (ii) the senescence of entire tissues and their conversion to litter, including the resorption of nutrients from foliage (SI Sect. 3.9).*"

• p. 6, l. 9: 'Microbes' or 'microbial' is mentioned at several instances, yet a microbial biomass pool is not explicitly modelled. Please specify how this is

to be understood.

We apologise for the confusion. The text has been revised to avoid using the word microbial or microbes unless it refers explicitly to the microbial processing of soil organic matter.

• p. 9, l. 3: Table 2 does not provide information about model performance. Can it be replaced by something that gives insight into performance?

Taking into consideration this comment (also the one below) and comments for Table 2 from Reviewer #2, we have decided to redo this table, by showing observed and simulated values of GPP, TER and leaf C:N -values for these four sites.

• p. 9, l. 5: Should mention modelled value next to observed value in the text.

In this version of the manuscript only the modelled values were in the table. In the new version we list both modelled and observed value in Table 2, and don't have their values in the text.

• p. 9, l. 18: Is there no data available to support this statement?

We are here referring to values of normalized standard deviation, that was not unfortunately clear in this context. The point we here try to make is that the modelled standard deviation was changing mostly because of model-data differences in the seasonal maximum values of the fluxes. We don't really see how we could use data to support this, since this is just a characteristic of the model behavior.

• p. 10, l. 22-23: How does this statement relate to the results shown in Fig. 8?

The reviewer is referencing to the statement "The model shows, as expected, clear dependencies between the rates of net N and P mineralisation, GPP, and carbon stock in vegetation and soil." We agree that this sentence can be confusing in this context and have added a new figure to highlight the dependencies between N mineralization and other variables in the LHS (S12). We have also included in the caption of Fig. 8, that the scalars shown in the figure were related to the annual means. These were unfortunately missing from the previous version.

• p. 11, l. 5-6: What does "decoupling of photosynthesis and growth" refer to?

This is relating to the implementation of the labile pool and meristem dynamics, which are described in the methods section and the SI. We have rephrased this now to read (p. 13 | 23-24):

"*explicit decoupling of the growth processes from C-supply due to photosynthesis by accounting for temperature, moisture and nutrient constraints in the formation of new tissue*"

• p. 11, l. 12-13: This is not shown, is it?

The Taylor plots (Figure 4) and the evaluation of the GFDB forest sites (Figure 6) show that there is no systematic model bias for any single PFT. Because none of the above directly evaluate the seasonal cycle, it is strictly speaking true that we do not show explicitly that the seasonal cycle is unbiased for more than just the four sites plotted in Figure 3, for which we do show the seasonal cycle. We have rephrased this sentence in p. 13 | 31-33, so that it points out to exactly what we have shown in the results section:

"*Despite the lack of any site-specific parameterisation, there is no systematic model bias for any single PFT for either the FLUXNET (Figs. 3 and 4) or the GFDB (Fig. 6) analyses.*"

• p. 11, l. 16: This does not seem to be what the figures suggest (substantial effect by CN and CNP vs. C)

This sentence is maybe a bit unclear. Indeed there is a substantial long-term productivity effect of CN and CNP compared to the C only version. It is the short term dynamics, which are similar between these different model versions. This point was also raised by reviewer #2. The text has now been revised to read (p. 13 | 33-37) :

"*Including a coupling of the carbon cycle to representations of the nitrogen and phosphorus cycle affects long-term average productivity through its effects on photosynthetic capacity (changed foliar nitrogen concentration) and leaf area (as a result of the changes in root:shoot allocation). However, short-term diurnal or sub-seasonal shortage of soil nitrogen or phosphorus does not directly and instantaneously affect simulated productivity because of the buffering introduced through the labile and reserve storage.*"

• p. 12, l. 12-13: give modelled values here too

In the new version of the manuscript we have both the observed and simulated values in a table or report the observed and simulated values in the text.

• Table 2: Just showing modelled values, without observational data is not very informative.

We mentioned now above how we have changed the table.

2.2 SI:

• p. 2, l. 8: Worth noting that layer 1 is the top layer.

We have added this to the text.

• p. 2., l. 9: Worth noting that this is the total canopy N content (if that's correct?).

We have added this to the text.

• Eq. 7: Why is the CO2 compensation point not subtracted from ci in the numerator?

This is not done in Eq 7, but Eq. 16a, as already noted in Kull and Kruijt (1998) eqs. 2 and 14.

• p. 4, l.19: Introduce the term Av again.

We've done this now.

• Eq. 15: It's described on p. 3, l. 26 that A is the minimum of two rates (Ac and Aj). It appears confusing that Ah is introduced here as another limiting rate. Isn't it just determining the Aj rate (actually, it may also appear confusing that Aj is independent of light, as of eq. 7).

On p. 3 l. 26 it is said that A is the minimum of the two rates (Ac and Aj) in the *light saturated* conditions. The Ah here is the photosynthesis taking place in the *light-limited* conditions. The formulation of the Farquhar model by Kull and Kruijt (1998) differs from some other formulations, as here it is assumed that each leaf layer has potentially both light-saturated and light-limited region, which is dependent on the leaf N concentration and the incident light environment of that layer (eq 16).

We have clarified this in the text in p. 4 | 3-8:

"*Photosynthesis and stomatal conductance are calculated for the mid-points of each canopy layer and light-quality class (sunlit and shaded; as defined in Sect. M6.1. For clarity, the subscript* $_{cl}$ *is omitted in this section. The calculation of leaf-level photosynthesis is based on Kull and Kruijt (1998), extended for C4 photosynthesis according to Friend et al. (2009). The Kull-photosynthesis scheme explicitly and dynamically separates each leaf (layer) into a fraction that is light-saturated, under which photosynthesis is controlled by Farquhar-type co-limitation model (Farquhar et al., 1982), and the remainder, which is light-harvesting limited, and therefore strongly depends in the leaf chlorophyll content (see for details Kull and Kruijt (1998)).*"

• Eq. 16: should spell out 'for' or use appropriate mathematical symbol

We have modified the equation accordingly.

• Eq. 17: Is aerodynamic conductance a fixed parameter?

No, it is not a fixed parameter, it is calculated from the aerodynamic resistance introduced in eq. 110. We have added a reference to this equation in the text.

• p. 8, l. 4: Why "co-limitation" and not (just) limitation?

Here we wanted to point out that both nitrogen and phosphorus can be limiting the growth, therefore we wrote co-limitation.

• p. 8, l. 4/5: Should mention here that this refers to the turnover rate of the labile pool and that the labile pool turnover defines this part of the growth limitation.

This has been done.

• Eq. 28: Should mention the exponent 2 also in the text below.

This has been done.

• Eq. 30: Better write functions as f(N, P, H2O) instead of arguments as subscripts. In general, Eq. 30 needs an explanation/motivation.

We write now (p. 10 | 20-25):

"*For both trees and grasses, fine root and leaves are assumed to be in homeostatic balance between transpiring leaf surface and root mass*

C_{leaf} = f^{ltor} \times k_{rtos} \times \frac{k_{latosa}}{sla \times \rho_{wood}}} \times C_{fine_root}

where k_{rtos}, sla, k_{latosa}, and ρ_{wood} are PFT-specific parameters. f^{ltor} is the long-term average (τ^{alloc}_{mavg}) of the nutrient and water limitation scalar, which represents the widely observed phenomenon of increased root allocation with water or nutrient shortage and is calculated here as the minimum of three functions describing N, P and water limitation respectively."

• Eq. 37: What are lambda and k?

Lambda and k are shape parameters, the values are shown in Table M3. We have added explanation and reference to the table in the text.

• Eq. 39b: k reserve not k store ?

Yes, we have corrected this.

• Eq. 45b, 'dt': clarify that this refers to daily.

We have corrected this in the revised version.

• p. 15, l. 5: Is the seed-bed pool and fruit production related?

Yes, the seed-bed pool is related to the fruit pool such that turnover from the fruit pool enters the seed bed pool, where it is either used for re-establishment of new seedlings, or turns over to form litter. This has already been described in the description of turnover, and we clarify now in the description of vegetation dynamics that (p. 16 | 5-7):

"*Different to Sitch et al. (2003) and Zaehle and Friend (2010), the establishment flux for a PFT is dependent on the size of the seed-bed pool, which itself is dependent on the turnover of the fruit pool, and an average, PFT-specific seed-bed turnover time ($\tau_{seed,est}$).*"

• p. 16, l. 3/4: But later, C pools of newly established individuals are averaged with C pools of existing ones, leading to a reduction in the average-individual C pool, right?

The mass and number of individuals from the newly established individuals are added to the mass and number of individuals from the existing average-individual population (i.e. this is an addition, not averaging at the grid-scale level), leading to a reduction of the mass per individual, just as in the LPJ model (Sitch et al. 2003). We will clarify this in the revised manuscript.

We have clarified this in the new version in p. 17 | 5-7 as:

"*...during establishment the total pool size increases, as mass is added to the labile pools, but the average size of individuals decreases due to the added number of (small) individuals.*"

• p. 16, l. 17: 'met, str, ...' Introduce these abbreviations at first mention.

We have added this.

• Eq. 65b: What is Ed,decomp?

This is the de-activation energy for decomposition, shown in Table M4. We have added an explanation now to the text p. 19 | 15-17:

"*The turnover times (τ_i^{base}) of the litter and SOM pools respond to soil temperature (T_{soil}) following a peaked Arrhenius function (with parameters for the activation ($E_{a,decomp}$) and de-activation ($E_{d,decomp}$) of soil organic matter decomposition, see Tab. M4, and the soil matrix potential (Ψ_{soil}) as follows:*"

• p. 19, l. 5: 'increased' At first I though this should be 'reduced'? I thought that the fast and slow SOM pools have a lower C:N ratio than the structural pool and mass transfer from the structural to fast/slow SOM leads to net immobilisation. If not, please state upfront which step of mass transfer leads to immobilisation and relate it to respective pool stoichiometries.

It is correct that the mass transfer from litter to SOM leads to net immobilisation. Shortage of nutrients causes the rate of the litter pool decomposition to decline so that the inflow of material into the SOM pools can maintain its stoichiometric ratio, and in consequence the litter turnover times increases. We have rephrased the model description to clarify this in p. 20 | 11-13:

"*In the case that the amount of available nitrogen ($\Phi_{l \rightarrow fast,NH4}$) is insufficient to ensure that the newly formed fast SOM has a C:N ratio of $\chi_{SOM\ C:N\ fast}$, the turnover times of the metabolic and structural litter pool are increased, leading to a reduced decomposition rate of litter and therefore a reduced immobilisation requirement for litter decomposition (Parton et al. (1993)):*"

• Eq. 73a: Point out in the main text that uptake is linear w.r.t. fine root biomass.

The revised main text says now p. 5 | 12-18: "*Plant nutrient uptake is assumed linearly dependent on fine root biomass density for each soil layer, and follows a Michealis-Menten parameterisation to simulate the effects of soil soluble NH_4, NO_3, and PO_4 concentrations (SI Sect. 4.5, Zaehle and Friend (2010)). As in Zaehle and Friend (2010), plant internal nutrient demand can up- or downregulate uptake, but rather than relying on instantaneous plant demand, the response of plant nutrient uptake to plant demand is modelled as a lagged response (of a few days) to balance short-term fluctuations in photosynthesis and soil nutrient availability and to represent memory effects in the plant's control of its nutrient uptake (Fig. S2).*"

• Eq. 94: Start with stating what the reflection coefficient determines. Maybe better to start with something "high-level", like the surface energy budget? Or just start with equation 97.

We have followed this suggestion and have re-organised this section to start with the general equation describing light absorption in the canopy to provide context for the following equations.

• Sec. 6.3: Start stating what sort of scheme is applied for soil hydrology, how many layers, . . .

This section now starts with an introduction (p. 30 | 22 - 27) :

"*Surface hydrology is represented in very simple terms in QUINCY, because it is meant to be replaced by the JSBACH 4 hydrology in a future version. The model largely follows JSBACH 3 (Roeckner et al. 2003), with some modifications. The model represents surface hydrology for a number of soil layers (see Section M1) and including a canopy skin layer (hereafter referred to as skin). It represents interception by and interception loss from the canopy, infiltration and surface runoff generation at the soil surface, water movement in the soil, as well as deep drainage.*"

• p. 29, l. 10: Need to introduce the meaning of "skin" here.

This is now done.

• p. 29, l. 19: I'm confused: field capacity is not part of Eqs. 114.

There was indeed a mistake in the equation. The entire section has been revised to be correct and easier to follow. In general, if the soil water per layer would exceed its field capacity, the amount of water exceeding the field capacity is moved into surface runoff or drained to the layer below.

• Eq. 114: Throughfall is not defined. Is sl=1 the topmost layer? In general, I don't understand Eq. 114.

Throughfall (Fthrough) is what is left from the precipitation after interception. Yes, sl=1 is the topmost layer. The description of surface hydrology has been revised (eq 113 - 116) in order to clarify what is happening in the model.

• Eq. 116: What is Ei? Evaporation of intercepted water? What is ra? aero-dynamic resistance? Repeat here to clarify. It would be helpful to start with the high-level water budget.

Yes, Ei is the evaporation of the intercepted water and ra is the aerodynamic resistance. We have added these to the text. We have re-organized this section as suggested.

• p. 30, l. 5: How is surface temperature calculated? Please add reference to equation.

The surface temperature is calculated by eq. 107. We have added here a reference to that.

• p. 31, l. 1: This is better put upwards (start with high level description of first principle (water/energy conservation).

Yes, as already mentioned above, this has been done.

A new ~~terrestrial biosphere~~ model ~~with~~ of the coupled carbon, nitrogen, and phosphorus cycles in the terrestrial biosphere (QUINCY v1.0; revision ~~1772~~1996)

Tea Thum[1], Silvia Caldararu[1], Jan Engel[1], Melanie Kern[1,2,3], Marleen Pallandt[1,2], Reiner Schnur[4], Lin Yu[1], and Sönke Zaehle[1,5]

[1]Max Planck Institute for Biogeochemistry, Hans-Knöll Str. 10, 07745 Jena, Germany
[2]International Max Planck Research School (IMPRS) for Global Biogeochemical Cycles, Jena, Germany
[3]Technical University Munich - School of Life Sciences, Weihenstephan, Germany
[4]Max Planck Institute for Meteorology, Hamburg, Germany
[5]Michael Stifel Center Jena for Data-driven and Simulation Science, Jena, Germany

Correspondence: Tea Thum (tthum@bgc-jena.mpg.de), Sönke Zaehle (szaehle@bgc-jena.mpg.de)

Abstract. The dynamics of terrestrial ecosystems are shaped by the coupled cycles of carbon, nitrogen, and phosphorus, and ~~strongly depend~~ these cycles are strongly dependent on the availability of water and energy. These interactions shape future terrestrial biosphere responses to global change. ~~Many process-based models of the terrestrial biosphere have been gradually extended from considering carbon-water interactions to also including nitrogen, and later, phosphorus dynamics. This evolutionary model development has hindered full integration of these biogeochemical cycles and the feedbacks amongst them. Here~~Here, we present a new terrestrial ecosystem model, QUINCY (QUantifying Interactions between terrestrial Nutrient CYcles and the climate system), which ~~is formulated around a consistent representation of element cycling~~ has been designed from scratch to allow for a seamless integration of the fully coupled carbon, nitrogen, and phosphorus cycles with each other and also with processes affecting the energy and water balances in terrestrial ecosystems. This new model includes i) a representation of plant growth which separates source (e.g. photosynthesis) and sink (growth rate of individual tissues, constrained by ~~nutrients, temperature , and water availability~~ temperature and the availability of water and nutrients) processes; ii) the acclimation of many ecophysiological processes to meteorological conditions and/or nutrient ~~availabilities~~availability; iii) an explicit representation of vertical soil processes to separate litter and soil organic matter dynamics; iv) a range of new diagnostics (leaf chlorophyll content; ^{13}C, ^{14}C, and ^{15}N isotope tracers) to allow for a more in-depth model evaluation. ~~We~~ In this paper, we present the model structure and provide an assessment of its performance against a range of observations from global-scale ecosystem monitoring networks. We demonstrate that ~~the framework~~ QUINCY v1.0 is capable of ~~consistently~~ simulating ecosystem dynamics across a ~~large gradient in climate and soil conditions~~wide climate gradient, as well as across different plant functional types. ~~To aid this understanding we~~ We further provide an assessment of the sensitivity of key model predictions to the model's ~~sensitivity to its parameterisationand the associated uncertainty~~parameterisation. This work lays the ground for future studies to test individual process hypotheses using the QUINCY v1.0 framework in the light of ecosystem manipulation observations, as well as global applications to investigate the large-scale consequences of nutrient-cycle interactions for projections of terrestrial biosphere dynamics.

1 Introduction

Past, present, and future changes in climatic conditions and atmospheric CO_2 concentrations affect terrestrial vegetation and soils (Hou et al., 2018; De Kauwe et al., 2013; Swann et al., 2016), which in turn ~~provide~~ induce biogeophysical and biogeochemical feedbacks to the atmosphere (Bonan, 2008; Friedlingstein et al., 2014; Zaehle et al., 2010). To predict the likely trajectories of terrestrial ecosystems under climate change and their climate feedbacks, it is important to develop and test advanced modelling tools for the terrestrial biosphere (Sitch et al., 2015). Global terrestrial biosphere models (TBMs) have evolved during the last decades alongside our understanding of soil and vegetation functioning (Bonan and Doney, 2018). Early vegetation models included only processes related to the carbon (C) and water cycle (e.g. Sitch et al., 2003; Krinner et al., 2005; Dickinson et al., 2006; Raddatz et al., 2007; Clark et al., 2011). The recognition that nitrogen (N) has a pivotal role in the future dynamics and C storage of terrestrial ecosystems (Vitousek and Howarth, 1991; Hungate et al., 2003) has led to the development of a new generation of models that include a comprehensive representation of the N cycle (Thornton et al., 2007; Zaehle and Friend, 2010; Gerber et al., 2010; Warlind et al., 2014). More recently, phosphorus (P) cycle processes have also been included in TBMs (Wang et al., 2010; Goll et al., 2017; Yang et al., 2014), as these can be important to understanding ecosystem response in naturally P limited tropical regions (Yang et al., 2014) or in regions with large atmospheric N deposition and ensuing increases in P limitation (Peñuelas et al., 2013; Vitousek et al., 2010).

~~The~~ Although the number of element cycles and thereby processes considered in TBMs has increased in an effort to provide more realistic models (Zaehle and Dalmonech, 2011; Prentice et al., 2015), ~~yet~~ there is little consensus on how to represent many of these processes in a realistic, but robust and computationally efficient manner. Often, small-scale soil and vegetation processes can lead to larger scale feedbacks (e.g. Hararuk et al., 2015; Bradford et al., 2016) and therefore need to be included in sufficient detail in terrestrial biosphere models. Recent model-data synthesis studies with observations from Free-Air CO_2 Enrichment (FACE) experiments have revealed a number of fundamental issues in the way that state-of-the-art models represent plant growth (De Kauwe et al., 2014), nitrogen dynamics (Zaehle et al., 2014), and water responses (De Kauwe et al., 2013) to elevated CO_2. This highlights the need for a modular framework that allows testing multiple hypothesis for uncertain processes, thereby gaining an understanding on how process information and importance propagates from site to regional and global scales (Knauer et al., 2016; Peng et al., 2014; Thum et al., 2017).

One important obstacle to such an approach is the gradual development of terrestrial biosphere models, which implies that new features, such as processes describing the dynamics of the N or P cycle~~(Gruber and Galloway, 2008; Arneth et al., 2010)~~, have been added to existing~~model formulations (Bonan, 2008)~~, carbon-cycle only land surface model formulations. This evolutionary approach can result in a situation where assumptions that were made in earlier versions of the model are incompatible with the new assumptions, or that the old model structure cannot appropriately accommodate new structures, therefore limiting the ability to take new ecophysiological understanding into account. To overcome ~~the issuesof evolutionary development~~such issues, we have developed a new terrestrial biosphere model, QUINCY (QUantifying Interactions between terrestrial Nutrient

CYcles and the climate system, Fig. 1), benefiting from advances in the understanding of global ecology. This new model is formulated based on:

- the recognition that plant growth may be limited by source (e.g. photosynthesis) or sink (growth rate of individual tissues, constrained by nutrients, temperature, and water availability) processes (Fatichi et al., 2013). We account for this decoupling by introducing a short-term ('labile') and a long-term ('reserve') storage pool for carbon and nutrients, which allow plants to adjust the carbon partitioning between growth, respiration, and storage according to nutrient availability, moisture stress and temperature.

- the consideration of gradual changes in nutrient availability over time and their effects on the surface carbon, water, and energy exchanges. The model represents all biogeochemical and biogeophysical processes in the model at a half-hourly time-step. Many processes, e.g. the response of photosynthesis, tissue stoichiometry and fine root growth to nutrient shortage, are assumed to have a process-specific 'memory' time scale, causing a lagged response to instantaneous variations in the environmental conditions. This includes a representation of the acclimation of both photosynthesis and maintenance respiration to the prevailing growth temperature (June et al., 2004; Atkin et al., 2014; Mercado et al., 2018). Together with a dynamic representation of photosynthetic capacity based on soil nutrient availability, this feature reduces the need for regionally defined plant functional types (e.g. boreal versus temperate type) needed to describe the vegetation in different regions.

- the recognition that biogeochemical processes in the soil (e.g. soil organic matter decomposition, nitrification, denitrification, and weathering) vary strongly within the soil profile (Ahrens et al., 2015; Koven et al., 2013). Therefore, soil physics~~and biogeochemical processes are explicitly vertically resolved and so is the interaction between plant root uptakeand turnover and soil biogeochemical processes~~, soil biogeochemical processes and their interaction with vegetation processes through plant nutrient / water uptake, as well as root turnover are explicitly vertically resolved.

~~We have formulated this model in a modular structure to facilitate the consistent testing of multiple hypothesis for one particular process. Additionally, we have added a number of important diagnostics, that will allow further ways of model evaluation in the future. The leaf chlorophyll content is explicitly modelled from the leaf N and used to model the light dependency of canopy photosynthesis (Kull and Kruijt, 1998), which allows for further ways to compare the simulation results with *in situ* and remotely sensed observations. The model also keeps track of the isotopic composition of C (in terms of , and) , and N (), which will allow to make use of natural abundance data and isotope tracer studies in the future~~The QUINCY model contains entirely newly written code, although certain process representations are adapted from literature and previous models, including but not limited to OCN (Zaehle and Friend, 2010) and JSBACH3 (Roeckner et al., 2003). This new code approach allows for an appropriate separation of model infrastructure (e.g. memory allocation) and scientific code, and a better integration of model components. This permits us to include an internally consistent representation of ecosystem processes and in particular nutrient effects on plant photosynthesis, growth and soil organic matter turnover through the inclusion of a common set of underlying hypotheses.

The aim of this paper is to present the basic structure and main features of the baseline version of this new model. We provide an assessment of the model's performance against a range of observations from global-scale ecosystem monitoring networks to demonstrate that the framework is capable of ~~consistently simulating C fluxes~~ simulating ecosystem C fluxes in agreement with these observations given the simulated N, P, and water availability across a large gradient in climate and soil conditions, as well as across different plant functional types. To aid this understanding we provide an assessment of the model's sensitivity to its parameterisation~~and the associated uncertainty. This information~~ .

The information from this paper provides the background for future process-specific studies to test and improve process representation. In particular, we have formulated this model in a modular structure to facilitate the testing of multiple hypotheses for one particular process, and to reduce the scope of the model (e.g. separately simulating canopy dynamics, vegetation dynamics, or soil biogeochemistry) to study the impact of particular processes (see SI for details). Additionally, we have added a number of important diagnostics, that will allow further ways of model evaluation. For instance, the leaf chlorophyll content is explicitly modelled from the leaf N to improve the simulated light response of photosynthesis throughout the canopy (Kull and Kruijt, 1998), but this will also allow for novel ways to compare the simulation results with *in situ* and remotely sensed observations in the future. The model also keeps track of the isotopic composition of C (in terms of ^{13}C, and ^{14}C), and N (^{15}N), which will allow to make use of natural abundance data and isotope tracer studies in the future.

2 Methods

2.1 Model description

The QUINCY model v1.0 (rev. 1772) represents the coupled biogeochemical cycles of carbon (C), nitrogen (N), and phosphorus (P) in terrestrial ecosystems, as well as their interaction with the terrestrial water and energy balance (Fig. 1). The model traces the flow of these elements as well as C and N isotopes (^{13}C and ^{14}C, and ^{15}N) through vegetation and soil at a half-hourly time-step. The model considers eight broadly defined plant functional types (PFTs, see Tab. 1), representing differences in leaf type (herbaceous, broadleaved, coniferous), phenology (evergreen, rain green, and summer green), growth form (grasses and trees), and photosynthesis-type (C3 versus C4 photosynthesis) with a set of traits describing time-invariant functional differences across types (see SI Tab. ~~7~~M7). Different to other TBMs, certain "soft" plant functional type characteristics, such as the photosynthetic capacity of leaves or the temperature sensitivity of photosynthesis and respiration acclimate to local environmental conditions, and therefore lead to a smoother transition of ecosystem functioning across eco-climatic gradients. The number of PFTs is not embedded into the code-structure and therefore new PFTs can be easily added if sufficient data to parameterise these are available.

A brief overview of the model structure and key processes is given in this section. The detailed mathematical description of the model processes can be found in the Supplementary Material.

Although conceived to be coupled to the land-surface scheme of an Earth system model, the model is currently applied stand-alone at the ecosystem scale. The stand-alone version requires half-hourly short- and longwave radiation, air temperature, precipitation and snowfall, wind velocity, atmospheric CO_2, $^{13}CO_2$, $^{14}CO_2$ mole fractions, as well as rates of NH_x, NO_y, and

PO_4 deposition as time-dependent driving data. In addition, the model requires input describing the geographical coordinates, vegetation type, and soil physical and chemical parameters (texture, bulk density, rooting and soil depth, as well as inorganic soil P content).

2.1.1 Vegetation processes

~~Vegetation~~ Expanding on the concept employed by LPJ (Sitch et al., 2003) and OCN (Zaehle and Friend, 2010), vegetation is characterised by an average individual representative of a PFT, composed of three fast-lived structural tissue types (pools: leaves, fine roots, and fruits), a respiring non-structural pool (labile), as well as a seasonal, non-respiring, and non-structural storage pool (reserve). In the case of tree vegetation types, three longer-lived structural tissue types (sapwood, heartwood, and coarse roots) are additionally represented, as are stand characteristics (height, diameter, individuum density).

~~Photosynthesis~~ Building on Zaehle and Friend (2010), photosynthesis is calculated for sunlit and shaded leaves separately, explicitly taking the vertical canopy gradient of light, foliar chlorophyll and photosynthetic N into account (Kull and Kruijt, 1998), with extensions for C4 photosynthesis (Friend et al., 2009), and the temperature response as in ~~Bernacchi et al. (2001, SI Sect. 2)~~Ber Different to OCN, temperature acclimation of photosynthesis is modelled to acclimate to air temperature according to Friend (2010). Photosynthetic parameters, including chlorophyll content, further are assumed to depend on leaf N concentration (Friend et al., 1997). As foliar mass and N concentrations both respond to soil N availability (Vicca et al., 2012; Hyvönen et al., 2007; Meyerholt and Zaehle, 20 this causes canopy photosynthesis to be directly affected by soil N availability in addition to meteorological variables. The stomatal conductance is coupled to the calculation of photosynthesis according to the Ball-Berry formulation (Ball et al., 1987; Knauer et al., 2015). ~~Maintenance~~ Different to Zaehle and Friend (2010), QUINCY v1.0 accounts for stomatal and biochemical limitations by soil moisture (Egea et al., 2011, SI Eq. 18). In addition, photosynthesis can become downregulated due to sink limitation, when nutrient or water availability or low temperatures limit growth and cause accumulation of photosynthates in the labile pool (Fatichi et al., 2013; Hartmann et al., 2018, see Fig. S1 for an example). Plant nutrient uptake is assumed linearly dependent on fine root biomass density for each soil layer, and follows a Michaelis-Menten parameterisation to simulate the effects of soil soluble NH_4, NO_3, and PO_4 concentrations (Zaehle and Friend, 2010, SI Sect. 4.5). As in Zaehle and Friend (2010), plant internal nutrient demand can up- or downregulate uptake, but rather than relying on instantaneous plant demand, the response of plant nutrient uptake to plant demand is modelled as a lagged response (of a few days) to balance short-term fluctuations in photosynthesis and soil nutrient availability and to represent memory effects in the plant's control of its nutrient uptake (Fig. S2).

As in LPJ and OCN, maintenance respiration is calculated for each tissue type as a function of its N content and tissue temperature ~~(SI Sect. 3.3, Lloyd and Taylor, 1994). Photosynthesis and respiration acclimate~~ (SI Sect. M3.3, Lloyd and Taylor, 1994). However, a novel feature of QUINCY v1.0 is that it does account for the observed acclimation of basal respiration rates to growth temperature ~~according to (Friend, 2010) and (Atkin et al., 2014), respectively. Plant nutrient uptake is dependent on fine root biomass density, soil soluble , , and concentrations as well as plant internal nutrient demand (SI Sect. 4.5, Zaehle and Friend, 2010)~~(Atk A second new feature is that the costs for actual nutrient transformation, which are dependent on the rate of uptake and source of nitrogen (SI Eq. 24, Zerihun et al., 1998), are included in the root maintenance respiration term. While maintenance respiration

takes priority over growth, under severe C deficit after the downregulation of photosynthesis, the maintenance respiration and nutrient uptake respiration can become downregulated by the meristem acticity.

Different to earlier model approaches that included a labile pool (Zaehle and Friend, 2010), plant growth is modelled as the balance of source processes (photosynthesis, ~~nutrient~~ nitrogen and phosphorus uptake) and the capacity of the plant to create sinks (production of new biomass tissue, respiration, and storage; SI Sect. 3.3). The capacity of the plant to generate sinks is dependent on (i) the activity of the plant's meristem controlling the usage of the labile pool for growth, which is reduced at low air temperature and/or soil moisture (Fatichi et al., 2013)~~.~~; (ii) the partitioning of its labile resource to new tissue growth and the availability of ~~nutrients~~ nitrogen and phosphorus to create these tissues (Zaehle and Friend, 2010); (iii) the need for longer-term storage production (Fisher et al., 2010); and (iv) respiration for maintenance, which is given priority over growth of new tissue. Short-term fluctuations in the balance between carbon acquisition through photosynthesis and nutrient acquisition by roots are balanced by the time-scale of the labile pool turnover. Seasonal and longer-term fluctuations are balanced to some extend by the build-up and use of the reserve pool. The flow of compounds between the labile and reserve pools (SI Sect. ~~3.6~~M3.6) is described by a set of pull (from the reserve pool) and push (to the reserve pool) mechanisms attempting to simulate the signalling related to the beginning of the growing season (phenological pull), the need for maintenance and growth (maintenance pull), as well as to provide resources for the next growing season or resilience against interannual variability (reserve push).

Tissue growth follows a set of allometric equations (Shinozaki et al., 1964; Sitch et al., 2003; Zaehle and Friend, 2010), describing size-dependent relationships of foliar, fine root, coarse root, sapwood and fruit biomass (SI Sect. ~~3.4~~M3.4). The allometric relationship between leaves and fine roots responds to N, P and water limitation and therefore increases uptake capacity under nutrient limitation. The C:N and N:P ratios of the leaves and fine roots are flexible within empirical bounds and respond dynamically to an imbalance between C and N, or N and P availability, respectively (SI Sect. ~~3.5~~M3.5). The allometric equations and the N and P content of each tissue give the stoichiometric constraint of plant growth. ~~Photosynthesis can be down-regulated through sink-limitation (Hartmann et al., 2018), if nutrient or water shortage leads to the accumulation of carbon in the labile pool (SI Sect. 3.6).~~

~~Turnover~~ Tissue turnover is considered at two time-scales: (i) the rapid breakdown of enzymes (N) and associated RNA (P) from tissue, and their ensuing replacement from the labile N and P pools (recycling; at the time scale of days, Zaehle and Friend, 2010), which allows for seasonal changes in tissue nutrient concentrations; and (ii) the senescence of entire tissues and their conversion to litter, including the resorption of nutrients from foliage (SI Sect. 3.9). ~~Tissue~~ The tissue senescence is calculated given a fixed turnover time for each tissue, with the exception of the leaves, where turnover is determined by the PFT-specific phenological timing (SI Sect. ~~3.8~~M3.8).

Stand-level vegetation dynamics are represented through ~~density-dependent mortality~~ the establishment and mortality of an average representative individual of the entire tree populations, following largely Sitch et al. (2003) and Zaehle and Friend (2010, ,see SI Se Mortality is simulated as density-dependent, constraining the number and size of individuals, as well as a dynamic background mortality related to the overall growth efficiency of the plant~~(Sitch et al., 2003; Zaehle and Friend, 2010, SI Sect. 3.10). Re-establishment/Recruitment is explicitly taking~~ . (Re-)establishment and recruitment is dependent on meteorological and

space constraints, but a new aspect of the re-establishment representation is that the model explicitly takes account of the available seed pool at the forest / grassland floor, ~~thereby depending amongst others~~ which depends on the vegetation's ability to grow and produce fruit.

2.1.2 Soil biogeochemical processes

The ~~vertical soil profile of biogeochemical pools and processes is explicitly represented, with exponentially increasing layer thickness with increasing soil depth. For each of these layers, the model represents different organic pools (metabolic, structural, and woody litter, as well as fast and slow overturning soil organic matter (SOM)), as well as inorganic pools of N and P (soluble inorganic , , as well as , , and , soluble inorganic , adsorbed , occluded and primary). For each soil layer, temperature and moisture are calculated based on soil physical characteristics, and the transport and atmospheric exchange of energy and water (SI Sect. 6.3).~~

~~The~~ turnover and formation of SOM follows, with some modifications, the CENTURY approach ~~(Parton et al., 1993, SISect. 4)~~(Parton et the turnover of litter and SOM pools are all calculated using first-order kinetics with temperature and moisture dependence. The litter stoichiometry is determined by the stoichiometry of senescent plant tissue and tissue-specific allocation fractions. The stoichiometry of the fast SOM pool adjusts to available inorganic nutrients, whereas the slow SOM pool is assumed to have fixed C:N:P stoichiometry. As a result, the decomposition of litter may become N and P limited, leading to the accumulation of an organic litter layer, and reducing the rate of N and P cycling in the ecosystem.

The soluble inorganic NH_4, NO_3 and PO_4 are assumed to be available for plant ~~and microbial uptake~~uptake and microbial immobilisation, as concluded by White (2006) and many others. ~~Plants and soil microbes~~ Plant uptake and SOM decomposition compete for these nutrients based on their respective demand and uptake capacity, which ~~varies~~ vary in time and with soil depth. In the aerobic part of the soil, NH_4 is oxidised to NO_3 through nitrification and in the anaerobic part of the soil NO_3 is reduced to N_2 through denitrification (Zaehle et al., 2011). Both processes produce NO_y and N_2O as by-products (SI Sect. ~~4.7~~M4.7). The representation of soil inorganic P dynamics (SI Sect. ~~4.8~~M4.8) follows the concept from Yang et al. (2014) and Wang et al. (2010). The available soluable PO_4 is exchanged via ad-/desorption with the mineral surface, leached with soil water, and replenished by atmospheric deposition, weathering, and biomineralisation of P that is bound in the slow SOM pool. The adsorbed P is further absorbed into the soil matrix and gradually becomes an inactive form of P (occluded P, Walker and Syers, 1976).

Different to the original CENTURY-style models, the vertical soil profile of biogeochemical pools and processes is explicitly represented, with exponentially increasing layer thickness with increasing soil depth. For each of these layers, the model represents different organic pools (metabolic, structural, and woody litter, as well as fast and slow overturning soil organic matter (SOM)), as well as inorganic pools of N and P (soluble inorganic NH_4, NO_3, as well as NO_y, N_2O, and N_2, soluble inorganic PO_4, adsorbed PO_4, occluded PO_4 and primary PO_4). For each soil layer, temperature and moisture are calculated based on soil physical characteristics, and the transport and atmospheric exchange of energy and water (SI Sect. M6.3). As an example of the benefit of QUINCY's modular approach, Fig. S3 shows that the explicit representation of the vertical soil profile, compared to a zero-dimensional, lumped soil approach, has little effect on the seasonal course of heterotrophic respiration.

However, it does affect the simulated nutrient dynamics because of the explicit separation of a nutrient immobilisation in the litter dominated layers from the gross-mineralisation dominated soil layers with a proportionally higher content of soil organic matter.

2.2 Data for model evaluation

We evaluate simulated diurnal and seasonal patterns of gross primary production and net ecosystem carbon exchange (GPP and NEE, respectively) at a subset of FLUXNET sites (see Table A1) available from the FLUXNET La Thuile Synthesis Dataset (NOA, 2007). The half-hourly CO_2 fluxes have been measured and processed using standard procedures (Papale et al., 2006) as well as gap-filling and partitioning algorithms (Reichstein et al., 2005). We further evaluate the mean annual estimates of gross and net primary production (GPP and NPP, respectively) and their ratio, the carbon-use efficiency (CUE = NPP / GPP) from a global forest database (GFDB, Vicca et al., 2012; Campioli et al., 2015). We further evaluate the simulated growing-season plant water-use efficiency, i.e. the ratio of plant water loss to carbon uptake, by comparing a proxy, foliar isotope discrimination of ^{13}C (Medlyn et al., 2017), against data reported by ~~(Cornwell et al., 2018a, b)~~Cornwell et al. (2018a, b). Fig. 2 provides an overview of the sites used for evaluation.

2.3 Model setup

2.3.1 Boundary conditions and meteorological forcing

The QUINCY model is applied at site scale for the dominant plant functional type (PFT) at each site. For the simulations at the FLUXNET sites, the site-specific observed meteorological data were used (NOA, 2007). For the GFDB sites, where site-level meteorology is not readily available, daily meteorological data for 1901 to 2015 was taken from CRUNCEP, version 7, (Viovy, 2016), and disaggregated to the model time-step using the statistical weather generator as in Zaehle and Friend (2010). The annually changing CO_2 mole fraction was obtained from Le Quéré et al. (2018), and the time series of ^{13}C, ^{14}C ~~are~~ were obtained from Graven et al. (2017). The time series of N deposition for each site ~~is~~ was taken from Lamarque et al. (2010) and Lamarque et al. (2011). For the P deposition model, estimates of nutrient and dust fluxes from ~~Brahney et al. (2015); Chien et al. (2016)~~ Brahney et al. (2015) and Chien et al. (2016) were used.

Soil physical properties (volumetric heat capacity and conductivity, water content at saturation, field capacity, and wilting points, as well as parameters describing the soil water retention curve are derived from soil texture according to Saxton and Rawls (2006). Where available, texture data are taken from site observations. Alternatively, they are obtained from the nearest gridcell of the SoilGrids dataset (Hengl et al., 2017). The rooting depth has been obtained from Jackson et al. (1996).

The vegetation is initialised as bare ground with a small amount of seed-bed mass to start vegetation growth. The soil organic matter profile is initialised with a default SOM content for each pool, 60% of which is allocated to the uppermost layer, and the remaining 40% is allocated to other soil layers in proportion to the assumed rooting profile. Previous tests have shown that the model is not very sensitive to the choice of the SOM initial ~~condition~~conditions. The soil inorganic P pools of the first 50 cm are initialised using the soil P dataset by Yang et al. (2013), extrapolated to the whole soil profile assuming i) a constant

total soil inorganic P density ($\mathrm{mol\ P\ kg^{-1}\ soil}$), and ii) an increasing fraction of primary P and decreasing fraction of labile P with increasing soil depth.

2.3.2 Spinup and model protocol

The QUINCY model is spun-up with repeated meteorological forcing for each site to obtain an near-equilibrium soil and vegetation state. For the GFBD sites, meteorology and other atmospheric forcing (atmospheric CO_2, its isotopes, as well as N and P deposition), are taken by randomly drawing years from the period 1901 to 1930. The same procedure is applied for FLUXNET sites, with the exception that meteorological forcing is only available for more recent years, and data from those years are used in random sequence. The P cycle is activated during the model spinup, but the more stable soil inorganic P pools, i.e. the primary, sorbed, occluded pools, are kept constant to ensure that the simulation initialises at the P status of Yang et al. (2013)'s dataset.

After spinup, the model is run for the period 1901-2015 using the annual values for atmospheric CO_2, $^{13}CO_2$ and $^{14}CO_2$, as well as N and P deposition, and the meteorology of the respective year. For the comparison to GFDB data, forest stands are clear-cut in the year provided by the database. Upon harvest, vegetation biomass is transferred to the litter pools, with the exception of the wood pool, of which a given fraction, $f_{harvest}^{wood}$, is removed from the site. In the case of FLUXNET sites, we retain the model output for the years covered by the available data at each individual site (Tab. A1). For the GFDB sites, we average over the period 1995-2004 to remove the effects of interannual climate variability and to have modelled forest age close to the actual forest age of each site, as the precise year of measurement is not recorded in the database for all sites.

To test the effect of the simulated N and P availability, we applied the model for the FLUXNET sites with three different setups. Next to the full CNP version of the model described above (referred to hereafter as 'CNP'), we performed a simulation ('CN') in which the P concentration of the soil was kept at concentrations not limiting ~~microbial or plant uptake~~ plant uptake or SOM decomposition, effectively removing the impact of the inorganic P sorption and weathering dynamics, and maintaining N:P stoichiometry at default values. We also added a version ('C'), in which in addition, biological N fixation in soil (asymbiotic fixation) and in vegetation (symbiotic fixation) was calculated so as to avoid any N limitation of soil turnover and vegetation growth while keeping the C:N stoichiometry at default values.

2.4 Model sensitivity to its parameterisation

We further test the sensitivity of the model to its parameterisation using a hierarchical latin hypercube design (LHS, Saltelli et al., 2000; Zaehle et al., 2005) to assess the stability of the model with respect to changing parameter values. As many parameters have unknown value ranges and distributions, we simply vary each parameter between 90% to 110% of its default value given in the Supplementary Material (Tables M1-M7), drawn with LHS sampling from a uniform distribution. We first generate LHS samples for each module (corresponding to one Section in the SI, *results not shown*), and evaluate the model output from these simulations in terms of long-term mean modelled GPP, leaf C:N:P, net N and P mineralisation, as well as total vegetation and ecosystem carbon storage. Based on these simulations we select parameters (n=45), which have a strong effect on the model outcome to form a new set of 1000 LHS samples, which are used for the model sensitivity ~~and uncertainty~~ analysis

presented in this paper. We measure parameter importance as the rank-transformed partial correlation coefficient (RPCC) to take account of potential non-linearities in the relationship between parameters and model output (Saltelli et al., 2000; Zaehle et al., 2005).

3 Results

3.1 Simulated diurnal to seasonal time-scale carbon dioxide fluxes at selected FLUXNET sites

We first compare the simulated mean monthly diurnal, as well as the mean seasonal cycle of gross primary production (GPP) at four forest sites, representing the major tree plant functional types, with *in situ* observations (Fig. 3, see Fig. S4 for a comparable evaluation of the latent heat flux). The model simulations agree reasonably well with the observations in that ~~the general~~ diurnal and seasonal timing and overall magnitude of fluxes are generally consistent. Importantly, while the N and P cycles dampen the overall magnitude of the fluxes at the beech forest site (temperate broad-leaved deciduous; FR-Hes) and the eucalyptus forest site (temperate broad-leaved evergreen; AU-Tum), they do not affect the shape of either the diurnal or seasonal cycles. In other words, the effect of diurnal and seasonal ~~changes in nutrient availability only affect the long-term, but not the short-term~~ variability in soil nutrient availability is buffered through the labile and reserve storage pools in the vegetation, such that it affects vegetation gross carbon uptake ~~.~~ only via slow processes such as foliar nutrient and allocation changes, but has no effect on variability at the daily to weekly time-scale. This is also demonstrated in the LAI values, that are influenced by the long-term dynamics. For instance, at FR-Hes and AU-Tum the LAI is lower at the nitrogen and phosphorus dynamics enabled version than with the C only version (6.0 compared to 6.2 $\mathrm{m^2 m^{-2}}$ at FR-Hes, 3.7 compared to 5.9 $\mathrm{m^2 m^{-2}}$ at AU-Tum), whereas it does not have a notable effect for the needle-leaved evergreen site of (FI-Hyy).

There is little overall effect of the nutrient cycles on the correlation between half-hourly simulated and observed GPP at FI-Hyy (all versions: r^2=0.76), FR-Hes (all versions: r^2=0.63), and BR-Ma2 (all versions: r^2=0.67), and only a minor reduction for AU-Tum (r^2 0.70 versus 0.65 for C and CN(P), respectively). The largest decrease of the model's root mean square error (RMSE) took place at FR-Hes, where introducing N and P cycling reduced the RMSE by nearly 20% to 5.17 $\mu\mathrm{molm^{-2}s^{-1}}$. For FI-Hyy the RMSE and the improvement were 2.42 and 0.11 $\mu\mathrm{molm^{-2}s^{-1}}$. For AU-Tum the RMSE and worsening of RMSE were 5.44 and 0.36 $\mu\mathrm{molm^{-2}s^{-1}}$. At BR-Ma2 the RMSE and the improvement were 7.78 and 0.09 $\mu\mathrm{molm^{-2}s^{-1}}$. At the tropical evergreen forest site BR-Ma2 (Fig. 3d, f) the different versions performed similarly. The lower GPP in the daily observation-based estimate between day of year 150 and 200, which are not replicated by the model, are largely caused by lower observation-based GPP at the start of the time-series during this time of year in 2003. There was no obvious cause for this behaviour visible in the meteorological drivers. The latent heat fluxes were generally well simulated at these four sites, with the exception of large summertime overestimation (73 %) at FR-Hes (Fig. S4).

Table **??** summarises the ~~key C, N and P stocks and fluxes simulated~~ observed and simulated GPP, total ecosystem respiration (TER) and foliar C:N with the CNP version of the model for these four FLUXNET sites, calculated for the time period of the flux observations (Table A1). The annual GPP from the CO_2 flux observations is in line with the modelled values for FI-Hyy ~~(observed 1016),~~ and FR-Hes~~(observed 1874)~~, while productivity at BR-Ma2 ~~(observed: 2557)~~ is somewhat

overestimated, and strongly underestimated at AU-Tum~~(observed : .~~ The TER is somewhat overestimated for FI-Hyy and FR-Hes, and strong overestimation occurs at BR-Ma2. However, the unusually large discrepancy between observed GPP and TER fluxes at BR-Ma2 suggests that these estimates should be considered with caution. At AU-Tum ~~: 2151)~~the TER is underestimated. Simulated foliar C:N was within the observational range reported in the La Thuille database (NOA, 2007) for all four sites~~(observed: 41, 21, 35 and 20-35, for FI-Hyy, FR-Hes, AU-Tum and BR-Ma2, respectively). Nutrient~~ . Observations for nutrient availability and fluxes are not consistently available ~~for~~ across these sites.

The Taylor plots of the half-hourly simulated and observation-based time-series of GPP and NEE (Fig. 4) demonstrate that the overall model performance noted in Fig. 3 holds across a wider set of sites, spanning a larger climatic gradient and also including grassland sites. The Taylor plot reports results obtained with the CNP version of the model; the plots for the C and CN version were very similar in terms of their correlation and moderately different in terms of the ratio of standard deviations. The simulated GPP shows slightly better performance over the different sites than NEE. Considering that i) the model has not been parameterised specifically for each site and ii) eddy-covariance observations at this time-scale are subject to considerable fluctuations, the model performance is acceptable in terms of the correlation. While there is a wide spread in the ratio of the simulated to observation-based standard deviation, mostly associated with site-based differences in the seasonal maximum of the flux, there is no systematic model bias for any PFT.

The inclusion of the N cycle (difference between C and CN model versions) reduces the root mean squared error (RMSE) between simulated and observation-based estimates of GPP for all PFTs apart from the tropical broad-leaved evergreen PFT (Fig. 5). The largest reductions of the RMSE between the different versions occurs for TeBE (34.0 %) and TeH (41.6 %). There is no strong effect of including the P cycle on simulated GPP, and in consequence there is no difference in the RMSE values of the CN and CNP versions, even for the tropical broad-leaved evergreen forest sites, which are in regions typically associated with P-limitation of biomass production.

3.2 Cross-site analysis of long-term mean GPP and NPP

Simulated GPP across all the GFDB sites (n=434), covering a range of tree PFTs, agrees reasonably well with data (r^2 = 0.55, RMSE=560 $\mathrm{gCm^{-2}yr^{-1}}$) (Fig. 6a), despite an underestimation of GPP for some sites, both in tropical forest ecosystems and needle-leaved evergreen forests. The data shown are restricted to forests older than 20 years, to avoid ambiguities in the model-data comparison as the exact method of forest regeneration after disturbance is not known and the model does not describe stand-level dynamics of very early succession forests that often have very high observed productivity. The model is also able to replicate the observations from low to modest NPP values albeit with a higher relative RMSE (Fig. 6b) (r^2 = 0.35, RMSE=305 $\mathrm{gCm^{-2}yr^{-1}}$). While there is no systematic over- or underestimation of NPP with PFT or magnitude of NPP, it is noteworthy that the highest NPP value simulated for this dataset was only 1441 $\mathrm{gCm^{-2}yr^{-1}}$, whereas for a few sites, observation-based estimates reached nearly 2000 $\mathrm{gCm^{-2}yr^{-1}}$. The model correctly predicts the range of carbon-use efficiency (CUE), i.e. the ratio of net to gross primary production, where the observed CUE values ranged between 0.21 and 0.76 $\mathrm{g\,g^{-1}}$, while the simulated values were between 0.19 and 0.61 $\mathrm{g\,g^{-1}}$. The model also predicts correctly a lower CUE in tropical compared to

temperate/boreal ecosystems. However, the model is not able to explain the within PFT-variability of the observed CUE values in the dataset (Fig. 6c).

~~The discrimination of leaf~~ Underlying these results are the emergent sensitivities of ecosystem processes to the model drivers. Fig. S5 and S6 show that the large-scale gradients of simulated GPP and NPP are largely controlled by mean annual temperature (MAT), with an additional clear effect of mean annual precipitation. For temperate and boreal forests, also N deposition is positively related to GPP and NPP. While the acclimation of photosynthesis to growth temperature does matter at the diurnal time-scale particularly on cloudy days (Figure S7), the positive and negative effects cancel each other out at the long-term annual mean, and therefore plays no role in the simulated GPP-MAT relationship. Despite a notable decline of maintenance respiration in higher temperatures due to the acclimation of respiration to growth temperature (see Figure S8), the spatial trend in simulated CUE is predominantly driven by MAT (Fig. S9). Trends apparent in the CUE response to MAP and N deposition are small and likely confounded by the MAT response. However, the general tendency of PFT-specific foliar C:N to decline with increasing N deposition (Fig. S10), something that is expected to happen based on observational evidence Hyvönen et al. (2007); Meyerholt and Zaehle (2015), suggest that the linearly increasing maintenance respiration rates per unit tissue drives whole-plant maintenance respiration up stronger than the saturating effect of increased leaf N on GPP, therefore reducing CUE with increasing N availability, counter to expectations (Vicca et al., 2012). The root to shoot ratio did not show strong dependency to any of these environmental variables (data now shown), probably contributing to the lack of a decline in CUE with declining N availability. Generally, PFT-wise foliar stoichiometry appears to be more strongly influenced by N deposition than MAT or MAP. This result occurs despite a clear dependency of the simulated biological N fixation on temperature and precipitation (Fig. S12), where the simulated range and response to climate drivers is consistent with the available evidence suggesting the highest N fixation in hot and moist environments (Fig. S11 Cleveland et al., 1999, 2013). In addition, in agreement with recent evidence, enhanced atmospheric N input suppresses simulated N fixation (Zheng et al., 2019).

The comparison of leaf $\Delta^{13}C$ ~~against an index of water availability (evapotranspiration divided by the potential evapotranspiration)(ET/P~~ based on observations (Cornwell et al., 2018b) and the GFDB simulations ~~are shown in Fig.7~~(Fig. 7) provide another look into the underlying processes of GPP evaluation, as they are documenting the simulated and observed trends in water-use efficiency with water availability. Both observations and model showed less discrimination of $\Delta^{13}C$ in drier conditions, indicating an effect of seasonal water availability in overall drought stress on photosynthesis. Comparing PFT-wise mean values, constrained to estimates of ET/PET > 0.25 to remove the effect of modelled outliers under high water-limitation, the average for broadleaf deciduous forest (BS) was 20.88 ‰ for the observations and 20.67 ‰ for the modelled values. For the needle-leaved deciduous (NS) PFT the average values were very similar (observations 20.29 ‰ and simulations 20.12 ‰). Somewhat larger discrepancies occurred for the needle-leaved evergreen PFT, where the average of the observations was 20.00 ‰ and the average of the simulation results was 19.59 ‰. For the broadleaf evergreen forests there was a large deviation between the observed (22.68 ‰) and modelled values (20.55 ‰), but also the sample sizes were very different (n=1617 for observations and n=54 for simulations). For the modelled values the difference between needle-leaved deciduous and evergreen forests was more pronounced than in the observations, but the sample size of modelled NS sites was very small (n=6).

3.3 Model sensitivity ~~and uncertainty~~ analysis

The parameter sensitivity study reveals that ~~the~~ from the many parameters introduced in this model (see SI), the model output is sensitive only to a limited amount of these parameters. The role of specific parameters varies across sites (Tab. **??**) and with the output quantity of interest (Tab. S1). A number of interesting things can be noted when looking at which parameters dominate across sites (Tab. **??**). In line with reports from other studies for other models (e.g. Zaehle et al., 2005; Zaehle and Friend, 2010; Wramneby the first set of parameters is related to those affecting the photosynthetic nitrogen-use efficiency, which directly affect the C assimilation per unit leaf area. In QUINCY v1.0, this is mostly related to the magnitude of leaf N assumed to be structural N (k_0^{struc}), the scaling of leaf N to leaf chlorophyll content (k_{fn}^{chl}, a_{chl}^n), and the efficiency of Rubisco-limited carboxylation rate per unit N (v_{cmax}^n).

The second set of parameters to which the model is sensitive, unlike other carbon-only models, relates to parameters determining the rate of litter and soil organic matter turnover ($T_{opt,decomp}$, τ_{slow}^{base}), the efficiency of microbial SOM processing ($\eta_{C,litter \rightarrow fast}$, $\eta_{C,fast \rightarrow slow}$), and the C:N of the slow decomposing soil organic matter ($\chi_{SOM_{slow}^{X:Y}}$). All these parameters control the rate at which nitrogen and phosphorus are released by SOM decomposition, which in the QUINCY 1.0 model is important for the growth of leaves and associated photosynthesis. Such a dependency is to be expected by a nutrient-cycle enabled model and this is clearly documented in the dependence of simulated GPP on simulated net N and P mineralisation (Fig. S12). It is important to note that for the effect of uncertainty in the temperature optimum of decomposition, $T_{opt,decomp}$, it is not the direct effect of the optimum point that matters, since it is larger than common soil temperatures for most of the sites, but a side-effect of changing the default turnover time of litter and SOM along with the change in optimum temperature. Consistent with expectation the rate of soil turnover is more important in cold that warm environments, soil-based parameters are less important that photosynthetic parameters for the tropical site compared to the three non-tropical sites.

The third set of parameters identified as sensitive can be characterised as being related to vegetation growth and dynamics. One one hand, these are parameters dominating the carbon allocation within plants (k_{latosa}, sla), also as noted by Zaehle et al. (2005) and Massoud et al. (2019) for other models, as well as the tissue stoichiometry ($\chi_{leaf}^{X:Y}$, $\chi_{leaf}^{X:Y}$). Important, also the scaling exponent k_{rp}, relating diameter to crown-area, and thereby determining the space-constraint for the establishment and mortality of tree PFTs plays some role in some of the sites due to its effect on LAI and total vegetation biomass. At the tropical BR-Ma2 site, despite temperature acclimation, the basal maintenance respiration rate for leaves and fine roots $f_{resp,maint}^{non-woody}$ is also a sensitive parameter, as is the scaling parameter for limiting nutrient uptake under high nutrient availability ($K_{demand}^{half,X}$).

The parameter sensitivities investigated here propagate to uncertainty in the model output. The inner-quartile range of the model output (Fig. 8) is well constrained and centred around the results of the standard parameterisation reported in Tab. **??**. Extreme parameter combinations cause larger variations, but do not fundamentally change the model behaviour. Including wider parameter ranges for some more uncertain parameters will likely affect the absolute mean and uncertainty range of particular model output. Therefore, the results shown in Fig. 8 should not be interpreted as an estimate of parameter-based model uncertainty. However, the results do suggest that despite introducing a complex ecosystem model with many non-linear equations and parameters, the model does not reveal fundamental model instabilities.

By varying parameters, we essentially generate an ensemble of simulations with identical climate and atmospheric nutrient input, but different soil nutrient ~~retention capacities and turnover rates, as well as~~ cycle rates, and vegetation nutrient-use efficiencies~~, thus a gradient of sites with identical climate, but different N and P availabilities. The~~. At the example of the broad-leaved deciduous forest site FR-Hes, the model shows, as expected, clear dependencies between the rates of net N and P mineralisation ~~, GPP, and~~ and GPP, which also propagate to the simulated carbon stock in vegetation ~~and soil.The correlation between~~ (Fig. S12) underlying the uncertainty ranges reported in Fig. 8. For this example, there is also a clearly negative correlation between the net N mineralisation and foliar C:N~~:P and biogeochemical fluxes is less clear, owing to the additional effects of productivity changes on foliar area and carbon partitioning belowground.~~

~~The role of specific parameters varies with the output quantity of interest and across sites, depending on the level of nutrient limitation at the sites. Table Tab. **??** lists the ten most important parameters for each site, clearly demonstrating that next to parameters affecting leaf mass and photosynthetic efficiency directly (e.g. k_0^{struc}, sla, a_{chl}^n, k_{latosa}), the assumed overall turnover time of the soil, affected through the optimum temperature of decomposition, $T_{opt,decomp}$, as well as the efficiencies of microbial SOM processing ($\eta_{C,litter \rightarrow fast}$, $\eta_{C,fast \rightarrow slow}$) play an important role due to the strong coupling of vegetation productivity to soil nutrient availability in the QUINCY v1.0 model~~which gives rise to a negative co-variation of GPP and leaf C:N. Interestingly, such a correlation does not exist for foliar N:P, probably owing to a lack of effect of foliar P concentrations on photosynthesis.

4 Discussion

~~Models of~~ Land surface models with coupled carbon-nitrogen and phosphorus cycles ~~for land surface models~~ have been published before (Goll et al., 2017; Wang et al., 2010; Yang et al., 2014). The QUINCY v1.0 model introduced in this paper distinguishes itself from these models in (i) that it seamlessly integrates nutrient dynamics with carbon, water and energy calculations (e.g. there is no difference in time-stepping between biogeophysical and biogeochemical processes) and (ii) that there is an explicit ~~consideration of the decoupling of photosynthesis and growth~~ decoupling of the growth processes from C-supply due to photosynthesis by accounting for temperature, moisture and nutrient constraints in the formation of new tissue, as opposed to the simpler treatment of these dynamics in Zaehle and Friend (2010), ~~as~~ and applied in Goll et al. (2017). The purpose of this paper is to provide a background for future studies on the effect of coupled biogeochemical cycles at large scales as well as on testing the effect alternative representations of important nutrient cycle related processes, for which the model is suitable due to its modular design. A detailed evaluation of all new submodules of the model is beyond the scope of this paper.

Overall, QUINCY v1.0 performs well in terms of diurnal, seasonal and annual carbon fluxes across a range of ecosystem monitoring flux sites, spanning a large geographic gradient and a variety of ecosystem types. Despite the lack of any site-specific parameterisation, there is no systematic model bias for any single PFT ~~at either time-scale~~for either the FLUXNET (Figs. 3 and 4) or the GFDB (Fig. 6) analyses. Including a coupling of the carbon cycle to representations of the nitrogen and phosphorus cycle affects long-term average productivity through its effects on photosynthetic capacity (changed foliar nitrogen concentration) and leaf area (as a result of the changes in root:shoot allocation)~~, but diurnal and seasonal variations in~~

. However, short-term diurnal or sub-seasonal shortage of soil nitrogen or phosphorus ~~availability do not~~ does not directly and instantaneously affect simulated productivity because of the buffering introduced through the labile and reserve storage.

Model predictions generally show an improvement in the prediction of GPP with the addition of the N cycle. This occurs despite a slight low bias in simulated foliar nitrogen concentration compared to the mean values of the TRY database ~~(BS: 2.1 (0.6-3.2) % versus 1.7 ± 0.3, TrBE/TeBE: 1.7 (0.5-3.9) % versus 1.7 ±, NE: 1.3 (0.5-1.9) % versus 1.0 ± 0.4, NS: 1.9 (0.9-3.0)~~ This comparison is indicative only, since there is a geographic mismatch between the spatial coverage and distribution of the modelled sites and the data in the TRY database. Note that these estimates are not fully independent because the minimum and maximum range of permissable foliar N were derived from (Kattge et al., 2011).

The P enabled version does not show additional improvement in simulating the regional differences in productivity. This is partly due to the fact that the sites with sufficient information on GPP and NPP available for model evaluation are as a majority located in temperate and boreal regions, where the main limiting nutrient is likely to be nitrogen (LeBauer and Treseder, 2008). However, even for the few tropical sites included in the analysis, where in general terms limitation of productivity by P would be expected (LeBauer and Treseder, 2008; Vitousek et al., 2010), we do not find any significant effect of the simulated P cycle. An important contributor is the fact that in QUINCY v1.0, the vertically explicit description of SOM dynamics permits very efficient recycling of organic P in the litter layer, where low mineral sorption capacities lead to efficient P uptake of soil microorganisms and vegetation. The efficient recycling in the litter layer is partially due to the biochemical mineralisation flux. Further observations are required in order to constrain this flux better (Reed et al., 2011). One further important factor is the unknown initial soil concentration of plant available P, as well as uncertainties in the rate of P weathering. Improving the understanding of P availability across the globe remains an important challenge for the representation of P effects on productivity (Wang et al., 2010; Goll et al., 2017), requiring detailed observations of soil and vegetation P dynamics and manipulation experiments (e.g. Medlyn et al., 2016). In addition, similar to other models (Goll et al., 2017; Yang et al., 2014), QUINCY v1.0 currently assumes that P limitation solely effects productivity due to a stoichiometric constraint on growth, while other mechanisms may also play an important role in the acclimation of plant processes to different levels of P availability (Jiang et al., 2019).

The predicted GPP and NPP across a large range of climatic and biogeographic situations is in good agreement with observations, and so is the average of the carbon-use efficiency (CUE = NPP/GPP). However, the model does not reproduce the observed range in CUE in temperate and boreal forests, and the analysis of the main drivers of CUE shows that in the current model version, CUE is mostly a function of mean annual temperature. Vicca et al. (2012) suggested that this variance is associated with altered carbon partitioning, and in particular increased belowground carbon allocation in response to nutrient shortage. The QUINCY v1.0 model simulates an increase of the root:shoot ratio with response to nutrient stress. However, the effect of this change on CUE is small, as increased root allocation not only decreases biomass production through increased allocation to higher turnover tissues, but also whole-plant mass-specific respiration, given the implicit model assumption that mass-specific fine root respiration is smaller than leaf-mass specific respiration. This inference is consistent with detailed observations at the FLUXNET site FI-Hyy (Ilvesniemi et al., 2009; Korhonen et al., 2013), where the QUINCY v1.0 model successfully simulated GPP, and vegetation C storage (~~observed 6.80~~ simulated/observed 7.0/6.8 $\mathrm{kgCm^{-2}}$, (Ilvesniemi et al.,

2009)), but substantially overestimated the NPP (~~observed:~~ simulated/observed: 536/242 $\mathrm{gCm^{-2}yr^{-1}}$). Additionally, the N uptake by the vegetation in addition to the N losses were in the same order of magnitude as the observations (Korhonen et al., 2013), suggesting that C partitioning rather than N availability is the source of the underestimation. ~~The QUINCY v1.0 model simulates an increase of the root:shoot ratio with response to nutrient stress. However, the effect of this change on CUE is small, as increased root allocation not only decreases biomass production through increased allocation to higher turnover tissue, but also whole-plant mass-specific respiration, given the implicit model assumption that mass-specific fine root respiration is smaller than leaf-mass specific respiration.~~ Further causes of this model-data mismatch include alternative pathways of carbon partitioning not represented in the model (e.g. exudation), changes in tissue turnover times with changes in nutrient availability, and the magnitude of mass-specific autotrophic respiration. For instance, the estimated autotrophic respiration in FI-Hyy was 714 $\mathrm{gCm^{-2}yr^{-1}}$ (Ilvesniemi et al., 2009), compared to ~~486~~ 494 in the model $\mathrm{gCm^{-2}yr^{-1}}$, which may be the combined result of allocation, temperature response and specific respiration rates, particularly below ground. The novel structure of the QUINCY v1.0 model that decouples photosynthesis from growth, and therefore permits to adjust carbon partitioning to different sinks at short timescales will allow to investigate the effect of these processes in the future. Finally, the intra-PFT variation of observed CUE likely depends on other site-specific factors that affect site fertility, which are currently not adequately represented in the model, such as the effects of soil pH, site history, and species-level variability.

The comparison of simulated leaf $^{13}\mathrm{C}$ discrimination to observations recorded in the global dataset by (Cornwell et al., 2018b) suggests that the overall parameterisation of long-term mean leaf- and ecosystem-level water-use efficiency, derived from instantaneous leaf-level gas exchange measurements (Lin et al., 2015), broadly conforms with observations. Notably, the model also simulates the trend in discrimination with respect to changing water availability in accordance with observations, which suggests that the overall effect of moisture availability on water-use efficiency is appropriately considered by the model. Discrepancies between the observation-based estimates of water-use efficiency derived from leaf-level flux and isotope measurements have been noted before (Medlyn et al., 2017), and these may contribute to the remaining model-data mismatch. One possible reason for this mismatch may be the omission of mesophyll conductance in model formulations, which may induce systematic shifts in chloroplast [$\mathrm{CO_2}$], and thereby affect the simulated value of leaf $\Delta^{13}\mathrm{C}$ without affecting leaf-level water-use efficiency (Knauer et al., in press).

5 Summary and future directions

In this paper, we presented the mathematical formulation of a new terrestrial biosphere model, QUINCY v1.0, that includes a number of ecophysiological processes (short-term and long-term storage pools, acclimation processes) that have not been represented in earlier TBMs. We evaluated QUINCY v1.0 against a range of observations from worldwide datasets and demonstrated that it is successful in simulating photosynthesis and plant dynamics across large geographical ranges and different ecosystem types with different levels of chronic nutrient input and water availability. We further demonstrated that despite increased complexity and therefore increased numbers of weakly constrained parameters, the model produces predictions of the coupled biogeochemical cycles at site level within reasonable and well-defined bounds. Whether or not the same parameter

and therefore process ranking applies also to perturbation situations, e.g. from the manipulation of C, N or P availability still remains to be evaluated. The model evaluation provided in this paper points to shortcomings of the baseline QUINCY model in terms of the responses of carbon partitioning to nutrient availability, and the interactions between plants and soil processes.

The next logical step in the model's evaluation is to subject it to a range of manipulative experimental settings that will test the realism of the coupling of the carbon-nitrogen-phosphorus cycle in different climate regimes (Zaehle et al., 2014; Yang et al., 2014; Medlyn et al., 2015). Such model evaluation can help point to the adequate representation of individual processes rather than just overall model performance. The inclusion of isotope tracers will increase the scope of such comparisons, since this will allow to better track carbon and nitrogen flows.

One of the motivations behind the development of the QUINCY v1.0 model was the recognition that there may be more than one adequate model representation for one process (Beven, 2008). Therefore the model has been constructed with a modular design, allowing to replace some of its components by alternative representations to test their effect on model predictions. Examples of future work with QUINCY v1.0 include the control of plants to shape carbon, nitrogen and phosphorus partitioning and thereby plant functioning in response to environmental change, and plant-soil processes by including better representations of the interactions between root growth/activity and SOM turnover and stabilisation.

These basic benchmarks provide a baseline test to integrate QUINCY v1.0 into the JSBACH land surface model (Mauritsen et al., 2019) to allow for a spatially explicit simulation, and integration of a range of important processes such as fire disturbance, land-use and permafrost dynamics. This integration will also allow more comprehensive and rigorous benchmarking against a wider variety of data products. In the mid-term, this will allow coupling to the Max Planck Institute's Earth System Model (MPI-ESM) framework ICON to address feedbacks between land biogeochemistry and climate on the basis of an improved representation of biological processes affecting land biogeochemical and biogeophysical processes.

Code availability. The scientific part of the code is available under a GPL v3 licence. The scientific code of QUINCY relies on on software infrastructure from the MPI-ESM environment, which is subject to the MPI-M-Software-License-Agreement in its most recent form (http://www.mpimet.mpg.de/en/science/models/license). The source code is available online (https://git.bgc-jena.mpg.de/quincy/quincy-model-releases) [TECHNICAL NOTE: WILL BE UPON ACCEPTANCE AND PRIOR TO PUBLICATION], but its access is restricted to registered users. Readers interested in running the model should request a username and password from the corresponding authors or via the git-repository. Model users are strongly encouraged to follow the fair-use policy stated on https://www.bgc-jena.mpg.de/bgi/index.php/Projects/QUINCYMode

Appendix A: FLUXNET sites

Table A1. FLUXNET sites

Site	Long	Lat	PFT	Start	End	Reference
AT-Neu	11.32	47.12	TeH	2002	2005	Wohlfahrt et al. (2008b)
AU-How	131.15	-12.49	TeBE	2002	2005	Beringer et al. (2011)
AU-Tum	148.15	-35.66	TeBE	2002	2005	Cleugh et al. (2007)
BE-Bra	4.52	51.31	TeNE	2000	2002	Carrara et al. (2004)
BR-Ma2	-60.21	-2.61	TrBE	2003	2005	Araújo et al. (2002)
CA-Man	-98.48	55.88	BNE	1999	2003	Dunn et al. (2007)
CA-Qfo	-74.34	49.69	BNE	2004	2006	Bergeron et al. (2007)
CA-SF1	-105.82	54.49	BNE	2004	2005	Mkhabela et al. (2009)
CH-Oe1	7.73	47.29	TeH	2002	2006	Ammann et al. (2007)
DE-Bay	11.87	50.14	TeNE	1997	1998	Rebmann et al. (2004)
DE-Hai	10.45	51.08	TeBS	2000	2006	Kutsch et al. (2008)
DE-Meh	10.66	51.28	TeH	2004	2006	Scherer-Lorenzen et al. (2007)
DE-Tha	13.57	50.96	TeNE	1998	2003	Grünwald and Bernhofer (2007)
DK-Sor	11.65	55.49	TeBS	1997	2006	Lagergren et al. (2008)
ES-ES1	-0.32	39.35	TeNE	1999	2004	Sanz et al. (2004)
ES-LMa	-5.77	39.94	TrH	2004	2006	Vargas et al. (2013)
FI-Hyy	24.29	61.85	BNE	2001	2006	Suni et al. (2003)
FR-Hes	7.06	48.67	TeBS	2001	2006	Granier et al. (2000)
FR-LBr	-0.77	44.72	TeNE	2003	2006	Berbigier et al. (2001)
FR-Pue	3.60	43.74	TeBE	2001	2006	Keenan et al. (2010)
IL-Yat	34.90	31.35	TeNE	2001	2002	Grünzweig et al. (2003)
IT-Cpz	12.38	41.71	TeBE	2001	2006	Tirone et al. (2003)
IT-MBo	11.05	46.02	TeH	2003	2006	Wohlfahrt et al. (2008a)
IT-Ro2	11.92	42.39	TeBS	2002	2006	Tedeschi et al. (2006)
IT-SRo	10.28	43.73	TeNE	2003	2006	Chiesi et al. (2005)
NL-Loo	5.74	52.17	TeNE	1997	2006	Dolman et al. (2002)

Table A1. FLUXNET sites (continued)

Site	Long	Lat	PFT	Start	End	Reference
SE-Fla	19.46	64.11	BNE	2000	2002	Lindroth et al. (2008)
SE-Nor	17.48	60.09	BNE	1996	1997	Lagergren et al. (2008)
US-Blo	-120.63	38.90	TeNE	2000	2006	Goldstein et al. (2000)
US-Ha1	-72.17	42.54	TeBS	1995	1999	Urbanski et al. (2007)
US-Ho1	-68.74	45.20	TeNE	1996	2004	Hollinger et al. (1999)
US-MMS	-86.41	39.32	TeBS	2000	2005	Schmid et al. (2000)
US-MOz	-92.20	38.74	TeBS	2005	2006	Gu et al. (2006)
US-SRM	-110.87	31.82	TeBE	2004	2006	Scott et al. (2009)
US-Syv	-89.35	46.242	TeNE	2002	2004	Desai et al. (2005)
US-Ton	-120.97	38.43	TeBE	2002	2006	Ma et al. (2007)
US-Var	-120.95	38.41	TrH	2001	2006	Ma et al. (2007)
US-WCr	-90.08	45.81	TeBS	2000	2005	Cook et al. (2004)
VU-Coc	167.19	-15.44	TrBE	2002	2003	Roupsard et al. (2006)
ZA-Kru	31.50	-25.02	TrBR	2001	2003	Archibald et al. (2010)

Author contributions. SZ conceived the model. TT, SC, LY, MK, and SZ developed the model. JE and RS helped with model implementation and testing. All authors contributed to the interpretation of the results and writing of the manuscript.

Competing interests. The authors declare that there are no competing interests

Acknowledgements. This work was supported by the European Research Council (ERC) under the European Union's Horizon 2020 research and innovation programme (QUINCY; grant no. 647204). LY was supported by the framework of Priority Program SPP 1685 "Ecosystem Nutrition: Forest Strategies for Limited Phosphorus Resources" of the German Research Foundation (DFG), grant No.ZA 763/2-1. We are grateful to Steffen Richter for technical assistance in developing the code, as well as to Sara Vicca for providing access to the GFDB data base. This work used eddy covariance data acquired by the FLUXNET community and in particular by the following networks: AmeriFlux (US Department of Energy, Biological and Environmental Research, Terrestrial Carbon Program (DE-FG02-04ER63917 and DE-FG02-04ER63911)), AfriFlux, AsiaFlux, CarboAfrica, CarboEuropeIP, CarboItaly, CarboMont, ChinaFlux, FluxnetCanada (supported by CFCAS, NSERC, BIOCAP, Environment Canada, and NRCan), GreenGrass, KoFlux, LBA, NECC, OzFlux, TCOS-Siberia, and USCCC. We acknowledge the financial support to the eddy covariance data harmonization provided by CarboEuropeIP, FAO-GTOS-TCO, iLEAPS, the Max Planck Institute for Biogeochemistry, the National Science Foundation, the University of Tuscia, Université Laval and Environment Canada, and the US Department of Energy and the database development and technical support from Berkeley Water Center, Lawrence Berkeley National Laboratory, Microsoft Research eScience, Oak Ridge National Laboratory, the University of California-Berkeley, and the University of Virginia.

References

Ahrens, B., Braakhekke, M. C., Guggenberger, G., Schrumpf, M., and Reichstein, M.: Contribution of sorption, DOC transport and microbial interactions to the 14C age of a soil organic carbon profile: Insights from a calibrated process model, Soil Biology and Biochemistry, 88, 390–402, 2015.

Ammann, C., Flechard, C., Leifeld, J., Neftel, A., and Fuhrer, J.: The carbon budget of newly established temperate grassland depends on management intensity, Agriculture, Ecosystems & Environment, 121, 5 – 20, https://doi.org/https://doi.org/10.1016/j.agee.2006.12.002, http://www.sciencedirect.com/science/article/pii/S0167880906004300, the Greenhouse Gas Balance of Grasslands in Europe, 2007.

Araújo, A. C., Nobre, A. D., Kruijt, B., Elbers, J. A., Dallarosa, R., Stefani, P., von Randow, C., Manzi, A. O., Culf, A. D., Gash, J. H. C., Valentini, R., and Kabat, P.: Comparative measurements of carbon dioxide fluxes from two nearby towers in a central Amazonian rainforest: The Manaus LBA site, Journal of Geophysical Research: Atmospheres, 107, LBA 58–1–LBA 58–20, https://doi.org/10.1029/2001JD000676, https://agupubs.onlinelibrary.wiley.com/doi/abs/10.1029/2001JD000676, 2002.

Archibald, S., Nickless, A., Govender, N., Scholes, R. J., and Lehsten, V.: Climate and the inter-annual variability of fire in southern Africa: a meta-analysis using long-term field data and satellite-derived burnt area data, Global Ecology and Biogeography, 19, 794–809, https://doi.org/10.1111/j.1466-8238.2010.00568.x, https://onlinelibrary.wiley.com/doi/abs/10.1111/j.1466-8238.2010.00568.x, 2010.

Arneth, A., Harrison, S. P., Zaehle, S., Tsigaridis, K., Menon, S., Bartlein, P. J., Feichter, J., Korhola, A., Kulmala, M., O'Donnell, D., Schurgers, G., Sorvari, S., and Vesala, T.: Terrestrial biogeochemical feedbacks in the climate system, Nat. Geosci., 3, 525, 2010.

Atkin, O. K., Meir, P., and Turnbull, M. H.: Improving representation of leaf respiration in large-scale predictive climate–vegetation models, New Phytologist, 202, 743–748, https://doi.org/10.1111/nph.12686, https://nph.onlinelibrary.wiley.com/doi/abs/10.1111/nph.12686, 2014.

Ball, J., Wooddrow, I., and Berry, J. A.: A model predicting stomatal conductance and its contribution to the control of photosynthesis under different environmental conditions, in: Progress in Photosynthesis Research, edited by Biggens, J., pp. 1–4, Dordrecht, The Netherlands, 1987.

Berbigier, P., Bonnefond, J.-M., and Mellmann, P.: CO2 and water vapour fluxes for 2 years above Euroflux forest site, Agricultural and Forest Meteorology, 108, 183 – 197, https://doi.org/https://doi.org/10.1016/S0168-1923(01)00240-4, http://www.sciencedirect.com/science/article/pii/S0168192301002404, 2001.

Bergeron, O., Margolis, H. A., Black, T. A., Coursolle, C., Dunn, A. L., Barr, A. G., and Wofsy, S. C.: Comparison of carbon dioxide fluxes over three boreal black spruce forests in Canada, Global Change Biology, 13, 89–107, https://doi.org/10.1111/j.1365-2486.2006.01281.x, https://onlinelibrary.wiley.com/doi/abs/10.1111/j.1365-2486.2006.01281.x, 2007.

Beringer, J., Hutley, L. B., Hacker, J. M., Neininger, B., and U, K. T. P.: Patterns and processes of carbon, water and energy cycles across northern Australian landscapes: From point to region, Agricultural and Forest Meteorology, 151, 1409 – 1416, https://doi.org/https://doi.org/10.1016/j.agrformet.2011.05.003, http://www.sciencedirect.com/science/article/pii/S016819231100147X, savanna Patterns of Energy and Carbon Integrated Across the Landscape (SPECIAL), 2011.

Bernacchi, C. J., Singsaas, E. L., Pimentel, C., Protis JR, A. R., and Long, S. P.: Improved temperature response functions for models of Rubisco-limited photosynthesis, Plant, Cell & Environment, 24, 253–259, 2001.

Beven, K.: On doing better hydrological science, Hydrological Processes, 22, 3549–3553, 2008.

Bonan, G. B.: Forests and Climate Change: Forcings, Feedbacks, and the Climate Benefits of Forests, Science, 320, 1444–1449, https://doi.org/10.1126/science.1155121, http://science.sciencemag.org/content/320/5882/1444, 2008.

Bonan, G. B. and Doney, S. C.: Climate, ecosystems, and planetary futures: The challenge to predict life in Earth system models, Science, 359, https://doi.org/10.1126/science.aam8328, http://science.sciencemag.org/content/359/6375/eaam8328, 2018.

Bradford, M. A., Wieder, W. R., Bonan, G. B., Fierer, N., Raymond, P. A., and Crowther, T. W.: Managing uncertainty in soil carbon feedbacks to climate change, Nature Climate Change, 6, https://doi.org/10.1038/nclimate3071, http://dx.doi.org/10.1038/nclimate3071, 2016.

Brahney, J., Mahowald, N., Ward, D. S., Ballantyne, A. P., and Neff, J. C.: Is atmospheric phosphorus pollution altering global alpine Lake stoichiometry?, Global Biogeochemical Cycles, 29, 1369–1383, https://doi.org/10.1002/2015GB005137, https://agupubs.onlinelibrary.wiley.com/doi/abs/10.1002/2015GB005137, 2015.

Campioli, M., Vicca, S., Luyssaert, S., and Bilcke, J.: Biomass production efficiency controlled by management in temperate and boreal ecosystems, Nature Geoscience, 8, 843–846, 2015.

Carrara, A., Janssens, I. A., Yuste, J. C., and Ceulemans, R.: Seasonal changes in photosynthesis, respiration and NEE of a mixed temperate forest, Agricultural and Forest Meteorology, 126, 15 – 31, https://doi.org/https://doi.org/10.1016/j.agrformet.2004.05.002, http://www.sciencedirect.com/science/article/pii/S0168192304001145, 2004.

Chien, C.-T., Mackey, K. R. M., Dutkiewicz, S., Mahowald, N. M., Prospero, J. M., and Paytan, A.: Effects of African dust deposition on phytoplankton in the western tropical Atlantic Ocean off Barbados, Global Biogeochemical Cycles, 30, 716–734, https://doi.org/10.1002/2015GB005334, https://agupubs.onlinelibrary.wiley.com/doi/abs/10.1002/2015GB005334, 2016.

Chiesi, M., Maselli, F., Bindi, M., Fibbi, L., Cherubini, P., Arlotta, E., Tirone, G., Matteucci, G., and Seufert, G.: Modelling carbon budget of Mediterranean forests using ground and remote sensing measurements, Agricultural and Forest Meteorology, 135, 22 – 34, https://doi.org/https://doi.org/10.1016/j.agrformet.2005.09.011, http://www.sciencedirect.com/science/article/pii/S0168192305002108, 2005.

Clark, D. B., Mercado, L. M., Sitch, S. A., Jones, C. D., Gedney, N., Best, M. J., Pryor, M., Rooney, G. G., Essery, R. L. H., Blyth, E., Boucher, O., Harding, R. J., Huntingford, C., and Cox, P. M.: The Joint UK Land Environment Simulator (JULES), model description – Part 2: Carbon fluxes and vegetation dynamics, Geoscientific Model Development, 4, 701–722, 2011.

Cleugh, H. A., Leuning, R., Mu, Q., and Running, S. W.: Regional evaporation estimates from flux tower and MODIS satellite data, Remote Sensing of Environment, 106, 285 – 304, https://doi.org/https://doi.org/10.1016/j.rse.2006.07.007, http://www.sciencedirect.com/science/article/pii/S0034425706002677, 2007.

Cleveland, C. C., Townsend, A. R., Schimel, D. S., Fisher, H., Howarth, R. W., Hedin, L. O., Perakis, S. S., Latty, E. F., Von Fischer, J. C., Elseroad, A., and Wasson, M. F.: Global patterns of terrestrial biological nitrogen (N-2) fixation in natural ecosystems, Global Biogeochemical Cycles, 13, 623–645, 1999.

Cleveland, C. C., Houlton, B. Z., Smith, W. K., Marklein, A. R., Reed, S. C., Parton, W. J., Del Grosso, S. J., and Running, S.: Patterns of new versus recycled primary production in the terrestrial biosphere, Proceedings of the National Academy of Sciences, pp. 1–16, 2013.

Cook, B. D., Davis, K. J., Wang, W., Desai, A., Berger, B. W., Teclaw, R. M., Martin, J. G., Bolstad, P. V., Bakwin, P. S., Yi, C., and Heilman, W.: Carbon exchange and venting anomalies in an upland deciduous forest in northern Wisconsin, USA, Agricultural and Forest Meteorology, 126, 271 – 295, https://doi.org/https://doi.org/10.1016/j.agrformet.2004.06.008, http://www.sciencedirect.com/science/article/pii/S0168192304001601, 2004.

Cornwell, W., Wright, I., Turner, J., Maire, V., Barbour, M., Cernusak, L., Dawson, T., Ellsworth, D., Farquhar, G., Griffiths, H., Keitel, C., Knohl, A., Reich, P., Williams, D., Bhaskar, R., Cornelissen, J., Richards, A., Schmidt, S., Valladares, F., C, K., Schulze, E.-D., Buchmann, N., and Santiago, L.: Leaf Δ^{13}C database, https://github.com/wcornwell/leaf13C/tree/v0.1.0, 2018a.

Cornwell, W. K., Wright, I. J., Turner, J., Maire, V., Barbour, M. M., Cernusak, L. A., Dawson, T., Ellsworth, D., Farquhar, G. D., Griffiths, H., Keitel, C., Knohl, A., Reich, P. B., Williams, D. G., Bhaskar, R., Cornelissen, J. H. C., Richards, A., Schmidt, S., Valladares, F., Körner, C., Schulze, E.-D., Buchmann, N., and Santiago, L. S.: Climate and soils together regulate photosynthetic carbon isotope discrimination within C3 plants worldwide, Global Ecology and Biogeography, 27, 1056–1067, 2018b.

De Kauwe, M. G., Medlyn, B. E., Zaehle, S., Walker, A. P., Dietze, M. C., Hickler, T., Jain, A. K., Luo, Y., Parton, W. J., Prentice, I. C., Smith, B., Thornton, P. E., Wang, S., Wang, Y.-P., Wårlind, D., Weng, E., Crous, Kristine, Y., Ellsworth, D. S., Hanson, P. J., Seok, K. H., Warren, J. M., Oren, R., and Norby, R. J.: Forest water use and water use efficiency at elevated CO2: a model-data intercomparison at two contrasting temperate forest FACE sites, Global Change Biology, 19, 1759–1779, https://doi.org/10.1111/gcb.12164, https://onlinelibrary.wiley.com/doi/abs/10.1111/gcb.12164, 2013.

De Kauwe, M. G., Medlyn, B. E., Zaehle, S., Walker, A. P., Dietze, M. C., Wang, Y.-P., Luo, Y., Jain, A. K., El-Masri, B., Hickler, T., Wårlind, D., Weng, E., Parton, W. J., Thornton, P. E., Wang, S., Prentice, I. C., Asao, S., Smith, B., McCarthy, H. R., Iversen, C. M., Hanson, P. J., Warren, J. M., Oren, R., and Norby, R. J.: Where does the carbon go? A model–data intercomparison of vegetation carbon allocation and turnover processes at two temperate forest free-air CO2 enrichment sites, New Phytologist, 203, 883–899, https://doi.org/10.1111/nph.12847, https://nph.onlinelibrary.wiley.com/doi/abs/10.1111/nph.12847, 2014.

Desai, A. R., Bolstad, P. V., Cook, B. D., Davis, K. J., and Carey, E. V.: Comparing net ecosystem exchange of carbon dioxide between an old-growth and mature forest in the upper Midwest, USA, Agricultural and Forest Meteorology, 128, 33 – 55, https://doi.org/https://doi.org/10.1016/j.agrformet.2004.09.005, http://www.sciencedirect.com/science/article/pii/S0168192304002369, 2005.

Dickinson, R. E., Oleson, K. W., Bonan, G., Hoffman, F., Thornton, P., Vertenstein, M., Yang, Z.-L., and Zeng, X.: The Community Land Model and Its Climate Statistics as a Component of the Community Climate System Model, Journal of Climate, 19, 2302–2324, https://doi.org/10.1175/JCLI3742.1, https://doi.org/10.1175/JCLI3742.1, 2006.

Dolman, A., Moors, E., and Elbers, J.: The carbon uptake of a mid latitude pine forest growing on sandy soil, Agricultural and Forest Meteorology, 111, 157 – 170, https://doi.org/https://doi.org/10.1016/S0168-1923(02)00024-2, http://www.sciencedirect.com/science/article/pii/S0168192302000242, 2002.

Dunn, A. L., Barford, C. C., Wofsy, S. C., Goulden, M. L., and Daube, B. C.: A long-term record of carbon exchange in a boreal black spruce forest: means, responses to interannual variability, and decadal trends, Global Change Biology, 13, 577–590, https://doi.org/10.1111/j.1365-2486.2006.01221.x, https://onlinelibrary.wiley.com/doi/abs/10.1111/j.1365-2486.2006.01221.x, 2007.

Egea, G., Verhoef, A., and Vidale, P. L.: Towards an improved and more flexible representation of water stress in coupled photosynthesisâ€“stomatal conductance models, Agricultural and Forest Meteorology, 151, 1370–1384, 2011.

Fatichi, S., Leuzinger, S., and Körner, C.: Moving beyond photosynthesis: from carbon source to sink-driven vegetation modeling, New Phytologist, 201, 1086–1095, 2013.

Fisher, R., McDowell, N., Purves, D., Moorcroft, P., Sitch, S. A., Cox, P. M., Huntingford, C., Meir, P., and Ian Woodward, F.: Assessing uncertainties in a second-generation dynamic vegetation model caused by ecological scale limitations, New Phytologist, 187, 666–681, 2010.

Friedlingstein, P., Meinshausen, M., Arora, V. K., Jones, C. D., Anav, A., Liddicoat, S. K., and Knutti, R.: Uncertainties in CMIP5 Climate Projections due to Carbon Cycle Feedbacks, Journal of Climate, 27, 511–526, https://doi.org/10.1175/JCLI-D-12-00579.1, https://doi.org/10.1175/JCLI-D-12-00579.1, 2014.

Friend, A. D.: Terrestrial plant production and climate change, Journal of Experimental Botany, 61, 1293–1309, 2010.

Friend, A. D., Stevens, A. K., Knox, R. G., and Cannell, M. G. R.: A process-based, terrestrial biosphere model of ecosystem dynamics (Hybrid v3.0), Ecological modelling, 95, 249–287, 1997.

Friend, A. D., Geider, R. J., Behrenfeld, M. J., and Still, C. J.: Photosynthesis in Global-Scale Models, in: Photosynthesis in silico: Understanding complexity from molecules to ecosystems, edited by Laisk, A., Nedbal, L., and Govindjee, pp. 465–497, Springer, 2009.

Gerber, S., Hedin, L. O., Oppenheimer, M., Pacala, S. W., and Shevliakova, E.: Nitrogen cycling and feedbacks in a global dynamic land model, Global Biogeochemical Cycles, 24, GB1001 doi:10.1029–2008GB003 336, 2010.

Goldstein, A., Hultman, N., Fracheboud, J., Bauer, M., Panek, J., Xu, M., Qi, Y., Guenther, A., and Baugh, W.: Effects of climate variability on the carbon dioxide, water, and sensible heat fluxes above a ponderosa pine plantation in the Sierra Nevada (CA), Agricultural and Forest Meteorology, 101, 113 – 129, https://doi.org/https://doi.org/10.1016/S0168-1923(99)00168-9, http://www.sciencedirect.com/science/article/pii/S0168192399001689, 2000.

Goll, D. S., Vuichard, N., Maignan, F., Jornet-Puig, A., Sardans, J., Violette, A., Peng, S., Sun, Y., Kvakic, M., Guimberteau, M., Guenet, B., Zaehle, S., Penuelas, J., Janssens, I., and Ciais, P.: A representation of the phosphorus cycle for ORCHIDEE (revision 4520), Geoscientific Model Development, 10, 3745–3770, https://doi.org/10.5194/gmd-10-3745-2017, https://www.geosci-model-dev.net/10/3745/2017/, 2017.

Granier, A., Ceschia, E., Damesin, C., Dufrêne, E., Epron, D., Gross, P., Lebaube, S., Le Dantec, V., Le Goff, N., Lemoine, D., Lucot, E., Ottorini, J. M., Pontailler, J. Y., and Saugier, B.: The carbon balance of a young Beech forest, Functional Ecology, 14, 312–325, https://doi.org/10.1046/j.1365-2435.2000.00434.x, https://besjournals.onlinelibrary.wiley.com/doi/abs/10.1046/j.1365-2435.2000.00434.x, 2000.

Graven, H., Allison, C. E., Etheridge, D. M., Hammer, S., Keeling, R. F., Levin, I., Meijer, H. A. J., Rubino, M., Tans, P. P., Trudinger, C. M., Vaughn, B. H., and White, J. W. C.: Compiled records of carbon isotopes in atmospheric CO_2 for historical simulations in CMIP6, Geoscientific Model Development, 10, 4405–4417, https://doi.org/10.5194/gmd-10-4405-2017, https://www.geosci-model-dev.net/10/4405/2017/, 2017.

Gruber, N. and Galloway, J. N.: An Earth-system perspective of the global nitrogen cycle, Nature, 451, 293–296, 2008.

Grünwald, T. and Bernhofer, C.: A decade of carbon, water and energy flux measurements of an old spruce forest at the Anchor Station Tharandt, Tellus B, 59, 387–396, https://doi.org/10.1111/j.1600-0889.2007.00259.x, https://onlinelibrary.wiley.com/doi/abs/10.1111/j.1600-0889.2007.00259.x, 2007.

Grünzweig, J. M., Lin, T., Rotenberg, E., Schwartz, A., and Yakir, D.: Carbon sequestration in arid-land forest, Global Change Biology, 9, 791–799, https://doi.org/10.1046/j.1365-2486.2003.00612.x, https://onlinelibrary.wiley.com/doi/abs/10.1046/j.1365-2486.2003.00612.x, 2003.

Gu, L., Meyers, T., Pallardy, S. G., Hanson, P. J., Yang, B., Heuer, M., Hosman, K. P., Riggs, J. S., Sluss, D., and Wullschleger, S. D.: Direct and indirect effects of atmospheric conditions and soil moisture on surface energy partitioning revealed by a prolonged drought at a temperate forest site, Journal of Geophysical Research: Atmospheres, 111, https://doi.org/10.1029/2006JD007161, https://agupubs.onlinelibrary.wiley.com/doi/abs/10.1029/2006JD007161, 2006.

Hararuk, O., Smith, M. J., and Luo, Y.: Microbial models with data-driven parameters predict stronger soil carbon responses to climate change, Global Change Biology, 21, 2439–2453, https://doi.org/10.1111/gcb.12827, https://onlinelibrary.wiley.com/doi/abs/10.1111/gcb.12827, 2015.

Hartmann, H., Adams, H. D., Hammond, W. M., Hoch, G., Landhäusser, S. M., Wiley, E., and Zaehle, S.: Identifying differences in carbohydrate dynamics of seedlings and mature trees to improve carbon allocation in models for trees and forests, Environmental and Experimental Botany, 152, 7–18, 2018.

Hengl, T., Mendes de Jesus, J., Heuvelink, G. B., Ruiperez Gonzalez, M., and Kilibarda, M.: ISoilGrids250m: global gridded soil information based on Machine Learning, PLoS ONE, 12, e0169 748, https://doi.org/10.1371/journal.pone.0169748, 2017.

Hollinger, D. Y., Goltz, S. M., Davidson, E. A., Lee, J. T., Tu, K., and Valentine, H. T.: Seasonal patterns and environmental control of carbon dioxide and water vapour exchange in an ecotonal boreal forest, Global Change Biology, 5, 891–902, https://doi.org/10.1046/j.1365-2486.1999.00281.x, https://onlinelibrary.wiley.com/doi/abs/10.1046/j.1365-2486.1999.00281.x, 1999.

Hou, E., Chen, C., Luo, Y., Zhou, G., Kuang, Y., Zhang, Y., Heenan, M., Lu, X., and Wen, D.: Effects of climate on soil phosphorus cycle and availability in natural terrestrial ecosystems, Global Change Biology, 24, 3344–3356, https://doi.org/10.1111/gcb.14093, https://onlinelibrary.wiley.com/doi/abs/10.1111/gcb.14093, 2018.

Hungate, B. A., Dukes, J. S., Shaw, M. R., Luo, Y., and Field, C. B.: Nitrogen and Climate Change, Science, 302, 1512–1513, https://doi.org/10.1126/science.1091390, http://science.sciencemag.org/content/302/5650/1512, 2003.

Hyvönen, R., Agren, G. I., Linder, S., Persson, T., Cotrufo, M. F., Ekblad, A., FREEMAN, M., Grelle, A., Janssens, I. A., Jarvis, P. G., Kellomäki, S., Lindroth, A., Loustau, D., Lundmark, T., Norby, R. J., Oren, R., PILEGAARD, K., RYAN, M. G., Sigurdsson, B. D., Strömgren, M., van OIJEN, M., and WALLIN, G.: The likely impact of elevated [CO 2], nitrogen deposition, increased temperature and management on carbon sequestration in temperate and boreal forest ecosystems: a literature review, New Phytologist, 173, 463–480, 2007.

Ilvesniemi, H., Levula, J., Ojansuu, R., Kolari, P., Kulmala, L., Pumpanen, J. Launiainen, S., Vesala, T., and Nikinmaa, E.: Long-term measurements of the carbon balance of a boreal Scots pine dominated forest ecosystem, Boreal Enrironment Research, 14, 731–753, 2009.

Jackson, R. B., Canadell, J., Ehleringer, J. R., Mooney, H. A., Sala, O. E., and Schulze, E. D.: A global analysis of root distributions for terrestrial biomes, Oecologia, 108, 389–411, 1996.

Jiang, M., Caldararu, S., Zaehle, S., Ellsworth, D. S., and Medlyn, B. E.: Towards a more physiological representation of vegetation phosphorus processes in land surface models, The New Phytologist, https://doi.org/10.1111/nph.15688, http://dx.doi.org/10.1111/nph.15688, 2019.

June, T., Evans, J. R., and Farquhar, G. D.: A simple new equation for the reversible temperature dependence of photosynthetic electron transport: a study on soybean leaf, Functional Plant Biology, 31, 275, 2004.

Kattge, J., Díaz, S., Lavorel, S., Prentice, I. C., Leadley, P., Bönisch, G., Garnier, E., Westoby, M., Reich, P. B., Wright, I. J., Cornelissen, J. H. C., Violle, C., Harrison, S. P., Van Bodegom, P. M., Reichstein, M., Enquist, B. J., Soudzilovskaia, N. A., Ackerly, D. D., Anand, M., Atkin, O., Bahn, M., Baker, T. R., Baldocchi, D., Bekker, R., Blanco, C. C., Blonder, B., Bond, W. J., Bradstock, R., Bunker, D. E., Casanoves, F., Caverner-Bares, J., Chambers, J. Q., Chapin III, F. S., Chave, J., Coomes, D., Cornwell, W. K., Craine, J. M., Dobrin, B. H., Duarte, L., Durka, W., Elser, J., Esser, G., Estiarte, M., Fagan, W. F., Fand, J., Fernández-Méndez, F., Fidelis, A., Finegan, B., Flores, O., Ford, H., Frank, D., Freschet, G. T., Fyllas, N. M., Gallagher, R. V., Green, W. A., Gutierrez, A. G., Thomas, H., Higgins, S. I., Hodgson, J. G., Jalili, A., Jansen, S., Joly, C. A., Kerkhoff, A. J., Kirkup, D., Kitajima, K., Kleyer, M., Klotz, S., Knops, J. M. H., Kramer, K., Kühn, I., Kurokawa, H., Laughlin, D., Lee, T. D., Leishman, M., Lens, F., Lenz, T., Lewis, S. L., Lloyd, J., Llusià, J., Louault, F., Ma, S., Mahecha, M. D., Manning, P., Massad, T., Medlyn, B. E., Messier, J., Moles, A. T., Müller, S. C., Nadrowski, K., Naeem, S., Niinemets, Ü., Nöllert, S., Nüske, A., Ogaya, R., Oleksyn, J., Onipchenko, V. G., Onoda, Y., Ordoñez, J., Overbeck, G., Ozinga, W. A., Patino, S., Paula, S., Pausas, J. G., Peñuelas, J., Phillips, O. L., Pillar, V., Poorter, H., Poorter, L., Poschlod, P., Prinzing, A., Proulx, R., Rammig, A.,

Reinsch, S., Reu, B., Sack, L., Salgado-Negret, B., Sardans, J., Shiodera, S., Shipley, B., Siefert, A., Sosinski, E., Soussana, J. F., Swaine, E., Swenson, N., Thompson, K., Thornton, P., Waldram, M., Weiher, E., White, M., White, S., Wright, S. J., Yguel, B., Zaehle, S., Zanne, A. E., and Wirth, C.: TRY - a global database of plant traits, Global Change Biology, 17, 2905–2935, 2011.

Keenan, T., Sabate, S., and Gracia, C.: Soil water stress and coupled photosynthesis–conductance models: Bridging the gap between conflicting reports on the relative roles of stomatal, mesophyll conductance and biochemical limitations to photosynthesis, Agricultural and Forest Meteorology, 150, 443 – 453, https://doi.org/https://doi.org/10.1016/j.agrformet.2010.01.008, http://www.sciencedirect.com/science/article/pii/S0168192310000110, 2010.

Knauer, J., Werner, C., and Zaehle, S.: Evaluating stomatal models and their atmospheric drought response in a land surface scheme: A multibiome analysis, Journal of Geophysical Research: Biogeosciences, 120, 1894–1911, 2015.

Knauer, J., Zaehle, S., Reichstein, M., Medlyn, B. E., Forkel, M., Hagemann, S., and Werner, C.: The response of ecosystem water-use efficiency to rising atmospheric CO2 concentrations: sensitivity and large-scale biogeochemical implications, New Phytologist, 213, 1654–1666, https://doi.org/10.1111/nph.14288, https://nph.onlinelibrary.wiley.com/doi/abs/10.1111/nph.14288, 2016.

Knauer, J., Zaehle, S., De Kauwe, M., Bahar, N. H., Evans, J. R., Medlyn, B. E., Reichstein, M., and Werner, C.: Effects of mesophyll conductance on vegetation responses to elevated CO2 concentrations in a land surface model, Global Change Biology, in press.

Korhonen, J. F. J., Pihlatie, M., Pumpanen, J., Aaltonen, H., Hari, P., Levula, J., Kieloaho, A.-J., Nikinmaa, E., Vesala, T., and Ilvesniemi, H.: Nitrogen balance of a boreal Scots pine forest, Biogeosciences, 10, 1083–1095, https://doi.org/10.5194/bg-10-1083-2013, https://www.biogeosciences.net/10/1083/2013/, 2013.

Koven, C. D., Riley, W. J., Subin, Z. M., Tang, J. Y., Torn, M. S., Collins, W. D., Bonan, G. B., Lawrence, D. M., and Swenson, S. C.: The effect of vertically resolved soil biogeochemistry and alternate soil C and N models on C dynamics of CLM4, Biogeosciences, 10, 7109–7131, 2013.

Krinner, G., Viovy, N., de Noblet-Ducoudré, N., Ogée, J., Polcher, J., Friedlingstein, P., Ciais, P., Sitch, S. A., and Prentice, I. C.: A dynamic global vegetation model for studies of the coupled atmosphere-biosphere system, Global Biogeochemical Cycles, 19, GB1015, 2005.

Kull, O. and Kruijt, B.: Leaf photosynthetic light response: a mechanistic model for scaling photosynthesis to leaves and canopies, Functional Ecology, 12, 767–777, 1998.

Kutsch, W. L., Kolle, O., Rebmann, C., Knohl, A., Ziegler, W., and Schulze, E.-D.: Advection and resulting CO2 exchange uncertainty in a tall forest in central Germany, Ecological Applications, 18, 1391–1405, https://doi.org/10.1890/06-1301.1, https://esajournals.onlinelibrary.wiley.com/doi/abs/10.1890/06-1301.1, 2008.

Lagergren, F., Lindroth, A., Dellwik, E., Ibrom, A., Lankreijer, H., Launiainen, S., Mölder, M., Kolari, P., Pilegaard, K., and Vesala, T.: Biophysical controls on CO2 fluxes of three Northern forests based on long-term eddy covariance data, Tellus B, 60, 143–152, https://doi.org/10.1111/j.1600-0889.2006.00324.x, https://onlinelibrary.wiley.com/doi/abs/10.1111/j.1600-0889.2006.00324.x, 2008.

Lamarque, J.-F., Bond, T. C., Eyring, V., Granier, C., Heil, A., Klimont, Z., Lee, D., Liousse, C., Mieville, A., Owen, B., Schultz, M. G., Shindell, D., Smith, S. J., Stehfest, E., Van Aardenne, J., Cooper, O. R., Kainuma, M., Mahowald, N., McConnell, J. R., Naik, V., Riahi, K., and van Vuuren, D. P.: Historical (1850–2000) gridded anthropogenic and biomass burning emissions of reactive gases and aerosols: methodology and application, Atmospheric Chemistry and Physics, 10, 7017–7039, https://doi.org/10.5194/acp-10-7017-2010, https://www.atmos-chem-phys.net/10/7017/2010/, 2010.

Lamarque, J.-F., Kyle, G. P., Meinshausen, M., Riahi, K., Smith, S. J., van Vuuren, D. P., Conley, A. J., and Vitt, F.: Global and regional evolution of short-lived radiatively-active gases and aerosols in the Representative Concentration Pathways, Climatic Change, 109, 191, https://doi.org/10.1007/s10584-011-0155-0, https://doi.org/10.1007/s10584-011-0155-0, 2011.

Le Quéré, C., Andrew, R. M., Friedlingstein, P., Sitch, S., Pongratz, J., Manning, A. C., Korsbakken, J. I., Peters, G. P., Canadell, J. G., Jackson, R. B., Boden, T. A., Tans, P. P., Andrews, O. D., Arora, V. K., Bakker, D. C. E., Barbero, L., Becker, M., Betts, R. A., Bopp, L., Chevallier, F., Chini, L. P., Ciais, P., Cosca, C. E., Cross, J., Currie, K., Gasser, T., Harris, I., Hauck, J., Haverd, V., Houghton, R. A., Hunt, C. W., Hurtt, G., Ilyina, T., Jain, A. K., Kato, E., Kautz, M., Keeling, R. F., Klein Goldewijk, K., Körtzinger, A., Landschützer, P., Lefèvre, N., Lenton, A., Lienert, S., Lima, I., Lombardozzi, D., Metzl, N., Millero, F., Monteiro, P. M. S., Munro, D. R., Nabel, J. E. M. S., Nakaoka, S.-I., Nojiri, Y., Padin, X. A., Peregon, A., Pfeil, B., Pierrot, D., Poulter, B., Rehder, G., Reimer, J., Rödenbeck, C., Schwinger, J., Séférian, R., Skjelvan, I., Stocker, B. D., Tian, H., Tilbrook, B., Tubiello, F. N., van der Laan-Luijkx, I. T., van der Werf, G. R., van Heuven, S., Viovy, N., Vuichard, N., Walker, A. P., Watson, A. J., Wiltshire, A. J., Zaehle, S., and Zhu, D.: Global Carbon Budget 2017, Earth System Science Data, 10, 405–448, https://doi.org/10.5194/essd-10-405-2018, https://www.earth-syst-sci-data.net/10/405/2018/, 2018.

LeBauer, D. S. and Treseder, K. K.: Nitrogen limitation of net primary productivity in terrestrial ecosystems is globally distributed, Ecology, 89, 371–379, 2008.

Lin, Y.-S., Medlyn, B. E., Duursma, R. A., Prentice, I. C., Wang, H., Baig, S., Eamus, D., de Dios, V. R., Mitchell, P., Ellsworth, D. S., de Beeck, M. O., Wallin, G., Uddling, J., Tarvainen, L., Linderson, M.-L., Cernusak, L. A., Nippert, J. B., Ocheltree, T. W., Tissue, D. T., Martin-StPaul, N. K., Rogers, A., Warren, J. M., De Angelis, P., Hikosaka, K., Han, Q., Onoda, Y., Gimeno, T. E., Barton, C. V. M., Bennie, J., Bonal, D., Bosc, A., Low, M., Macinins-Ng, C., Rey, A., Rowland, L., Setterfield, S. A., Tausz-Posch, S., Zaragoza-Castells, J., Broadmeadow, M. S. J., Drake, J. E., Freeman, M., Ghannoum, O., Hutley, L. B., Kelly, J. W., Kikuzawa, K., Kolari, P., Koyama, K., Limousin, J. M., Meir, P., Lola da Costa, A. C., Mikkelsen, T. N., Salinas, N., Sun, W., and Wingate, L.: Optimal stomatal behaviour around the world, Nature Climate Change, 5, 459–464, 2015.

Lindroth, A., Klemedtsson, L., Grelle, A., Weslien, P., and Langvall, O.: Measurement of net ecosystem exchange, productivity and respiration in three spruce forests in Sweden shows unexpectedly large soil carbon losses, Biogeochemistry, 89, 43–60, https://doi.org/10.1007/s10533-007-9137-8, https://doi.org/10.1007/s10533-007-9137-8, 2008.

Lloyd, J. and Taylor, J. A.: On the temperature dependence of soil respiration, Functional ecology, pp. 315–323, https://www.jstor.org/stable/2389824, 1994.

Ma, S., Baldocchi, D. D., Xu, L., and Hehn, T.: Inter-annual variability in carbon dioxide exchange of an oak/grass savanna and open grassland in California, Agricultural and Forest Meteorology, 147, 157 – 171, https://doi.org/https://doi.org/10.1016/j.agrformet.2007.07.008, http://www.sciencedirect.com/science/article/pii/S016819230700189X, 2007.

Massoud, E. C., Xu, C., Fisher, R., Knox, R., Walker, A., Serbin, S., Christoffersen, B., Holm, J., Kueppers, L., Ricciuto, D. M., Wei, L., Johnson, D., Chambers, J., Koven, C., McDowell, N., and Vrugt, J.: Identification of key parameters controlling demographicallystructured vegetation dynamics in a Land Surface Model [CLM4.5(ED)], Geoscientific Model Development Discussions, 2019, 1–44, https://doi.org/10.5194/gmd-2019-6, https://www.geosci-model-dev-discuss.net/gmd-2019-6/, 2019.

Mauritsen, T., Bader, J., Becker, T., Behrens, J., Bittner, M., Brokopf, R., Brovkin, V., Claussen, M., Crueger, T., Esch, M., Fast, I., Fiedler, S., Fläschner, D., Gayler, V., Giorgetta, M., Goll, D. S., Haak, H., Hagemann, S., Hedemann, C., Hohenegger, C., Ilyina, T., Jahns, T., Jimenez de la Cuesta Otero, D., Jungclaus, J., Kleinen, T., Kloster, S., Kracher, D., Kinne, S., Kleberg, D., Lasslop, G., Kornblueh, L., Marotzke, J., Matei, D., Meraner, K., Mikolajewicz, U., Modali, K., Möbis, B., Müller, W. A., Nabel, J. E. M. S., Nam, C. C. W., Notz, D., Nyawira, S.-S., Paulsen, H., Peters, K., Pincus, R., Pohlmann, H., Pongratz, J., Popp, M., Raddatz, T., Rast, S., Redler, R., Reick, C. H., Rohrschneider, T., Schemann, V., Schmidt, H., Schnur, R., Schulzweida, U., Six, K. D., Stein, L., Stemmler, I., Stevens, B., von Storch, J.-S., Tian, F., Voigt, A., de Vrese, P., Wieners, K.-H., Wilkenskjeld, S., Winkler, A., and Roeckner, E.: Developments in the MPI-M Earth

System Model version 1.2 (MPI-ESM 1.2) and its response to increasing CO_2, Journal of Advances in Modeling Earth Systems, pp. 1–110, 2019.

Medlyn, B. E., Zaehle, S., De Kauwe, M. G., Walker, A. P., Dietze, M. C., Hanson, P. J., Hickler, T., Jain, A. K., Luo, Y., Parton, W., Prentice, I. C., Thornton, P. E., Wang, S., Wang, Y.-P., Weng, E., Iversen, C. M., McCarthy, H. R., Warren, J. M., Oren, R., and Norby, R. J.: Using ecosystem experiments to improve vegetation models, Nature Climate Change, 5, 528–534, 2015.

Medlyn, B. E., De Kauwe, M. G., Zaehle, S., Walker, A. P., Duursma, R. A., Luus, K., Mishurov, M., Pak, B., Smith, B., Wang, Y.-P., Yang, X., Crous, K. Y., Drake, J. E., Gimeno, T. E., Macdonald, C. A., Norby, R. J., Power, S. A., Tjoelker, M. G., and Ellsworth, D. S.: Using models to guide field experiments: a priori predictions for the CO_2 response of a nutrient- and water-limited native Eucalypt woodland, Global Change Biology, 22, 2834–2851, 2016.

Medlyn, B. E., De Kauwe, M. G., Lin, Y.-S., Knauer, J., Duursma, R. A., Williams, C. A., Arneth, A., Clement, R., Isaac, P., Limousin, J. M., Linderson, M.-L., Meir, P., Martin-StPaul, N., and Wingate, L.: How do leaf and ecosystem measures of water-use efficiency compare?, New Phytologist, 216, 758–770, 2017.

Mercado, L. M., Medlyn, B. E., Huntingford, C., Oliver, R. J., Clark, D. B., Sitch, S. A., Zelazowski, P., Kattge, J., Harper, A. B., and Cox, P. M.: Large sensitivity in land carbon storage due to geographical and temporal variation in the thermal response of photosynthetic capacity., The New phytologist, 218, 1462–1477, 2018.

Meyerholt, J. and Zaehle, S.: The role of stoichiometric flexibility in modelling forest ecosystem responses to nitrogen fertilization, New Phytologist, pp. n/a–n/a, 2015.

Mkhabela, M., Amiro, B., Barr, A., Black, T., Hawthorne, I., Kidston, J., McCaughey, J., Orchansky, A., Nesic, Z., Sass, A., Shashkov, A., and Zha, T.: Comparison of carbon dynamics and water use efficiency following fire and harvesting in Canadian boreal forests, Agricultural and Forest Meteorology, 149, 783 – 794, https://doi.org/https://doi.org/10.1016/j.agrformet.2008.10.025, http://www.sciencedirect.com/science/article/pii/S0168192308003080, 2009.

NOA: FLUXNET Data Download, http://www.fluxdata.org/DataDownload/default.aspx, last access: 17 February 2015, 2007.

Papale, D., Reichstein, M., Aubinet, M., Canfora, E., Bernhofer, C., Kutsch, W., Longdoz, B., Rambal, S., Valentini, R., Vesala, T., and Yakir, D.: Towards a standardized processing of Net Ecosystem Exchange measured with eddy covariance technique: algorithms and uncertainty estimation, Biogeosciences, 3, 571–583, https://doi.org/10.5194/bg-3-571-2006, https://www.biogeosciences.net/3/571/2006/, 2006.

Parton, W. J., Scurlock, J. M. O., Ojima, D. S., Gilmanov, T. G., Scholes, R. J., Schimmel, D. S., Kirchner, T., Menaut, J. C., Seastedt, T., Moya, E. G., Kamnalrut, A., and Kinyamario, J. I.: Observations and modelling of biomass and soil organic matter dynamics for the grassland biome worldwide, Global Biogeochemical Cycles, 7, 785–809, 1993.

Peng, J., Dan, L., and Huang, M.: Sensitivity of Global and Regional Terrestrial Carbon Storage to the Direct CO2 Effect and Climate Change Based on the CMIP5 Model Intercomparison, PLOS ONE, 9, 1–17, https://doi.org/10.1371/journal.pone.0095282, https://doi.org/10.1371/journal.pone.0095282, 2014.

Peñuelas, J., Poulter, B., Sardans, J., Ciais, P., van der Velde, M., Bopp, L., Boucher, O., Godderis, Y., Hinsinger, P., Llusia, Joan Nardin, E., Vicca, S., Obersteiner, M., and Janssens, I. A.: Human-induced nitrogen–phosphorus imbalances alter natural and managed ecosystems across the globe, Nature Communications, 4, https://doi.org/10.1038/ncomms3934, http://dx.doi.org/10.1038/ncomms3934, 2013.

Prentice, I. C., Liang, X., Medlyn, B. E., and Wang, Y. P.: Reliable, robust and realistic: the three R's of next-generation land-surface modelling, Atmospheric Chemistry and Physics, 15, 5987–6005, 2015.

Raddatz, T. J., Reick, C. H., Knorr, W., Kattge, J., Roeckner, E., Schnur, R., Schnitzler, K.-G., Wetzel, P., and Jungclaus, J.: Will the tropical land biosphere dominate the climate–carbon cycle feedback during the twenty-first century?, Climate Dynamics, 29, 565–574, https://doi.org/10.1007/s00382-007-0247-8, https://doi.org/10.1007/s00382-007-0247-8, 2007.

Rebmann, C., Anthoni, P., E., F., Göckede, M., Mangold, A., Subke, J.-A., Thomas, C., Wichura, B., Schulze, E.-D., Tenhunen, J. D., and Foken, T.: Carbon Budget of a Spruce Forest Ecosystem, in: Biogeochemistry of Forested Catchments in a Changing Environment, edited by Matzner, E., pp. 143–159, Springer, https://doi.org/https://doi.org/10.1007/978-3-662-06073-5_8, 2004.

Reed, S. C., Townsend, A. R., Taylor, P. G., and Cleveland, C. C.: Phosphorus Cycling in Tropical Forests Growing on Highly Weathered Soils, in: Phosphorus in Action Biological Processes in Soil Phosphorus Cycling, edited by Bünemann, E., Oberson, A., and Frossard, E., pp. 339–369, Springer Berlin Heidelberg, Berlin, Heidelberg, https://doi.org/10.1007/978-3-642-15271-9, 2011.

Reichstein, M., Falge, E., Baldocchi, D., Papale, D., Aubinet, M., Berbigier, P., Bernhofer, C., Buchmann, N., Gilmanov, T., Granier, A., Grünwald, T., Havránková, K., Ilvesniemi, H., Janous, D., Knohl, A., Laurila, T., Lohila, A., Loustau, D., Matteucci, G., Meyers, T., Miglietta, F., Ourcival, J.-M., Pumpanen, J., Rambal, S., Rotenberg, E., Sanz, M., Tenhunen, J., Seufert, G., Vaccari, F., Vesala, T., Yakir, D., and Valentini, R.: On the separation of net ecosystem exchange into assimilation and ecosystem respiration: review and improved algorithm, Global Change Biology, 11, 1424–1439, https://doi.org/10.1111/j.1365-2486.2005.001002.x, https://onlinelibrary.wiley.com/doi/abs/10.1111/j.1365-2486.2005.001002.x, 2005.

Roeckner, E., Tompkins, A., Bäuml, G., Bonaventura, L., Brokopf, R., Esch, M., Giorgetta, M., Hagemann, S., Kirchner, I., Kornblueh, L., Manzini, E., Rhodin, E., Schlese, U., and Schulzweida, U.: The atmospheric general circulation model ECHAM5 - Part I: Model description, Tech. Rep. 349, Max Planck Institute for Meteorology, Hamburg, 2003.

Roupsard, O., Bonnefond, J.-M., Irvine, M., Berbigier, P., Nouvellon, Y., Dauzat, J., Taga, S., Hamel, O., Jourdan, C., Saint-André, L., Mialet-Serra, I., Labouisse, J.-P., Epron, D., Joffre, R., Braconnier, S., Rouzière, A., Navarro, M., and Bouillet, J.-P.: Partitioning energy and evapo-transpiration above and below a tropical palm canopy, Agricultural and Forest Meteorology, 139, 252 – 268, https://doi.org/https://doi.org/10.1016/j.agrformet.2006.07.006, http://www.sciencedirect.com/science/article/pii/S0168192306001663, 2006.

Saltelli, A., Chan, K., and Scott, E. M.: Sensitivity Analysis, John Wiley & Sons, ltd., Chichester, New York, 2000.

Sanz, M., Carrara, A., Gimeno, C., Bucher, A., and Lopez, R.: Effects of a dry and warm summer conditions on CO_2 and energy fluxes from three Mediterranean ecosystems, Geophysical Research Abstracts, 6, 3239–3239, 2004.

Saxton, K. E. and Rawls, W. J.: Soil Water Characteristic Estimates by Texture and Organic Matter for Hydrologic Solutions, Soil Science Society of America Journal, 70, 1569–10, 2006.

Scherer-Lorenzen, M., Schulze, E.-D., Don, A., Schumacher, J., and Weller, E.: Exploring the functional significance of forest diversity: A new long-term experiment with temperate tree species (BIOTREE), Perspectives in Plant Ecology, Evolution and Systematics, 9, 53 – 70, https://doi.org/https://doi.org/10.1016/j.ppees.2007.08.002, http://www.sciencedirect.com/science/article/pii/S1433831907000339, 2007.

Schmid, H. P., Grimmond, C. B., Cropley, F., Offerle, B., and Su, H.-B.: Measurements of CO2 and energy fluxes over a mixed hardwood forest in the mid-western United States, Agricultural and Forest Meteorology, 103, 357 – 374, https://doi.org/https://doi.org/10.1016/S0168-1923(00)00140-4, http://www.sciencedirect.com/science/article/pii/S0168192300001404, 2000.

Scott, R. L., Jenerette, G. D., Potts, D. L., and Huxman, T. E.: Effects of seasonal drought on net carbon dioxide exchange from a woody-plant-encroached semiarid grassland, Journal of Geophysical Research: Biogeosciences, 114, https://doi.org/10.1029/2008JG000900, https://agupubs.onlinelibrary.wiley.com/doi/abs/10.1029/2008JG000900, 2009.

Shinozaki, K., Yoda, K., Hozumi, K., and Kira, T.: A quantitative analysis of the plant form - the pipe model theory, Japanes Journal of Ecology, 14, 98–104, 1964.

Sitch, S., Friedlingstein, P., Gruber, N., Jones, S. D., Murray-Tortarolo, G., Ahlström, A., Doney, S. C., Graven, H., Heinze, C., Huntingford, C., Levis, S., Levy, P. E., Lomas, M., Poulter, B., Viovy, N., Zaehle, S., Zeng, N., Arneth, A., Bonan, G., Bopp, L., Canadell, J. G., Chevallier, F., Ciais, P., Ellis, R., Gloor, M., Peylin, P., Piao, S. L., Le Quere, C., Smith, B., Zhu, Z., and Myneni, R.: Recent trends and drivers of regional sources and sinks of carbon dioxide, Biogeosciences, 12, 653–679, https://doi.org/10.5194/bg-12-653-2015, https://www.biogeosciences.net/12/653/2015/, 2015.

Sitch, S. A., Smith, B., Prentice, I. C., Arneth, A., Bondeau, A., Cramer, W., Kaplan, J. O., Levis, S., Lucht, W., Sykes, M. T., and Venevsky, S.: Evaluation of ecosystem dynamics, plant geography and terrestrial carbon cycling in the LPJ Dynamic Global Vegetation Model, Global Change Biology, 9, 161–185, 2003.

Suni, T., Rinne, J., Reissell, A., Altimir, N., Keronen, P., Rannik, Ü., Dal Maso, M., Kulmala, M., and Vesala, T.: Long-term measurements of surface fluxes above a Scots pine forest in Hyytiälä, southern Finland, 1996-2001, Boreal Enrironment Research, 8, 287–301, 2003.

Swann, A. L. S., Hoffman, F. M., Koven, C. D., and Randerson, J. T.: Plant responses to increasing CO2 reduce estimates of climate impacts on drought severity, Proceedings of the National Academy of Sciences, 113, 10 019–10 024, https://doi.org/10.1073/pnas.1604581113, http://www.pnas.org/content/113/36/10019, 2016.

Tedeschi, V., Rey, A., Manca, G., Valentini, R., Jarvis, P. G., and Borghetti, M.: Soil respiration in a Mediterranean oak forest at different developmental stages after coppicing, Global Change Biology, 12, 110–121, https://doi.org/10.1111/j.1365-2486.2005.01081.x, https://onlinelibrary.wiley.com/doi/abs/10.1111/j.1365-2486.2005.01081.x, 2006.

Thornton, P., Lamarque, J.-F., Rosenbloom, N. A., and Mahowald, N. M.: Influence of carbon-nitrogen cycle coupling on land model response to CO2 fertilization and climate variability, Global Biogeochemical Cycles, 21, https://doi.org/10.1029/2006GB002868, https://agupubs.onlinelibrary.wiley.com/doi/abs/10.1029/2006GB002868, 2007.

Thum, T., Zaehle, S., Köhler, P., Aalto, T., Aurela, M., Guanter, L., Kolari, P., Laurila, T., Lohila, A., Magnani, F., Van Der Tol, C., and Markkanen, T.: Modelling sun-induced fluorescence and photosynthesis with a land surface model at local and regional scales in northern Europe, Biogeosciences, 14, 1969–1987, https://doi.org/10.5194/bg-14-1969-2017, https://www.biogeosciences.net/14/1969/2017/, 2017.

Tirone, G., Dore, S., Matteucci, G., Greco, S., and Valentini, R.: Evergreen Mediterranean Forests. Carbon and Water Fluxes, Balances, Ecological and Ecophysiological Determinants, in: Fluxes of Carbon, Water and Energy of European Forests, edited by Valentini, R., pp. 125–149, Springer Berlin Heidelberg, Berlin, Heidelberg, https://doi.org/10.1007/978-3-662-05171-9_7, https://doi.org/10.1007/978-3-662-05171-9_7, 2003.

Urbanski, S., Barford, C., Wofsy, S., Kucharik, C., Pyle, E., Budney, J., McKain, K., Fitzjarrald, D., Czikowsky, M., and Munger, J. W.: Factors controlling CO2 exchange on timescales from hourly to decadal at Harvard Forest, Journal of Geophysical Research: Biogeosciences, 112, https://doi.org/10.1029/2006JG000293, https://agupubs.onlinelibrary.wiley.com/doi/abs/10.1029/2006JG000293, 2007.

Vargas, R., Sonnentag, O., Abramowitz, G., Carrara, A., Chen, J. M., Ciais, P., Correia, A., Keenan, T. F., Kobayashi, H., Ourcival, J.-M., Papale, D., Pearson, D., Pereira, J. S., Piao, S., Rambal, S., and Baldocchi, D. D.: Drought Influences the Accuracy of Simulated Ecosystem Fluxes: A Model-Data Meta-analysis for Mediterranean Oak Woodlands, Ecosystems, 16, 749–764, https://doi.org/10.1007/s10021-013-9648-1, https://doi.org/10.1007/s10021-013-9648-1, 2013.

Vicca, S., Luyssaert, S., Peñuelas, J., Campioli, M., Chapin III, F. S., Ciais, P., Heinemeyer, A., Hogberg, P., Kutsch, W. L., Law, B. E., Malhi, Y., Papale, D., Piao, S. L., Reichstein, M., Schulze, E. D., and Janssens, I. A.: Fertile forests produce biomass more efficiently, Ecology Letters, 15, 520–526, 2012.

Viovy, N.: CRU-NCEP dataset, v7, https://vesg.ipsl.upmc.fr/thredds/catalog/store/p529viov/cruncep/V7_1901_2015/catalog.html, 2016.

Vitousek, P. M. and Howarth, R. W.: Nitrogen limitation on land and in the sea - how it can occur, Biogeochemistry, 13, 87–115, 1991.

Vitousek, P. M., Porder, S., Houlton, B. Z., and Chadwick, O. A.: Terrestrial phosphorus limitation: mechanisms, implications, and nitrogen–phosphorus interactions, Ecological Applications, 20, 5–15, https://doi.org/10.1890/08-0127.1, 2010.

Walker, T. W. and Syers, J. K.: The fate of phosphorus during pedogenesis, Geoderma, 15, 1–19, https://doi.org/10.1016/0016-7061(76)90066-5, http://linkinghub.elsevier.com/retrieve/pii/0016706176900665, 1976.

Wang, Y. P., Law, R. M., and Pak, B.: A global model of carbon, nitrogen and phosphorus cycles for the terrestrial biosphere, Biogeosciences, 7, 2261–2282, 2010.

Warlind, D., Smith, B., Hickler, T., and Arneth, A.: Nitrogen feedbacks increase future terrestrial ecosystem carbon uptake in an individual-based dynamic vegetation model, Biogeosciences, 11, 6131–6146, 2014.

White, R. E.: Principles and Practice of Soil Science The soil as a Natural Resource, vol. 32, Blackwell Publishing, Malden, 4th edn., https://doi.org/10.1177/0340035206070163, 2006.

Wohlfahrt, G., Anderson-Dunn, M., Bahn, M., Balzarolo, M., Berninger, F., Campbell, C., Carrara, A., Cescatti, A., Christensen, T., Dore, S., Eugster, W., Friborg, T., Furger, M., Gianelle, D., Gimeno, C., Hargreaves, K., Hari, P., Haslwanter, A., Johansson, T., Marcolla, B., Milford, C., Nagy, Z., Nemitz, E., Rogiers, N., Sanz, M. J., Siegwolf, R. T., Susiluoto, S., Sutton, M., Tuba, Z., Ugolini, F., Valentini, R., Zorer, R., and Cernusca, A.: Biotic, Abiotic, and Management Controls on the Net Ecosystem CO2 Exchange of European Mountain Grassland Ecosystems, Ecosystems, 11, 1338–1351, https://doi.org/10.1007/s10021-008-9196-2, https://doi.org/10.1007/s10021-008-9196-2, 2008a.

Wohlfahrt, G., Hammerle, A., Haslwanter, A., Bahn, M., Tappeiner, U., and Cernusca, A.: Seasonal and inter-annual variability of the net ecosystem CO2 exchange of a temperate mountain grassland: Effects of weather and management, Journal of Geophysical Research: Atmospheres, 113, https://doi.org/10.1029/2007JD009286, https://agupubs.onlinelibrary.wiley.com/doi/abs/10.1029/2007JD009286, 2008b.

Wramneby, A., Smith, B., Zaehle, S., and SYKES, M. T.: Parameter uncertainties in the modelling of vegetation dynamics - Effects on tree community structure and ecosystem functioning in European forest biomes, Ecological Modelling, 216, 277–290, 2008.

Yang, X., Post, W. M., Thornton, P. E., and Jain, A.: The distribution of soil phosphorus for global biogeochemical modeling, Biogeosciences, 10, 2525–2537, https://doi.org/10.5194/bg-10-2525-2013, 2013.

Yang, X., Thornton, P. E., Ricciuto, D. M., and Post, W. M.: The role of phosphorus dynamics in tropical forests – a modeling study using CLM-CNP, Biogeosciences, 11, 1667–1681, https://doi.org/10.5194/bg-11-1667-2014, https://www.biogeosciences.net/11/1667/2014/, 2014.

Zaehle, S. and Dalmonech, D.: Carbon–nitrogen interactions on land at global scales: current understanding in modelling climate biosphere feedbacks, Current Opinion in Environmental Sustainability, 3, 311–320, 2011.

Zaehle, S. and Friend, A. D.: Carbon and nitrogen cycle dynamics in the O-CN land surface model: 1. Model description, site-scale evaluation, and sensitivity to parameter estimates, Global Biogeochemical Cycles, 24, GB 1005, 2010.

Zaehle, S., Sitch, S. A., Smith, B., and Hatterman, F.: Effects of parameter uncertainties on the modeling of terrestrial biosphere dynamics, Global Biogeochemical Cycles, 19, doi:10.1029–2004GB002 395, https://doi.org/doi:10.1029/2004GB002395, 2005.

Zaehle, S., Friedlingstein, P., and Friend, A. D.: Terrestrial nitrogen feedbacks may accelerate future climate change, Geophysical Research Letters, 37, https://doi.org/10.1029/2009GL041345, https://agupubs.onlinelibrary.wiley.com/doi/abs/10.1029/2009GL041345, 2010.

Zaehle, S., Ciais, P., Friend, A. D., and Prieur, V.: Carbon benefits of anthropogenic reactive nitrogen offset by nitrous oxide emissions, Nature Geoscience, 4, 601–605, 2011.

Zaehle, S., Medlyn, B. E., De Kauwe, M. G., Walker, A. P., Dietze, M. C., Hickler, T., Luo, Y., Wang, Y.-P., El-Masri, B., Thornton, P., Jain, A., Wang, S., Warlind, D., Weng, E., Parton, W., Iversen, C. M., Gallet-Budynek, A., McCarthy, H., Finzi, A., Hanson, P. J., Prentice, I. C., Oren, R., and Norby, R. J.: Evaluation of 11 terrestrial carbon–nitrogen cycle models against observations from two temperate Free-Air CO2 Enrichment studies, New Phytologist, 202, 803–822, https://doi.org/10.1111/nph.12697, https://nph.onlinelibrary.wiley.com/doi/abs/10.1111/nph.12697, 2014.

Zerihun, A., McKenzie, B. A., and Morton, J. D.: Photosynthate costs associated with the utilization of different nitrogen–forms: influence on the carbon balance of plants and shoot–root biomass partitioning, The New Phytologist, 138, 1–11, 1998.

Zheng, M., Zhou, Z., Luo, Y., Zhao, P., and Mo, J.: Global pattern and controls of biological nitrogen fixation under nutrient enrichment: A meta-analysis., Global Change Biology, 25, 3018–3030, 2019.

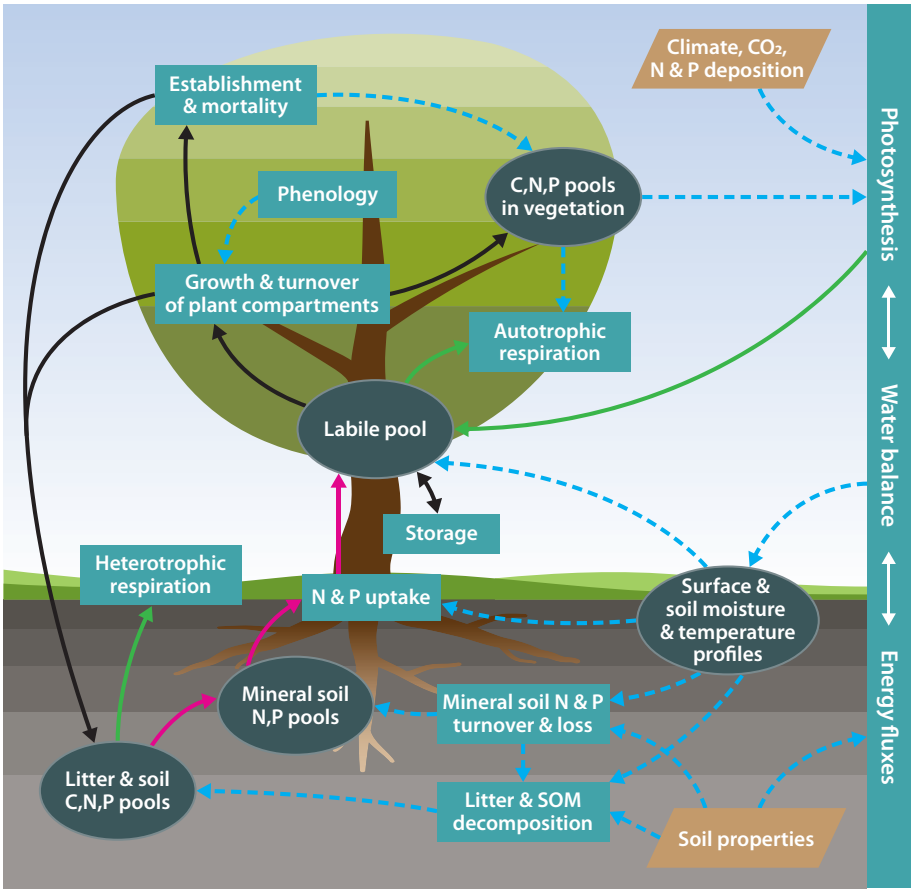

Figure 1. Schematic representation of the model structure. Elipses: biogeochemical pools and other state variables; rectangles: biogeochemical processes; tetraeders: model input; solid green lines: carbon fluxes; solid dark red lines: nitrogen and phosphorus fluxes; solid black lines: carbon, nitrogen and phosphorus fluxes; dotted blue lines: effects.

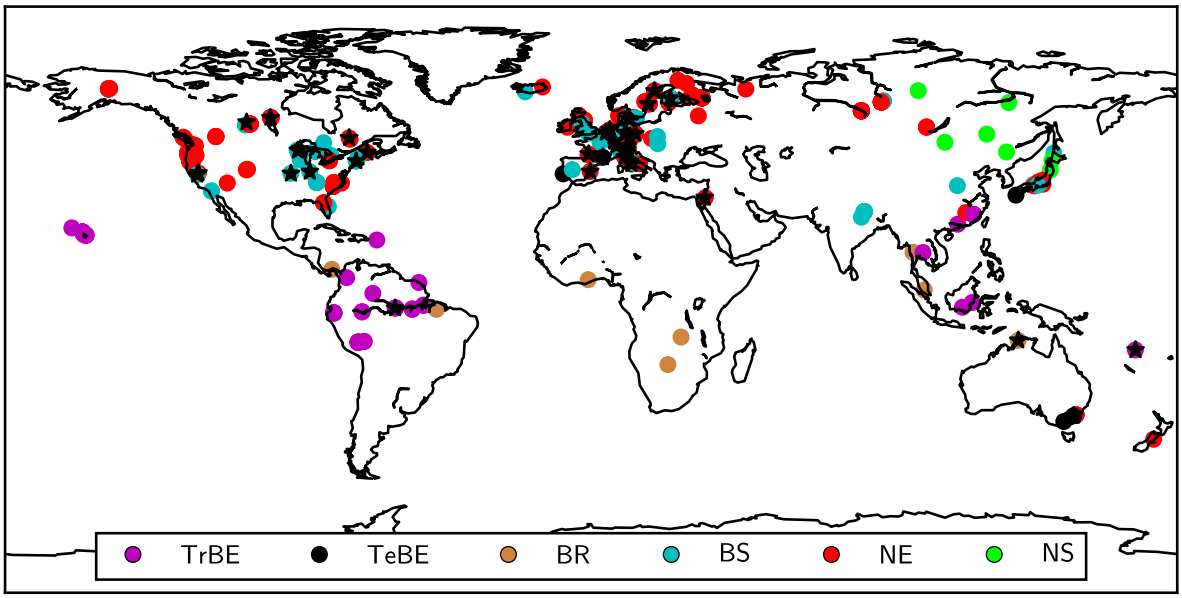

Figure 2. Locations of the sites used for model evaluation. Black stars: FLUXNET sites; circles: GFDB sites with circles having colors corresponding to different PFTs (see Table 1).

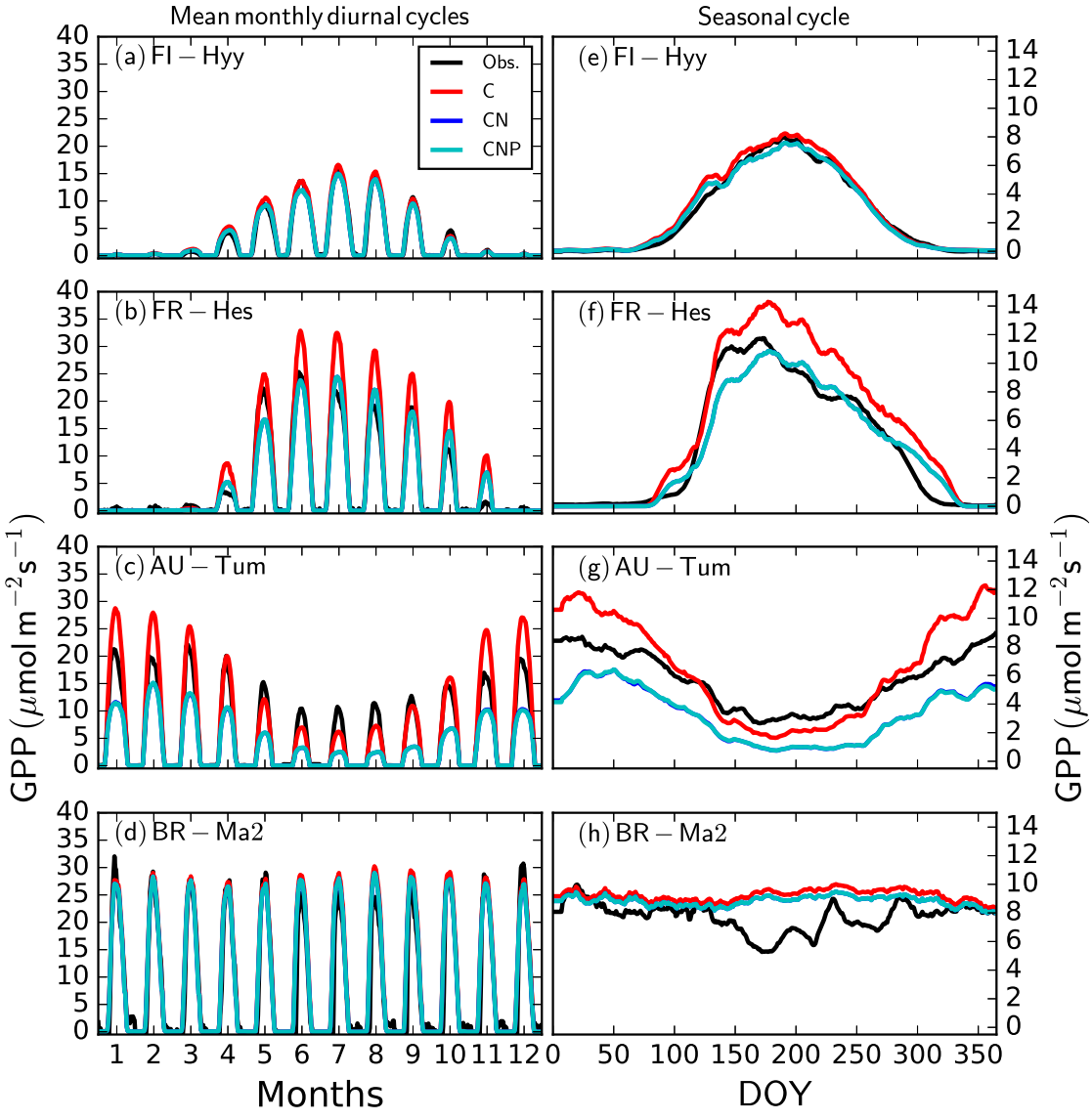

Figure 3. Simulated and observed mean monthly diurnal (a, b, c, d) and seasonal (e, f, g, h) cycles of gross primary production (GPP) at four FLUXNET sites (FI-Hyy, FR-Hes, AU-Tum, BR-Ma2, see Tab. A1) representing the major QUINCY PFTs (NE, BS, TeBE, and TrBE, respectively, see Tab. 1). 'Obs' correspond to micrometeorological observations. 'C', 'CN' and 'CNP' refer to the model simulations with C, C&N and C&N&P options enabled. Seasonal cycles have been smoothed by a 16-day running mean.

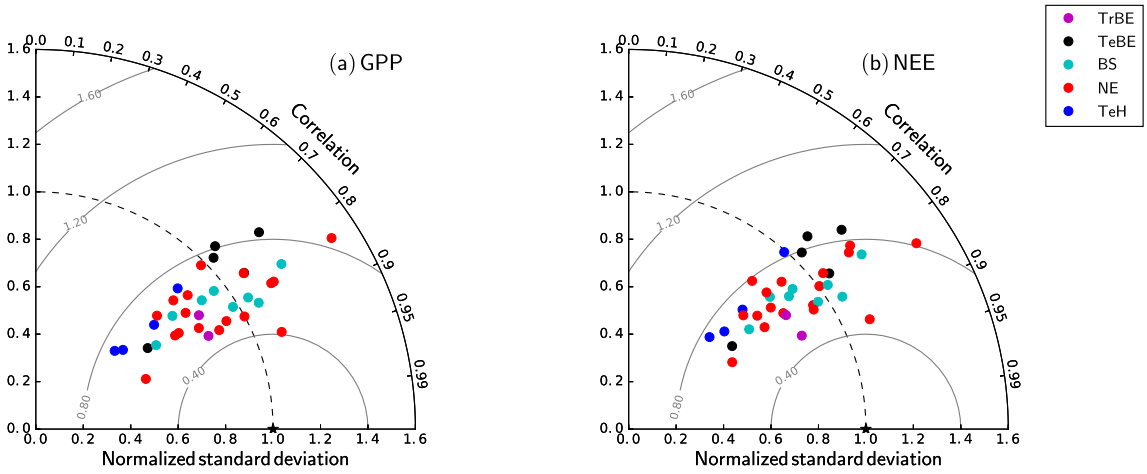

Figure 4. Taylor plots for gross primary production (GPP) and net ecosystem exchange (NEE) showing the model-data agreement for the FLUXNET sites used in this study (Tab. A1), separated according to the dominant plant functional type (Tab. 1). The standard deviation was normalized against the standard deviation of the observations for the corresponding variable. The grey lines correspond to the euclidean distance from the point of perfect model-data agreement, where both the normalised standard deviation and the correlation coefficient are 1.0, shown as a black star in the figure.

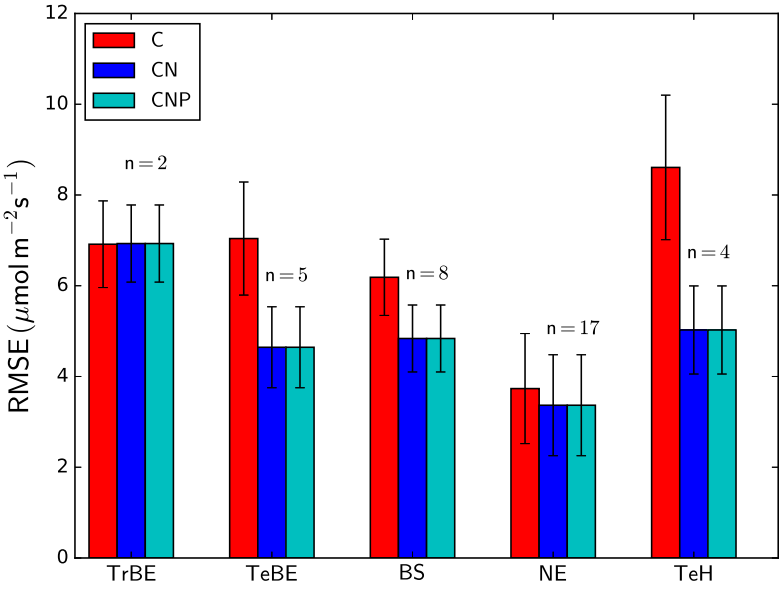

Figure 5. Root mean square error (RMSE) for simulated gross primary production (GPP) by dominant plant functional type (see Tab. 1). The number of sites used in the calculation of the PFT-specific RMSE value (n) is shown above the bars for each PFT. The error bars denote the standard deviation of the RMSE values of the different sites within each PFT. 'C', 'CN' and 'CNP' refer to the model simulations with C, C&N and C&N&P options enabled.

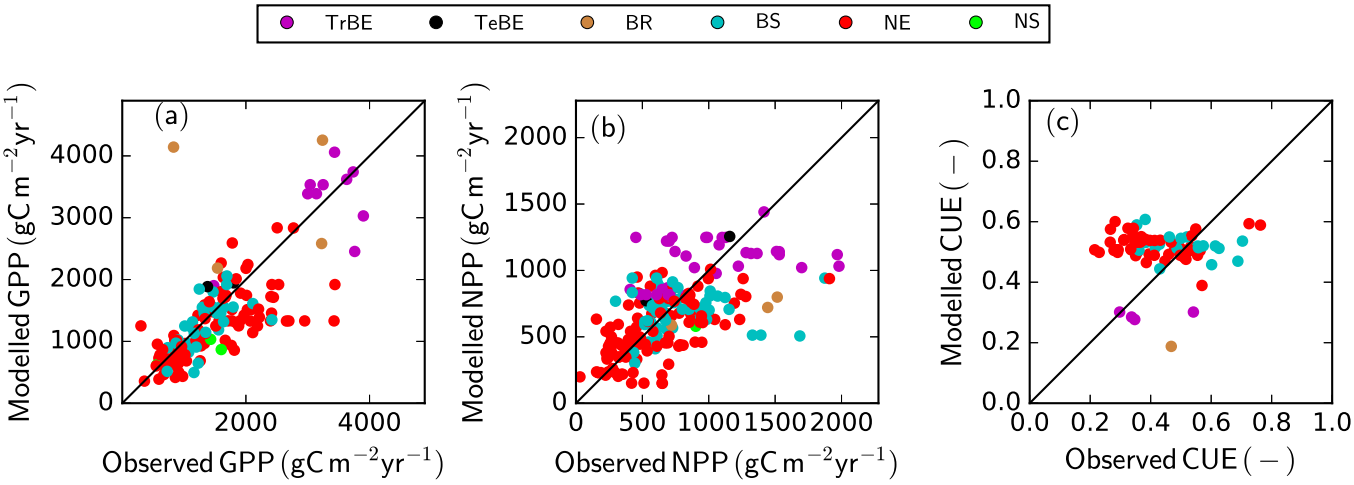

Figure 6. Simulated versus observed gross primary productivity (GPP) (a), net primary productivity (NPP) (b) and carbon use efficiency (CUE=NPP/GPP) (c) at GFDB sites against observations. For PFT abbreviations, see Table 1. Note that observations of GPP and NPP are not consistently available for all sites.

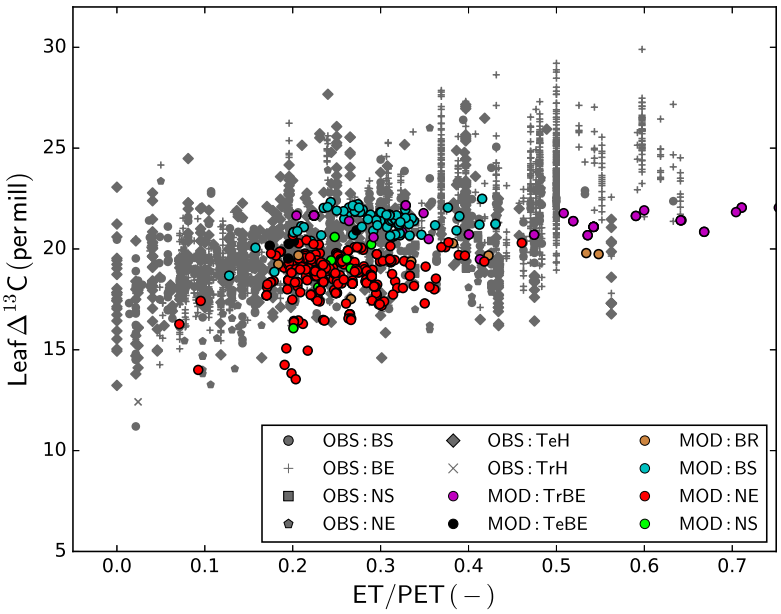

Figure 7. Observed and simulated leaf Δ^{13}C. Observations are taken from the global database of (Cornwell et al., 2018b), simulations are derived from the GFDB set of sites (see Fig. 2). As there is no direct correspondence between data and model location, the data are plotted as a function of climatic water deficit, measured as the ratio of actual to potential evapotranspiration (ET/PET). For model PFT abbreviations, see Table 1.

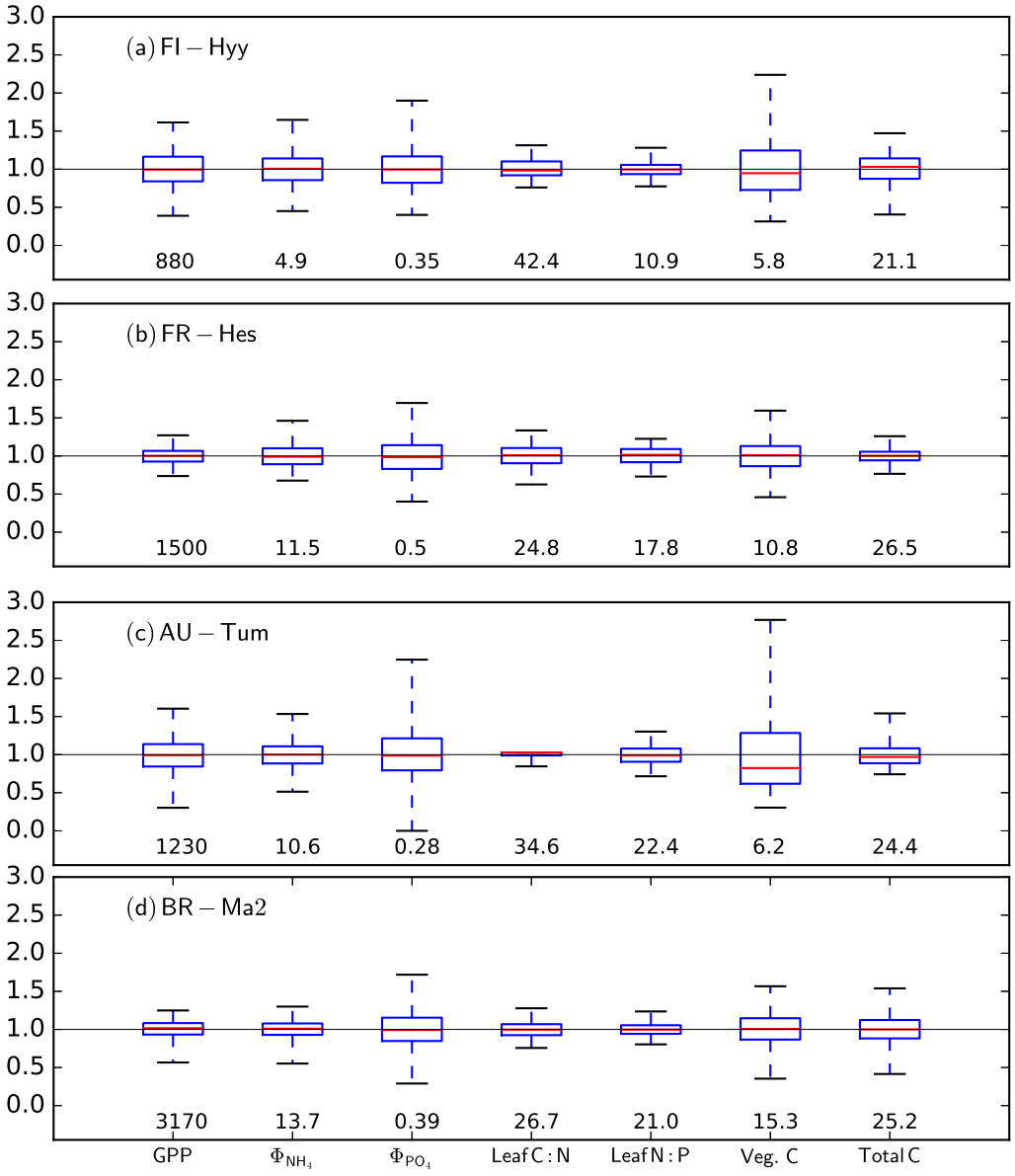

Figure 8. Median, inner-quartile range and absolute range of simulated gross primary production (GPP), net mineralisation of NH_4 (Φ_{NH_4}) and PO_4 (Φ_{PO_4}), leaf C:N and N:P, as well as vegetation C (veg. C) and total ecosystem C (up to a depth of ~~1m~~1 m) obtained for the four FLUXNET sites in Fig. 3 using latin-hypercube sampling (n=1000) for 45 parameters. Values have been normalised to the ensemble mean, given as number for each site and variable, to improved readability. The numbers below each individual box correspond the median value for each variable, GPP in units gC m^{-2} yr^{-1}, Φ_{NH_4} in units gN m^{-2} yr^{-1}, Φ_{PO_4} in units gP m^{-2} yr^{-1} and vegetation and total carbon in units gC m^{-2}.

Table 1. Description of plant functional types used in the model

Number	Abbreviation	Description
1	TrBE	Tropical broad-leaved evergeen
2	TeBE	Temperate broad-leaved evergreen
3	BR	(Tropical) broad-leaved rain deciduous (rain green)
4	BS	(Temperate & Boreal) Broad-leaved winter deciduous (summer green)
5	NE	(Temperate & Boreal) Needle-leaved evergreen (coniferous evergreen)
6	NS	(Temperate & Boreal) Needle-leaved winter deciduous (summer green)
7	TeH	C3 grass
8	TrH	C4 grass

Supplementary material for: A new ~~terrestrial biosphere~~ model ~~with~~ of the coupled carbon, nitrogen, and phosphorus cycles in the terrestrial biosphere (QUINCY v1.0; revision ~~1772~~1996)

Tea Thum[1], Silvia Caldararu[1], Jan Engel[1], Melanie Kern[1,2,3], Marleen Pallandt[1,2], Reiner Schnur[4], Lin Yu[1], and Sönke Zaehle[1,5]

[1]Max Planck Institute for Biogeochemistry, Hans-Knöll Str. 10, 07745 Jena, Germany
[2]International Max Planck Research School (IMPRS) for Global Biogeochemical Cycles, Jena, Germany
[3]Michael Stifel Center Jena for Data-driven and Simulation Science, Jena, Germany

Correspondence: Tea Thum (tthum@bgc-jena.mpg.de), Sönke Zaehle (szaehle@bgc-jena.mpg.de)

This Supplementary Material includes a detailed model description with equations. Section M1 summarises the general structure and vertical discretisation of vegetation and soil, and introduces general parameters (Tab M1). Section M2 describes the canopy processes, such as photosynthesis and stomatal coupling, with parameters in Tab. M2. Section M3 introduces vegetation growth, turnover and dynamics and the corresponding parameters are in Tab. M3. The soil biochemistry is described in Section M4, and its parameters are in Tab. M4. Section M5 describes the implementation of the isotope code, with parameters in Tab. M5. Section M6 describes the radiation scheme, surface energy balance and soil hydrology, with parameters described in Tab. M6. The PFT-specific parameters are listed in Tab. M7. Where no explicit reference to other studies is given, the equations have been developed in this study.

M1 General model structure, modularity, and discretisation

Each gridcell of the model is subdivided into nested tiles, each of which is occupied by one specific vegetation-type, representing a plant functional type (PFT). The number of tiles per gridcell is flexible, making it is easy to implement more/different PFTs in the future. In the model, vegetation is represented by an average individual composed of a range of structural pools (leaves, sapwood, heartwood, coarse roots, fine roots, and fruit), a fast overturning, respiring non-structural pool (labile), as well as a seasonal, non-respiring, and non-structural storage pool (reserve). Tree vegetation types are furthermore characterised by their height (m), diameter (m), and stand density (m^{-2}). Soil biogeochemistry is represented using five organic pools: metabolic (met), structural (str) and and woody (wl) litter, as well as fast (f) and slow (s) overturning soil organic matter. Each of these pools contains carbon (C), nitrogen (N) and phosphorus (P), as well as $^{13}\mathrm{C}$, $^{14}\mathrm{C}$, and $^{15}\mathrm{N}$. The unit of the pools is $\mathrm{mol\ X\ m}^{-2}$ for vegetation and $\mathrm{mol\ X\ m}^{-3}$ for soil biogeochemical pools, where X represents any of these elements. In addition, the model represents the following soil biogeochemical pools ($\mathrm{NH_4}$, $\mathrm{NO_3}$, $\mathrm{NO_y}$, $\mathrm{N_2O}$, $\mathrm{N_2}$, and $\mathrm{PO_4}$), with equivalent units.

The model operates on a half-hourly time-scale (denoted as dt). Vegetation processes, e.g. the photosynthesis and respiration responses to temperature, the responses of nutrient uptake and foliar nutrient concentrations to nutrient availability, are assumed to respond to these instantaneous conditions and associated fluxes with a process-specific lag time ($\tau_{mavg}^{process}$, see Tab. M1), representing a form of memory for instance in the calculation of allocation or vegetation dynamic responses. Where appropriate, the fluxes or pool sizes are calculated as running means with a time-averaging filter as

$$X_{mavg,new}^{process} = X_{mavg,old}^{process} \times (1-\omega) + X_{current} \times \omega, where \tag{1a}$$

$$\omega = \frac{dt}{\tau_{mavg}^{process}} \tag{1b}$$

where $X_{current}$ is the instantaneous state or flux of interest, and $X_{mavg,old}^{process}$, as well as $X_{mavg,new}^{process}$ are the averaged values of the previous and current time step, respectively. The equations where these lag times are playing a role are also shown in Tab. M1.

M1.1 Vertical discretisation

The canopy is discretised into 10 layers (denoted by subscript cl), with exponentially increasing layer depth (LAI_{cl}) to allow for a better resolution of ~~canopy processes in areas of~~ top-of-canopy processes with high light and nitrogen gradients. ~~Total foliage N~~ In accordance with observations of canopy N distribution (Niinemets et al., 1998), less N is allocated to the lower, darker canopy layers: as in Zaehle and Friend (2010), the total canopy N content (N_{leaf}) is distributed to each canopy layer cl ~~,~~following

$$N_{leaf,cl} = N_{leaf,cl=1} \times e^{-k_n \times LAI_c}, where \tag{2a}$$

$$N_{leaf,cl=1} = \frac{k_n}{1-e^{-k_n \times LAI}} N_{leaf} \tag{2b}$$

where LAI_c is the cumulative leaf area above the centre-point of the canopy layer, and LAI the total leaf area, ~~such that less N is allocated to the lower, darker canopy layers, in accordance with observations of canopy N distribution (Niinemets et al., 1998)~~and $cl = 1$ is the top layer.

All soil state-variables (temperature, moisture, texture, soil biogeochemical pools) and fluxes are discretised into 15 soil layers (denoted by subscript (sl). Layer thickness increases exponentially with increasing layer depth up to a total depth of 9.5 m, and with a minimum layer thickness for the top layer of 0.065 m. ~~Fine~~ Following observations presented by Jackson et al. (1996), fine roots and coarse roots are assumed to be distributed in exponentially decreasing density along the soil profile according to

$$X_{root,sl} = X_{root,sl=1} \times e^{-k_{root\_dist} \times depth_{sl}}, where \tag{3a}$$

$$X_{root,sl=1} = \frac{k_{rd}}{1-e^{-k_{root\_dist} \times depth_r}} X_{root} \tag{3b}$$

where k_{rd} is a PFT-specific parameter (see Tab. M7~~, Jackson et al. (1996)~~), $depth_{sl}$ the depth of the soil layer's mid point, $depth_r$ the rooting depth, derived from site characteristics and X_{root} the respective fine or coarse root mass.

For clarity in the following, the subscript for canopy and soil layer is ignored if processes are treated similarly across layers.

M1.2 Modularity

The code structure of QUINCY has been designed in a modular way, with two intentions.

Modularity regarding the scope of the model The model can be run configured as a canopy flux scheme (simplified representation of LAI dynamics given the phenology subroutines, full consideration of soil hydrology, surface energy, canopy radiation and photosynthesis), a stand-alone vegetation model (all of the canopy flux schemes, but with LAI dependent on vegetation growth and dynamics, however without biogeochemical soil feedbacks), a stand-alone soil biogeochemical model (driven by pre-calculated soil moisture and temperature as well as atmospheric and plant litter inputs), a configuration of any of the former without considering soil moisture constraints, and the fully coupled canopy, vegetation and soil model as applied here. This approach allows for testing the implications of particular processes at reduced model complexity.

Modularity regarding the ability to test different hypothesis regarding specific process representations that the subroutine structure of the model facilitates the testing of alternative process hypotheses. These include alternative assumptions about temperature acclimation, the vertical structure of the soil (bulk or one-dimensional with flexible numbers of layers), as well as submodules to be tested in future studies.

M2 Canopy processes

M2.1 Canopy nitrogen allocation

The leaf area index (LAI) and canopy nitrogen content (N_{leaf}) are dynamic properties of the model, as described in Section M3, and are discretised to canopy layers given by Eq. 2. $N_{leaf,cl}$ is partitioned into photosynthetic and non-photosynthetic, or structural, N. The fraction of structural N ($fN_{struc,cl}$) is calculated as a function of the total leaf N in the respective canopy layer (Zaehle and Friend, 2010):

$$fN_{struc,cl} = k_0^{struc} - k_1^{struc} N_{leaf,cl} \tag{4}$$

where k_0^{struc} is a PFT-specific parameter and k_1^{struc} is an empirical constant.

The photosynthetic N is further separated into the fraction that is associated with Rubisco (fN_{rub}), electron transport (fN_{et}), chlorophyll (fN_{chl}) and in the case of C4 plants, a fourth fraction for PEP carboxylase fN_{pepc}.

~~The~~ As in (Zaehle and Friend, 2010), the fraction of N in chlorophyll for each layer is calculated as decreasing with canopy depth:

$$fN_{chl} = \frac{k_0^{chl} - k_1^{chl} e^{-k_{fn}^{chl} LAI_c}}{a_{chl}^n}, \tag{5}$$

where k_0^{chl}, k_1^{chl} and k^{chl} are empirical parameters ~~,~~and a_{chl}^n is the molecular N content of chlorophyll.

The values of fN_{rub} and fN_{et} are calculated assuming a fixed ratio of the V_{cmax} and J_{max} photosynthetic parameters at 25°C, r_{J2V}, given the calculated values of the structural and photosynthetic fractions. The PEP carboxylase fraction, fN_{pep}, is considered to be a constant.

M2.2 Leaf-level net photosynthesis

Photosynthesis and stomatal conductance are calculated for the mid-points of each canopy layer and light-quality class (sunlit and shaded; as defined in Sect. M6.1). For clarity, the subscript $_{cl}$ is omitted in this section. The calculation of leaf-level photosynthesis is based on Kull and Kruijt (1998), extended for C4 photosynthesis according to Friend et al. (2009)~~, and with the~~ . The Kull-photosynthesis scheme explicitly and dynamically separates each leaf (layer) into a fraction that is light-saturated, under which photosynthesis is controlled by Farquhar-type co-limitation model (Farquhar et al., 1982), and the remainder, which is light-harvesting limited, and therefore strongly depends in the leaf chlorophyll content (see Kull and Kruijt, 1998, for details).

The temperature response curves as described in Bernacchi et al. (2001). Unless stated otherwise, temperature sensitivities follow the form:

$$f_x(T_{air}) = e^{E_0^x - E_1^x/(R \times T_{air})} \tag{6}$$

where T_{air} is the air temperature (K), R is the universal gas constant ($\mathrm{Jmol^{-1}K^{-1}}$), and the process-wise E_0^x and E_1^x are given in Table M2.

~~Photosynthesis and stomatal conductance are calculated for the mid-points of each canopy layer and light-quality class (sunlit and shaded; as defined in Sect. M6.1). For clarity, the subscript $_{cl}$ is omitted in this section~~Note that the current version of QUINCY does not include a representation of canopy temperature and we are therefore using air temperature for all aboveground processes.

In light-saturated conditions, gross photosynthesis (A_g) in C3 plants is calculated as the minimum of two potential rates, The electron-transport capacity limited carboxylation (A_j) and the Rubisco-limited rate of photosynthesis (A_v). A_j is given by

$$A_j = m_1 \times J_{max}, where \tag{7a}$$

$$m_1 = \frac{c_i}{c_i + 2 \times \Gamma^*}, \tag{7b}$$

$$J_{max} = n_1 \times N_{leaf}, \tag{7c}$$

$$n_1 = g_{jmax}(T_{air}) \times \beta_{soil}^{ps} \times \beta_{sinklim}^{ps} \times \beta_{soa}^{ps} \times j_{max}^n \times fN_{et} \tag{7d}$$

where c_i is the intercellular partial pressure of CO_2 (Pa, Eq. 17), and Γ^* is the CO_2 compensation point in the absence of dark respiration. $\beta_{sinklim}^{ps}$ is a signal to reduce photosynthesis in the case of C sink limitation (Eq. 43) and β_{soa}^{ps} is accounting

for the effect of low-temperature acclimation in the evergreen species (Eq. 46). Excessive soil moisture stress constraints (as discussed in Rogers et al. (2017)) are assumed to reduce light-saturated photosynthetic activity by:

$$\beta_{soil}^{ps} = 1 - \frac{\Psi_{soil}}{\Psi_{leaf}^{min}}, \tag{8}$$

where Ψ_{soil} is the soil water potential in the root zone (Eq. 121) and Ψ_{leaf}^{min} is the PFT-specific minimum leaf water potential. The temperature sensitivity of electron transport is assumed to follow the bell-shaped form described by June et al. (2004), where T_{jmax}^{opt} is the optimum temperature for J_{max} according to Friend (2010), as follows:

$$g_{jmax}(T_{air}) = e^{-\left(\frac{T_{air}-\bar{T}_{jmax}^{opt}}{T_\Omega}\right)^2}, \tag{9a}$$

$$T_{jmax}^{opt} = k0_{jmax}^{topt} + k1_{jmax}^{topt} \times T_{air}; T_{jmax,min}^{opt} < T_{jmax}^{opt} \leq T_{jmax,max}^{opt}, \tag{9b}$$

where T_Ω is a PFT-specific parameter, $k0_{jmax}^{topt}$ and $k1_{jmax}^{topt}$ are parameters, T_{air} is the air temperature, and $\bar{T}_{jmax}^{opt}$ in Eq. 9 is the mean of the daytime T_{jmax}^{opt} over the past few days (τ_{mavg}^{jmax}), thereby accounting for temperature acclimation of photosynthesis as in Friend (2010).

A_v, the Rubisco-limited rate of photosynthesis, is given by

$$A_v = m_2 \times V_{cmax}, where \tag{10a}$$

$$m_2 = \frac{c_i}{c_i + k_c(1 + O_i/k_o)}, \tag{10b}$$

$$V_{cmax} = n_2 \times N_{leaf} \tag{10c}$$

$$n_2 = f_{vcmax}(T_{air}) \times \beta_{soil}^{ps} \times \beta_{sinklim}^{ps} \times \beta_{soa}^{ps} \times v_{cmax}^n \times fN_{rub} \tag{10d}$$

where O_i is the intercellular partial pressure of O_2, and k_c and k_o are the Michaelis-Menten constants for CO_2 and O_2 respectively, derived E_0^{kc}, E_1^{kc}, or E_0^{ko}, E_0^{ko} using Eq. 6.

The N-specific light-saturated rate of C3 photosynthesis can then be calculated as:

$$m_{sat} = min(n_1 \times m_1, n_2 \times m_2) \tag{11}$$

Friend et al. (2009) adjusted the scheme by Kull and Kruijt (1998) using the Collatz formulation of C4 photosynthesis Collatz et al. (1992). The simplified assumption is that A_j and A_v can be calculated as above, but at saturating c_i ($c_{i,max}$). Bundle-sheath transport limitation (A_p) is then further limiting C4 photosynthesis, given by

$$A_p = V_{pmax} \times m_3, where \tag{12a}$$

$$V_{pmax} = n_3 \times N_{leaf} \tag{12b}$$

$$n_3 = g_{pepc}(T_{air}) \times v_{pepc}^n \times fN_{pepc}, \tag{12c}$$

$$m_3 = \frac{c_i}{p}, \tag{12d}$$

where the temperature response is

$$g_{pepc}(T_{air}) = 2^{(T_{air}-T_{ref}^{pepc})/T_{base}^{pepc}} \tag{13}$$

The N-specific light-saturated rate of C4 photosynthesis can be calculated as

$$m_{sat} = min(n_1 \times m_1, n_2 \times m_2, n_3 \times m_3) \tag{14}$$

The light-harvesting limited rate of photosynthesis (A_h) can be written as

$$A_h = m_1 \times \alpha_i \times PPFD_a, \tag{15a}$$

$$PPFD_a = PPFD_0(1 - e^{-k_a \times C_{chl}}), where \tag{15b}$$

$$C_{chl} = a_{chl}^n \times fN_{chl} \times N_{leaf} \tag{15c}$$

where α_i is the intrinsic quantum efficiency for CO_2 uptake, $PPFD_0$ is the photosynthetic photon flux density (PPFD) penetrating sunlit or shaded foliage, converted from the adsorbed radiation of the canopy layer (Eq. 102), and k_a as well as a_{chl}^n are parameters specified in Table M2.

As Kull and Kruijt (1998) show, this system of equations (Eq. 7-15) can be solved to yield gross photosynthesis (A_g) for one canopy layer and light-class as:

$$A_g = (1 - \frac{\Gamma^*}{c_i})[m_{sat}N_{sat} + \alpha_i PPFD_a(e^{-k_a \times a_{chl}^n \times fN_{chl} \times N_{sat}} - e^{-k_a \times a_{chl}^n \times fN_{chl} \times N_{leaf}}), where \tag{16a}$$

$$for N_{sat} = 0: \; N_{lim} < 0 \tag{16b}$$

$$for N_{sat} = N_{lim}: \; N_{lim} < N_{leaf} \tag{16c}$$

$$for N_{sat} = N_{leaf}: \; N_{lim} \geq N_{leaf}, and \tag{16d}$$

$$N_{lim} = -\frac{ln(m_{sat}/[\alpha_i \times PPFD \times k_a \times a_{chl}^n \times fN_{chl} \times m_1])}{k_a \times a_{chl}^n \times fN_{chl}} \tag{16e}$$

(16f)

M2.3 Stomatal coupling

The combination of leaf-level net photosynthesis ($A_{n,cl}$), stomatal conductance ($g_{s,cl}$), and leaf internal CO_2 concentration ($c_{i,cl}$) satisfying Eq. 17 is sought iteratively for each canopy layer (following broadly Ball et al., 1987):

$$A_n = (A_{g,sunlit} \times f_{sunlit} + A_{g,shaded} \times (1 - f_{sunlit})) - R_l \tag{17a}$$

$$g_s = [g_0 + g_1 \frac{A_n \beta_{air} \beta_{soil}^{gs}}{c_a}] \times R \times T_{air}/p \tag{17b}$$

$$c_i = c_1 \times c_a - c_2 \times A_n \times (\frac{D_{air}^{wv2co2}}{g_s} + \frac{D_{turb}^{wv2co2}}{g_a}) \times R \times T_{air} \tag{17c}$$

where f_{sunlit} is the fraction of sunlit leaves in a canopy layer (see Eq. 101), R_l is the maintenance respiration of leaves (see Sect. M3.2), g_0 and g_1 are PFT-specific parameters, R is the molar gas constant, T_{air} is air temperature (K), p air pressure (Pa), c_1 converts CO_2 concentration from ppm to Pa, c_2 converts $\mu mol m^{-2} s^{-1}$ to $mol m^{-2} s^{-1}$, g_a is the aerodynamic conductance (calculated following Eq. 110), and the D's are the diffusion coefficient corrections for CO_2 and water (Bonan, 2015).

β_{air} is taken as relative humidity (Ball et al., 1987; Knauer et al., 2015) and β^{gs}_{soil} is the stomatal response to soil moisture, described by:

$$\beta^{gs}_{soil} = 1 - \frac{\Psi_{soil}}{\Psi^{min}_{leaf}} \tag{18}$$

where Ψ_{soil} is the soil water potential in the root zone (Eq. 121) and Ψ^{min}_{leaf} is the PFT-specific minimum leaf water potential.

M2.4 Canopy integration

Canopy-level fluxes are derived by summing the product of layer-level fluxes or state-variables and the depth of the layer

$$F = \sum_{cl=1}^{ncanopy} F_{cl} \times LAI_{cl}, \tag{19}$$

where F is the canopy-level equivalent of a leaf-level variable F_{cl} (per unit leaf-area), such as gross photosynthesis (A_g), net photosynthesis (A_n), and leaf-level stomatal conductance (g_s), (see Sect. ?? M2.2 and M2.3) and LAI_{cl} is the leaf area index of the canopy layer. The resulting canopy net assimilation A_g is used as input to the vegetation model (Eq. 20), the canopy conductance (G_s) is used for the calculation of ecosystem transpiration (Eq. 118).

M3 Vegetation growth, turnover and dynamics

M3.1 Labile pool dynamics

The general equation for labile pool dynamics resembles Zaehle and Friend (2010), and similar approaches: growth of a plant is modelled dependent on the partitioning of its labile resource to new tissue growth, storage production, as well as – in the case of C – respiration for maintenance and resource uptake:

$$\frac{dC_{labile}}{dt} = A_g + \Delta S_C - R_m - R_r - (1 + f_{resp,growth}) \times G_C \tag{20a}$$

$$\frac{dN_{labile}}{dt} = U_{root,N} + \Delta S_N - G_N \tag{20b}$$

$$\frac{dP_{labile}}{dt} = U_{root,P} + \Delta S_P - G_P \tag{20c}$$

where R_m is maintenance respiration, R_r is resource uptake respiration (for both see Sect. M3.2), ΔS_X is the net exchange between the labile and reserve pool (Sect. M3.6), $f_{resp,growth}$ is the constant fraction of respiration associated with growth, G_X are the growth rates to build new tissues, $U_{root,X}$ are nutrient rates of root uptake.

M3.2 Maintenance respiration

~~Maintenance respiration~~ Following (Sprugel et al. (1995), as in (Zaehle and Friend, 2010)), maintenance respiration ($R_{m,i}$) for every vegetation pool (i) is estimated from its N content (N_i) as

$$R_{m,i} = f_{temp} \times f^{i}_{resp,maint} \times N_i \tag{21}$$

where $f^{i}_{resp,maint}$ is the maintenance respiration per unit N, which differs between woody and non-woody pools, and f_{temp} is the instantaneous temperature response of respiration (Lloyd and Taylor (1994))

$$f_{temp} = e^{t_{k1}(\frac{1}{t_{k2}} - \frac{1}{T - t_{k3}})} \tag{22}$$

where t_{k1}, t_{k2} and t_{k3} are temperature sensitivity parameters and T is the instantaneous air or soil temperature for above- and belowground tissues, respectively. Following Atkin et al. (2014), the basal respiration rate acclimates to temperature

$$f_{maint\_rate} = f_{maint\_rate\_ref} 10^{f_{resp\_acclim}(T_{acclim} - T_{acclim,ref})} \tag{23}$$

where $f_{maint\_rate,ref}$ is the N-specific maintenance respiration rate at the temperature $T_{acclim,ref}$, f_{resp_acclim} is the slope of the temperature acclimation and T_{acclim} is the running average of air or soil temperature (τ^{resp}_{mavg}), respectively.

Resource uptake respiration for nutrients is given by specific costs ($cost_i$, Zerihun et al. (1998)) to transform nutrients from mineral sources (i) into organic material and the actual plants uptake $U_{plant,i}$ (M4.5) as

$$R_{r,i} = cost_i \times U_{plant,i} \tag{24}$$

where i is either NH_4 or NO_3.

M3.3 Growth

The equations in this section have been developed for the QUINCY model. The potential, source-limited growth rate (G^{*}_{X}) is given by the product of the maximum turnover rate of the labile pool ($1/\tau_{labile}$) and the actual labile pool size (X_{labile}). Three sink limitation processes operate, which control the down-regulation of this potential growth rate to the actual growth rates (G_X):

- the temperature and moisture sensitivity of the meristem (Eq. 25);
- the requirement for maintenance respiration (Eq. 21), which takes priority over new growth; and
- the co-limitation of growth by the nutrients required to grow specific pools (Eq. 28).

The ~~meteorological/environmental~~ temperature and moisture control on the meristem~~mechanism~~, and therefore the growth rate, is represented by a reduction of the maximum turnover rate of the labile pool at low temperatures and low soil moisture conditions.

$$k^{*}_{labile} = \frac{1}{\tau_{labile}} \times e^{-(\lambda^{labile}_{temp} \times T_{air})^{k^{labile}_{temp}}} \times e^{-(\lambda^{labile}_{\Theta} \times \Theta)^{k^{labile}_{\Theta}}} \tag{25}$$

where T_{air} is air temperature in degrees Celsius, Θ is the fractional soil moisture content (Eq. 120), and the λ and k are parameters. k^*_{labile} is set to zero outside the growing season (see Sect. M3.8).

Respiration is assumed to have priority over growth. However, under severe C deficit, the meristem activity also down-regulates maintenance and resource uptake respiration.

To ensure that carbon growth (G_C) does not exceed the size of the labile carbon pool, the turnover rate of the labile pool to growth is corrected by the current respiration rate, and constrained to positive solutions:

$$G^*_C = k^*_{labile} \times C_{labile} \times dt - R_m - R_r; G^*_C \geq 0 \tag{26}$$

Given G^*_C, and the stoichiometric requirements for biomass growth (req^{growth}_{NC}, and req^{growth}_{PN}, respectively):

$$req^{growth}_{XY} = \sum_i^{pools} f^i_{alloc} \times \frac{X_i}{Y_i} \tag{27}$$

where f^i_{alloc} are the allocation fractions (Sect. M3.4) to each pool i, and $\frac{X_i}{Y_i}$ are the target stoichiometries of C:N:P (Sect. M3.5) of the leaf, fine root, coarse root, sapwood, and fruits pools. The actual growth rates can be calculated as

$$G_P = req^{growth}_{N:P} \times G_N = req^{growth}_{P:N} \times req^{growth}_{N:C} \times G_C \tag{28a}$$

$$G_C \leq G^*_C \tag{28b}$$

$$G_N \leq \frac{k^{nut}_{labile}}{\tau_{labile}} \times N_{labile} \times dt \tag{28c}$$

$$G_P \leq \frac{(k^{nut}_{labile})^2}{\tau_{labile}} \times P_{labile} \times dt, \tag{28d}$$

Note that only the minimum of the three rates in eq. 28a can actually be realised. The other two growth rates are adjusted, implying a relative accumulation of these elements in the labile pool. The use of k^{nut}_{labile}, and $(k^{nut}_{labile})^2$ for phosphorus, implies a stronger mobilisation capacity for ~~nutrients than for carbon~~ nitrogen (amino-acids) and phosphorus (a inorganic anion) than for reserve carbon (starch), which requires transformation to be used for growth. The assumption behind this is that the temperature and moisture control of the meristem is already accounted for by G_C, and that the plant is able to mobilise the required nutrients from the labile pool to support this growth.

Outside the growing season, all growth fluxes are set to zero (see Sect. M3.8).

M3.4 Growth partitioning

The labile pool partitioned to growth is first split into reproductive (fruit pool) and structural (leaves, fine and coarse roots and sap wood) growth. ~~The latter is then further subdivided following a functional balance relationship between the structural pools (Zaehle and Friend, 2010).~~

The fraction of carbon growth allocated to fruit depends on the ability of the plant to build reserves (ΔS_C, see Sect. M3.6), implying that fruit growth is suppressed during phases of rapid leaf growth (beginning of the growing season), as well as periods of C starvation (e.g. severe drought).

$$f_{alloc,C}^{fruit} = k1_{alloc}^{fruit} + (k2_{alloc}^{fruit} - k1_{alloc}^{fruit}) \times exp^{-(\lambda_{alloc}^{fruit} \times (\Delta S_C + k3_{alloc}^{fruit}))^{k4_{alloc}^{fruit}}} \quad (29)$$

where the maximum fraction of allocation to fruits ($k2_{alloc}^{fruit}$) is a PFT-specific parameter ~~.~~ (this study).

The allocation of the remaining growth ($(1 - f_{alloc,C}^{fruit}) \times G_C$) to the structural pools leaves, fine root, coarse roots, and sapwood follows a set of following allometric relationships (Zaehle and Friend, 2010).

~~For both trees and grasses, fine root and leaves are assumed to be in homeostatic balance described as~~

$$C_{leaf} = f_{N|P|H_20}^{ltor} \times k_{rtos} \times \frac{C_{leaf}}{C_{sap\_wood}} \times C_{fine\_root}$$

~~where k_{rtos} is a PFT-specific parameter and f^{ltor} is a function describing the response of the leaf to root ratio to nutrient and water limitation. It is calculated as the minimum of three functions describing N, P and water limitation respectively, calculated as:~~

$$f^{ltor} = min(\frac{N_{labile}/C_{labile}}{req_{NC}^{growth}}, \frac{P_{labile}/N_{labile}}{req_{PN}^{growth}}, \frac{W_{soil,root}}{W_{soil,crit}^{alloc}})$$

~~X_{labile} refers to the content of the respective element in the labile pool and req_{NC}^{growth} and req_{PN}^{growth} are the N:C and P:N ratios required for growth, respectively (see eqn. 27). For the water limited allocation, $W_{soil,crit}^{alloc}$ is the critical level of soil moisture below which root allocation increases and $W_{soil,root}$ is calculated as the ratio between the current water content in the root zone and the water content in the root zone at field capacity.~~

In grasses, halms are assumed to be a proportion of leaf mass, and no height restrictions apply.

$$C_{leaf} = k_{htol} \times C_{sap\_wood} \quad (30)$$

In trees and shrubs, leaf and woody biomass are linked through the pipe-model hypothesis (requiring a constant ratio of leaf area, LA, to sapwood area, SA)

$$C_{leaf} = \frac{k_{latosa} \times C_{sap\_wood}}{sla \times \rho_{wood} \times H} <=> LA = k_{latosa} \times SA, \quad (31)$$

where sla, k_{latosa}, and ρ_{wood} are the PFT-specific specific leaf area, leaf to sapwood area ratio, and wood density, respectively. H is the mean forest canopy height calculated as:

$$H = k1_{allom} \times D^{k2_{allom}}, \quad (32)$$

where the diameter at breast height (D) is determined from woody biomass, assuming that the entire trunk is a cylinder. As an extension to the pipe-model theory below-ground, coarse root biomass is assumed to be proportional to sap wood mass:

$$C_{coarse\_root} = k_{ctos} \times C_{sap\_wood} \tag{33}$$

where k_{ctos} is a PFT-specific parameters.

For both trees and grasses, fine root and leaves are assumed to be in homeostatic balance between transpiring leaf surface and root mass

$$C_{leaf} = f^{ltor} \times k_{rtos} \times \frac{k_{latosa}}{sla \times \rho_{wood}} \times C_{fine\_root} \tag{34}$$

where k_{rtos}, sla, k_{latosa}, and ρ_{wood} are PFT-specific parameters. f^{ltor} is the long-term average (τ^{alloc}_{mavg}) of the nutrient and water limitation scalar, which represents the widely observed phenomenon of increased root allocation with water or nutrient shortage and is calculated here as the minimum of three functions describing N, P and water limitation respectively, calculated as:

$$f^{ltor} = min(\frac{N_{labile}/C_{labile}}{req^{growth}_{NC}}, \frac{P_{labile}/N_{labile}}{req^{growth}_{PN}}, \frac{W_{soil,root}}{W^{alloc}_{soil,crit}}) \tag{35}$$

X_{labile} refers to the content of the respective element in the labile pool and req^{growth}_{NC} and req^{growth}_{PN} are the N:C and P:N ratios required for growth, respectively (see eqn. 27). For the water limited allocation, $W^{alloc}_{soil,crit}$ is the critical level of soil moisture below which root allocation increases and $W_{soil,root}$ is calculated as the ratio between the current water content in the root zone and the water content in the root zone at field capacity.

M3.5 Tissue stoichiometry

Following Meyerholt and Zaehle (2015), C:N:P stoichiometry for slow-overturning structural tissues (sap wood, coarse roots) as well as fruits, is assumed to be time-invariant and modelled as dependent on the PFT-specific mean foliar stoichiometry ($\chi^{C:N}_{leaf}$, and $\chi^{N:P}_{leaf}$) and set ratios (see Table M3). Heartwood stoichiometry differs from sapwood stoichiometry because a fraction of the nutrients are retranslocated (k^{wood}_{resorb}) to the labile pool upon heartwood formation.

Following Zaehle and Friend (2010), the C:N and N:P ratios of leaves are varied in response to the nutrient demand and supply so that:

$$\chi^{X:Y}_{leaf|t+1} = \chi^{X:Y}_{leaf} \times (1 + \delta^{\chi}_{leaf} \times \Gamma_{XY}) \tag{36}$$

where $\chi_{leaf}^{X:Y}$ denotes either the C:N or N:P ratio of the leaves, δ_{leaf}^{χ} is a parameter denoting the maximum amount that leaf nutrients can change per timestep and $\Gamma_{X:Y}$ heuristically accounts for limits to the plasticity of foliar stoichiometry as:

$$\Gamma_{X:Y} = \begin{cases} e^{-(\lambda_{leaf}^{\chi} \frac{\chi_{leaf}^{X:Y}}{\chi_{leaf,min}^{X:Y} + \chi_{leaf,max}^{X:Y}})^{k_{leaf}^{\chi}}} & \text{if } \chi_{labile}^{Y:X} \leq req_{Y:X}^{growth} \\ -(1 - e^{-(\lambda_{leaf}^{\chi} \frac{\chi_{leaf}^{X:Y}}{\chi_{leaf,min}^{X:Y} + \chi_{leaf,max}^{X:Y}})^{k_{leaf}^{\chi}}}) & \text{if } \chi_{labile}^{Y:X} > req_{Y:X}^{growth} \end{cases} \tag{37}$$

In the above, $\chi_{leaf,min}^{X:Y}$ and $\chi_{leaf,max}^{X:Y}$ are PFT-specific parameters. The λ_{leaf}^{χ} and k_{leaf}^{χ} are parameters (Tab. M3) The condition refers to the relationship between the nutrients available for growth in the labile pool and the nutrients required for growth (Eq. 27), averaged at the time-scale of τ_{mavg}^{χ}. The stoichiometric ratios of the fine roots vary proportionally to those of the leaves, whereas the stoichiometry of wood is assumed time-invariant (Meyerholt and Zaehle, 2015). The stoichiometry of the labile and reserve pools are prognostic properties, as described in Sect. M3.6.

M3.6 Long-term reserve dynamics

While labile-reserve dynamics have been part of the OCN model (Zaehle and Friend, 2010), the underlying equations have been reworked to increase robustness and traceability. The target leaf carbon pool (C_{leaf}^{target}) is determined by the current allometry, and corresponds to the leaf area index implied by current sapwood area.

The target labile carbon pool size buffers short term fluctuations in GPP, and is assumed to correspond to the maximum of the cumulated GPP or R_m over the turnover time of the labile pool, while the target of the labile nitrogen and phosphorus pool corresponds to the average stoichiometric growth requirement over the turnover time of the labile pool:

$$C_{labile}^{target} = max(\int_{t=-\tau_{labile}^{0}}^{t=0} GPP \times dt, \int_{t=-\tau_{labile}^{0}}^{t=0} R_m \times dt) \tag{38a}$$

$$N_{labile}^{target} = req_{NC}^{growth} \times C_{labile}^{target} \tag{38b}$$

$$P_{labile}^{target} = req_{PN}^{growth} \times N_{labile}^{target} \tag{38c}$$

The target size of the reserve pool depends on the C required to replace the annual growth of leaves and fine roots. It is scaled by a PFT-specific constant as a measure of risk avoidance ($k_{reserve}^{target}$), with larger values indicating a preference for storage over growth.

$$C_{reserve}^{target} = min(k_{reserve} \times (1 + f_{resp,growth}) \times \frac{LAI^{target}}{sla}, \sum_{i=l,f,s} f_{reserve,max,i} \times C_i), where \tag{39a}$$

$$k_{storereserve} = k_{reserve}^{target} \times (min(1, \frac{1}{\tau_{leaf}}) + \frac{1}{\tau_{fine\_root} \times R_{leaf:fine\_root}}) \tag{39b}$$

where LAI^{target} is the target leaf area index, which is constrained to values below LAI_{max}^{target} (see Sect. M3.4) and sla the PFT-specific specific leaf area, τ_{leaf} and τ_{fine_root} are the PFT-specific turnover times of foliage and fine roots, and

$R_{leaf:fine\_root}$ is the leaf to root ratio (Eq. 35) averaged over the lifetime of the fine roots (τ^{root}_{mavg}). The N and P target pools are defined in an equivalent manner, respecting the current target stoichiometry of leaves and fine roots (Sect. M3.5).

The net exchange between the labile and reserve pool is calculated as

$$\Delta S_X = \frac{1}{\tau_{labile}} \times (\Phi^X_{maint} \times X_{reserve} - \Phi^X_{store} \times X_{labile}) \times dt; with \tag{40a}$$

$$\Phi^X_{maint} = e^{-(\lambda^{\Phi}_{maint} \times \frac{X_{labile}}{X^{target}_{labile}})^{k^{\Phi}_{maint}}}, and \tag{40b}$$

$$\Phi^X_{store} = 1 - e^{-(\lambda^{\Phi}_{store} \times \frac{X_{reserve}}{X^{target}_{reserve}})^{k^{\Phi}_{store}}} \tag{40c}$$

where λ^{Φ}_{maint}, k^{Φ}_{maint}, λ^{Φ}_{store}, and k^{Φ}_{store} are parameters of a Weibull-type function. Under conditions of severe resource stress (i.e. low labile pool size corresponding to its target size), the build up of reserves, is reduced according to

$$\Phi^X_{store} = \frac{1 - \Phi^X_{maint}}{1 - k_{\Phi,inter}} \Phi^X_{store},\ if\ \Phi^X_{maint} > k_{\Phi,inter} \tag{41}$$

where $k_{\Phi,inter}$ is a parameter. To support leaf and fine-root growth at the beginning of the growing season, ΔS_X is further modified by the phenological pull (Φ^X_{phen}) during the growing season as follows:

$$\Delta S_X = \Delta S_X + k^*_{labile} \times \Phi^X_{phen} \times X_{reserve} \times dt, with \tag{42a}$$

$$\Phi^X_{phen} = e^{-(\lambda^{\Phi}_{phen} \times \frac{X_{leaf}}{X^{target}_{leaf}})^{k^{\Phi}_{phen}}} \tag{42b}$$

where λ^{Φ}_{phen}, and k^{Φ}_{phen} are parameters of a Weibull-type function.

M3.7 Photosynthetic sink limitation

~~In the case that~~ The observation that growth and photosynthesis may differ in their response to environmental stressors (Hartmann et al., 2018) is considered in QUINCY such that in case the labile carbon pool exceeds its target size substantially because growth is limited by temperature, moisture, or because sufficient nutrients are lacking to allow growth (Eq. 28a), sink-limitation down-regulates photosynthetic activity so that:

$$\beta^{ps}_{sinklim} = \beta^{ps}_{sinklim,min} + (1 - \beta^{ps}_{sinklim,min}) \times e^{-(\lambda^{ps}_{sinklim} \times X)^{k^{ps}_{sinklim}}}, where \tag{43a}$$

$$X = \frac{C_{labile} - C^{target}_{labile}}{C^{target}_{labile}} \tag{43b}$$

Here, $\beta_{sinklim,min}$, $\lambda^{ps}_{sinklim}$ and $k^{ps}_{sinklim}$ are parameters (see Table M3) and C^{target}_{labile} is the target value for the labile pool (Eq. 38).

In addition, if the C:N or N:P ratios of the labile pool exceed those of the target labile pool, indicating strong nutrient stress, the sink limitation factor is further modified as a function of the stoichiometric ratio of the labile pool and that of the labile target as:

$$\beta^{ps}_{sinklim} = \beta^{ps}_{sinklim} \times min(1, \frac{\chi^{N:C}_{labile}}{k^{CNP}_{sinklim} \times \chi^{N:C}_{labile,target}}, \frac{\chi^{P:N}_{labile}}{k^{CNP}_{sinklim} \times \chi^{P:N}_{labile,target}}) \quad (44)$$

where $k^{CNP}_{sinklim}$ is a parameter.

M3.8 Phenology

The phenology of vegetation, describing the seasonal development of foliage biomass, is simulated prognostically given the ability of the plant to grow new tissues, which depends on the size and turnover of the meristems (Eq. 28), as well as the fractional allocation of growth to plant organs (see Sect. M3.3). The start and end of the the growing season are determined by meteorological triggers and soil moisture, with plant growth set to zero outside the growing season (Eq. 28). The meteorological variables determining these phenological triggers are averaged over τ^{phen}_{mavg}, to smooth out the effect of day-to-day climate variability. While the beginning and ending mark the start and end of tissue production, only the turnover of the leaves is directly affected by phenological triggers. The turnover of all other tissues is assumed to be constant (see Sect. M3.9).

The model differentiates evergreen, cold deciduous, rain deciduous tree and shrub phenological strategies, as well as herbaceous perennial phenological strategies.

The growing season start for cold deciduous and herbaceous PFTs is described as a function of the accumulated growing degree days (GDD_{acc}) as:

$$GDD_{acc} > GDD^{max}_{req} \times exp^{-k^{GDD}_{dormance} \times NDD}, where \quad (45a)$$

$$\frac{GDD_{acc}}{dt} = GDD_{acc} + MAX(t_{air} - t^{GDD}_{tair}, 0.0) \quad (45b)$$

where GDD_{acc} denotes the current growing degree days above the temperature threshold (t^{GDD}_{air}) since the last beginning of dormancy, NDD is the number of dormancy days, taken as days since the last growing season, and $k^{GDD}_{dormance}$ is a PFT-specific parameter relating dormancy to the PFT-specific maximum growing degree days requirement (GDD^{max}_{req}) to account for the chilling requirements of the buds (Krinner et al., 2005), and dt denotes time-step in days.

For rain deciduous phenology, the start of the growing season is triggered when the soil moisture stress factor (β^{gs}_{soil}, see Eq. 18) is larger than a PFT-specific threshold (β^{flush}_{soil}). This criterion is also applied for herbaceous PFTs in addition to the GDD-criterion.

~~For the evergreen phenology, recovery of photosynthesis in spring is delayed according to the state of acclimation (S) to air temperature, which reduces photosynthesis in spring until acclimation is reached (Mäkelä et al., 2004). S is calculated as~~

$$\frac{dS}{dt} = \frac{1}{\tau_{soa}}(T_{air} - S)$$

,

where τ_{soa} is a time constant. The reduction factor for Rubisco- and electron transport limited photosynthesis (β_{soa}) is calculated as

$$\beta_{soa} = \frac{(S - T^{soa}_{min})}{(T^{soa}_{max} - T^{soa}_{min})}$$

where T^{soa}_{min} and T^{soa}_{max} are parameters and β_{soa} is constrained to the range 0.1 and 1.

The end of the growing season for cold deciduous and herbaceous PFTs is triggered by decreasing average air temperatures below a PFT-specific temperature threshold (t^{sen}_{air}). For raingreen and herbaceous PFTs the end of the growing season is triggered when the soil moisture stress factor (β^{gs}_{soil}) becomes lower than a PFT-specific threshold (β^{sen}_{soil}). In addition, herbaceous PFTs end their growing season, once the weekly carbon balance ($GPP - R_m$) becomes negative. Senescence is generally only introduced once the leaf age has become larger than a PFT-specific threshold (age^{leaf}_{min}).

For the evergreen phenology, recovery of photosynthesis in spring is delayed according to the state of acclimation (S) to air temperature, which reduces photosynthesis in spring until acclimation is reached (Mäkelä et al., 2004). S is calculated as

$$\frac{dS}{dt} = \frac{1}{\tau_{soa}}(T_{air} - S) \tag{46}$$

,

where τ_{soa} is a time constant. The reduction factor for Rubisco- and electron transport limited photosynthesis (β_{soa}) is calculated as

$$\beta_{soa} = \frac{(S - T^{soa}_{min})}{(T^{soa}_{max} - T^{soa}_{min})} \tag{47}$$

where T^{soa}_{min} and T^{soa}_{max} are parameters and β_{soa} is constrained to the range 0.1 and 1. S is updated according to this equation starting from a set initial value.

M3.9 Turnover

~~The~~ As in OCN (Zaehle and Friend, 2010), the breakdown of leaf and fine-root nutrients occurs at the time-scale of $\tau_{nut\_recycle}$. The freed nutrients enter the labile pool and are replaced by new nutrients of the labile pool according to the current target C:N:P of the respective pool.

$$\frac{X_{pool}}{dt} = (Y_{pool}\frac{X_{pool}^{target}}{Y_{pool}^{target}} - X_{pool}) \times 1/\tau_{nut\_recycle}, \tag{48}$$

where X is either N or P, and Y C or N, respectively. The flux from the labile pool is limited by the turnover rate and size of the labile pool to ascertain that the latter cannot be exhausted.

The turnover time of most tissue types (fine and coarse roots, sapwood, and fruits) is assumed constant for each PFT (τ_{fine_root}, τ_{coarse_root}, τ_{sap_wood}, and τ_{fruit}, respectively). ~~While roots and fruit~~ The fruit pool is turning into seed bed pool, which is either used for re-establishment of new seedlings or turned over to form litter. While roots turn directly into litter, only a small fraction of sapwood ($f_{sap\_wood}^{branch}$) is turned to litter, assuming it is lost as branches ($\tau_{branches}$), whereas the predominant fraction of sapwood turns into non-respiring hardwood at the timescale of τ_{sap_wood}. In evergreen trees, foliar turnover to litter is assumed to be constant (τ_{leaves}). For deciduous and herbaceous PFTs only minor turnover happens at τ_{leaves} during the growing season. At the end of the growing season (see Sect. M3.8), foliar turnover is set to a constant rate

$$f_{turn}^{leaf} = min(f_{shed,max} \times \frac{LAI^{target}}{LAI}, 1) \tag{49}$$

Resorption of nutrients to the labile pool during litterfall is assumed to only occur during foliage turnover ~~and heartwood formation~~ (leaf scenescence) and the conversion from life sap-wood to dead heartwood (see for instance data in White et al., 2000) at a constant fraction (k_{resorb}^{X}), whereas fine root turnover is assumed to be dominated by predation and therefore no nutrient resorption is assumed to occur. so that:

$$flux_{pool\rightarrow litter}^{X} = (1 - k_{resorb}^{X}) \times \frac{X_{pool}}{\tau_{pool}} \times dt, and \tag{50a}$$

$$flux_{pool\rightarrow labile}^{X} = k_{resorb}^{X} \times \frac{X_{pool}}{\tau_{pool}} \times dt, \tag{50b}$$

where $flux_{pool\rightarrow litter}^{X}$ is the litterfall from any one pool, and $flux_{pool\rightarrow labile}^{X}$ the retranslocated flux into the labile pool.

M3.10 Vegetation dynamics

Vegetation dynamics follow largely Sitch et al. (2003). To assess stand density, we define for tree functional types the crown area as:

$$CA = k_{CA} \times D^{k_{rp}} \tag{51}$$

where k_{CA} and k_{rp} are parameters, D is the tree diameter at breast hight and CA is constrained to be less then a maximum crown area (CA_{max}). Using stand-scale LAI, individuum density ($dens_{ind}$, see Eq. 58) and crown area, the LAI of an individual tree is defined (LAI_{ind}), which is used to ~~calculated~~ calculate the foliage projective cover (FPC) as:

$$FPC = CA \times dens_{ind}(1 - e^{-k_{fpc} \times LAI_{ind}}) \tag{52}$$

where k_{fpc} is a ~~paramter~~parameter. To avoid strong seasonal cycles in foliage projective cover for the calculation of vegetation dynamics (Krinner et al., 2005; Zaehle and Friend, 2010), LAI_{ind} is diagnosed from the sapwood area implied by the pipe-model (Eq. 31), implying that FPC is essentially representing last year's maximum LAI. For grasses, the calculation of FPC is not required and it is set to zero.

~~The~~ Differently to Sitch et al. (2003) and Zaehle and Friend (2010), the establishment flux for a PFT is dependent on the size of the seed-bed pool~~and the~~, which itself is dependent on the turnover of the fruit pool, and an average, PFT-specific seed-bed turnover time ($\tau_{seed,est}$)~~:~~. The motivation for this change is that this allows to close the carbon and nutrient budgets during re-establishment and avoids the addition of extra mass during re-establishment of a population.

$$flux_{est,X} = f_{dens} \times f_{temp} \times f_{moist} \times \frac{X_{seed\_bed}}{\tau_{seed,est}} \tag{53}$$

where f_{temp} and f_{moist} represent limitations for establishment at low temperature and low moisture availability in the form of Weibull-functions with parameters λ_{est}^{env} and k_{est}^{env}, where env refers to either weekly air temperature (T_{air}) or weekly top-soil moisture (Θ_1). Density dependency of establishment (f_{dens}) is modelled as in Sitch et al. (2003):

$$f_{dens} = MAX(FPC_{max} - FPC, 0) \tag{54}$$

Three types of mortality are considered as additive processes, growth-efficiency related mortality ($mort_{greff}$), density dependent mortality ($mort_{dens}$), and a PFT-specific background mortality, representing currently unaccounted for processes such as disturbance or grazing.

$$f_{mort} = MIN(mort_{greff} + mort_{dens} + mort_{bg,PFT}, 1) \tag{55}$$

Growth-efficiency mortality, represents any kind of mortality associated with trees lacking the ability to defend themselves against stress (e.g. pathogens) and is calculated as:

$$mort_{greff} = \frac{k1_{mort\_greff}}{1 + k2_{mort\_greff} \times eff_{growth}}, where \tag{56a}$$

$$eff_{growth} = \frac{NPP - \sum Turnover_i}{LAI} \tag{56b}$$

where, as in Sitch et al. (2003), $k1_{mort\_greff}$ and $k2_{mort\_greff}$ are parameters and growth efficiency depends on net primary production minus tissue turnover (of all tissues i) per unit leaf area, calculated as running means over $\tau_{mavg}^{dynamics}$.

Space constraints in tree populations (as for grasses FPC is zero) are considered by constraining the foliage projected cover to a prescribed maximum (FPC_{max}):

$$mort_{dens} = MAX(FPC - FPC_{max}, 0) \tag{57}$$

Litterfall from vegetation dynamics is then the product of the current pool size and f_{mort}, scaled to the timestep of the model.

For trees, the appropriate number of individuals is also removed following mortality. This does not affect the size of trees, as woody biomass and stand density are modified proportionally. On the other hand, during establishment the total pool size increases, as mass is added to the labile pools, but the average size of individuals decreases due to the added number of (small) individuals. In total, the change in vegetation individual density following establishment and mortality is written as:

$$\frac{dens_{ind}}{dt} = f_{mort} \times dens_{ind} + \frac{flux_{est,C}}{k_{seed}} \tag{58}$$

where $flux_{est,C}$ is the carbon flux defined by Eq. 53, and k_{seed} is the PFT-specific seed size.

M4 Soil biogeochemistry

The dynamics of the soil organic pools (~~X) are~~ X_i; i = met (metabolic litter), str (structural litter), wl (woody litter), fast, slow; see Section M4.3) are structurally simplified from Parton et al. (1993), but applied here for a vertically explicit soil including a vertical transport term and are described in general as:

$$\frac{\partial}{\partial t}X_{met} = \sum(f_{vp\rightarrow met}F_{L_{vp}}) + f_{wl\rightarrow met}\eta_{wl\rightarrow met}\frac{X_{wl}}{\tau_{wl}} - \frac{X_{met}}{\tau_{met}} \tag{59a}$$

$$\frac{\partial}{\partial t}X_{str} = \sum(f_{vp\rightarrow str}F_{L_{vp}}) + f_{wl\rightarrow str}\eta_{wl\rightarrow str}\frac{X_{wl}}{\tau_{wl}} - \frac{X_{str}}{\tau_{str}} \tag{59b}$$

$$\frac{\partial}{\partial t}X_{wl} = \sum(f_{vp\rightarrow wl}F_{L_{vp}}) - \frac{X_{wl}}{\tau_{wl}} \tag{59c}$$

$$\frac{\partial}{\partial t}X_{fast} = \eta_{l\rightarrow fast}(\frac{X_{met}}{\tau_{met}} + \frac{X_{str}}{\tau_{str}}) + \eta_{slow\rightarrow fast}\frac{X_{slow}}{\tau_{slow}} - \frac{X_{fast}}{\tau_{fast}} + \Phi_{l\rightarrow fast} + \Phi_{slow\rightarrow fast} + \frac{\partial}{\partial z}(D_b\frac{\partial X_{fast}}{\partial z}) \tag{59d}$$

$$\frac{\partial}{\partial t}X_{slow} = \eta_{fast\rightarrow slow}\frac{X_{fast}}{\tau_{fast}} - \frac{X_{slow}}{\tau_{slow}} + \Phi_{fast\rightarrow slow} + \frac{\partial}{\partial z}(D_b\frac{\partial X_{slow}}{\partial z}) \tag{59e}$$

where $F_{L_{vp}}$ is the litterfall of the various plant tissue types, $f_{vp\rightarrow i}$ are the coefficients determining the partitioning of this litterfall to the litter pools (see Section M4.1), τ_i are temperature and moisture adjusted, nitrogen-limited turnover times of the respective pools (X; i = met ~~, str, wl~~(metabolic litter), str (structural litter), wl (woody litter), fast, slow; see Section M4.3)~~,~~. In the following sections we refer to the fast pool as the microbial pool, as while microbes are not explicitly modelled in the

current model version, the fast pool is meant to largely represent the microbial pool. $\eta_{i\rightarrow j}$ are the mass transfer from pool i to j (see Section M4.3), the Φ_x are the net mineralisation terms for N and P, respectively, required to balance the carbon inflow to the fast and slow SOM pools and their respective C:N:P stoichiometry (see Sect. M4.3). The transfer of soil organic matter through bioturbation is represented with a prescribed diffusion constant (see Sect. M4.4).

The dynamics of the inorganic nitrogen pools ~~are described as~~generally follow Zaehle and Friend (2010, but with updated process formul
are given by:

$$\frac{\partial}{\partial t}NH_4 = F_{dep,NH_4} - U_{plant,NH_4} - \sum(\Phi_{i,NH_4}) - U_{nit} - \frac{\partial v_{NH_4} NH_4}{\partial z} \tag{60a}$$

$$\frac{\partial}{\partial t}NO_3 = F_{dep,NO_3} + F_{nit,NO3} - U_{plant,NO_3} - \sum(\Phi_{i,NO_3}) - U_{denit} - \frac{\partial v_{NO_3} NO_3}{\partial z} \tag{60b}$$

$$\frac{\partial}{\partial t}NO_y = F_{nit,NO_y} + F_{denit,NO_y} - E_{NO_y} \tag{60c}$$

$$\frac{\partial}{\partial t}N_2O = F_{nit,N_2O} + F_{denit,N_2O} - E_{N_2O} \tag{60d}$$

$$\frac{\partial}{\partial t}N_2 = F_{nit,N_2} + F_{denit,N_2} - E_{N_2} \tag{60e}$$

where U are the uptake rates of plants, or (de-)nitrifying bacteria, respectively (see Section M4.5 and M4.7, respectively); the F_{dep} are the atmospheric deposition fluxes; the $F_{nit,i}$, and $F_{denit,i}$ are the production of NO_y, N_2O and N_2 by nitrification and denitrification, respectively; ~~,~~and $\frac{\partial v_x X}{\partial z}$ the vertical transport loss term given by the product of ion concentration and water mass flow between soil layers (see Sect. M6.3). Sorption of NH_4 is not explicitly modelled, and is accounted for by a reduced mobility in water (f_{leach,NH_4}).

The dynamics of the inorganic phosphorus pools generally follows Wang et al. (2010) are described as:

$$\frac{\partial}{\partial t}PO_4 = F_{dep,PO_4} + F_{weath,PO_4} + F_{biomin,PO_4} - U_{plant,PO_4} - F_{adsorp,PO_4} - \sum(\Phi_{i,PO_4}) - \frac{\partial v_{PO_4} PO_4}{\partial z} \tag{61a}$$

$$\frac{\partial}{\partial t}P_{lab} = F_{adsorp,PO_4} - F_{desorp,PO_4} + \frac{\partial}{\partial z}(D_b \frac{\partial P_{lab}}{\partial z}) \tag{61b}$$

$$\frac{\partial}{\partial t}P_{sorb} = F_{desorp,PO_4} - F_{occlusion,PO_4} + \frac{\partial}{\partial z}(D_b \frac{\partial P_{sorb}}{\partial z}) \tag{61c}$$

$$\frac{\partial}{\partial t}P_{ocl} = k_{ocl} P_{sorb} + \frac{\partial}{\partial z}(D_b \frac{\partial P_{ocl}}{\partial z}) \tag{61d}$$

$$\frac{\partial}{\partial t}P_{primary} = -F_{weath,PO_4} \tag{61e}$$

where P_{lab}, P_{sorb}, P_{ocl}, and $P_{primary}$ are labile, absorbed, occluded, and primary P, respectively; the F_{dep,PO_4}, F_{weath,PO_4}, F_{biomin,PO_4}, F_{adsorp,PO_4}, and F_{adsorp,PO_4} are the atmospheric deposition, weathering, fast adsorption, and phosphorus fluxes, respectively (see Section M4.8). All pools except the primary phosphorus pool are assumed to be affected by bioturbation (see Sect. M4.4).

M4.1 Partitioning of litterfall to litter pools

Non-woody litterfall is partitioned to the metabolic and structural litter according to the CENTURY approach (Parton et al., 1993). Litter from labile and reserve pools is assumed to enter the metabolic pools, litter from sap- and heartwood enters the

woody pool. The metabolic fraction of litterfall from each vegetation pool ($_{vp}$, i.e. leaves, fine and coarse roots, fruits and seed-bed) is determined as:

$$f_{vp\rightarrow met,C} = f_{met,max,C} - k_{met,C} \times LC_{vp} \frac{C_{vp}}{N_{vp}} \tag{62}$$

where $f_{vp\rightarrow met,C}$ is constrained to positive solutions, $f_{met,max,C}$ is the maximum fraction allocated to the metabolic pool, $k_{met,C}$ a factor relating the metabolic litter fraction to the lignin to nitrogen ratio, LC_{vp} the tissue-specific fraction of the lignin content of that tissue type, and $\frac{C_{vp}}{N_{vp}}$ the C:N ratio of litterfall from that tissue. The lignin content is assumed constant for all but the leaf tissues. For the latter, an empirical dependency between lignin content and specific leaf-area (sla) is used (White et al., 2000).

$$LC_{leaf} = LC_{leaf,max} + k_{leaf2sla} \times sla \tag{63}$$

The remainder of litterfall is allocated to the structural pool. For N and P, the partitioning assumes that the relative proportions of C:N and N:P are preserved in the partitioning according to:

$$f_{vp\rightarrow met,X} = \frac{1}{1 + \frac{1-f_{vp\rightarrow met,C}}{k_{met,vp,X} \times f_{vp\rightarrow met,C}}} \tag{64}$$

~~Woody~~ Contrary to versions of the CENTURY model, woody decomposition is assumed to be a two-stage process to account for the large fraction of CO_2 loss during woody decomposition. The first step implies physical destabilisation and a first level of biochemical processing, which releases a constant fraction of carbon (1 - $\eta_{C,wl\rightarrow met,str}$) to heterotrophic respiration. During this step, a fraction of the nutrients (1 - $\eta_N|\eta_P$) is leached to the mineral phase to account for inefficiencies of the microbiota in mineral processing decomposing wood. The ~~remainder~~ remaining destabilised woody material ($\eta_{C,wl\rightarrow met,str}$) is assumed to enter the metabolic and structural litter (Eq. 62 and 64) and is then decomposed as such.

M4.2 SOM and litter turnover rates

The turnover times (τ_i^{base}) of the litter and SOM pools respond to soil temperature (T_{soil}) ~~and~~ following a peaked Arrhenius function (with parameters for the activation ($E_{a,decomp}$) and de-activation ($E_{d,decomp}$) of soil organic matter decomposition, see Tab. M4), and the soil matrix potential (Ψ_{soil}) as follows:

$$\tau_i^* = \tau_i^{base} \times f(T_{soil}) \times g(\Psi_{soil}),\ where \tag{65a}$$

$$f(T_{soil}) = \frac{E_{d,decomp} \times e^{E_{a,decomp} \times T}}{E_{d,decomp} - E_{a,decomp} \times (1 - e^{E_{d,decomp} \times T})},\ with \tag{65b}$$

$$T = \frac{T_{soil} - T_{opt,decomp}}{T_{soil} \times T_{opt,decomp} \times R},\ and \tag{65c}$$

$$g(\Psi_{soil}) = 1 - \Psi_{soil}/\Psi_{dec,min} \tag{65d}$$

M4.3 SOM formation

Matter entering the fast and slow SOM pool (Eq. 59) is required to fulfill the prescribed stoichiometry of the SOM pools (χ_{SOM}). These are assumed constant with the exception of the fast SOM C:N ratio, which varies with available NH_4 following

CENTURY (Parton et al., 1993):

$$\chi_{SOM_{fast}^{C:N}} = MAX(\chi_{SOM_{fast,max}^{C:N}} - f_\chi \times NH_4, \chi_{SOM_{fast,min}^{C:N}}) \tag{66}$$

where $\chi_{SOM_{fast,min}^{C:N}}$, $\chi_{SOM_{fast,max}^{C:N}}$ and f_χ are parameters.

The difference in stoichiometry of the matter entering the pool and the required stoichiometry of the pool leads to the estimate of the potential immobilisation flux:

$$\Phi^*_{l\rightarrow fast,NH_4} = \frac{\eta_{C,litter\rightarrow fast}}{\chi_{SOM_{fast}^{C:N}}}\left(\frac{C_{met}}{\tau^*_{met}} + \frac{C_{str}}{\tau^*_{str}}\right) - \eta_N\left(\frac{N_{met}}{\tau^*_{met}} + \frac{N_{str}}{\tau^*_{str}}\right) \tag{67}$$

where τ^*_i are the temperature and moisture constrained turnover times (Eq. 65).

The actual immobilisation rate ($\Phi_{l\rightarrow fast,NH_4}$) is limited to the amount of ammonium (NH_4 available, subject to co-occurring potential N uptake from plants ($U^*_{NH_4,plant}$, Eq. 73), and nitrifiers (U^*_{nit}; Eq. 76). Note that, similar as for the plant uptake, the uptake of ammonium is limited ~~with~~ by Michaelis-Menten kinetics to account for reduced accessibility of N at very low values.

$$\Phi_{l\rightarrow fast,NH_4} = \frac{NH_4}{max(NH_4,\, U^*_{NH_4,plant} + U^*_{nit} + \Phi^*_{l\rightarrow fast,NH_4})} \times \Phi^*_{l\rightarrow fast,NH_4} \tag{68}$$

In the case that the amount of available nitrogen ($\Phi_{l\rightarrow fast,NH_4}$) is insufficient to ensure that the newly formed fast SOM has a C:N ratio of $\chi_{SOM_{fast}^{C:N}}$, the turnover times of the metabolic and structural litter pool ~~is increasedto match the N available for immobilisation~~ are increased, leading to a reduced decomposition rate of litter and therefore a reduced immobilisation requirement for litter decomposition (Parton et al. (1993)):

$$\tau_{met|str} = \tau^*_{met|str} \frac{\frac{\eta_{l\rightarrow fast,C}}{\chi_{SOM_{fast}^{C:N}}}\left(\frac{C_{met}}{\tau^*_{met}} + \frac{C_{str}}{\tau^*_{str}}\right) - \eta_N\left(\frac{N_{met}}{\tau^*_{met}} + \frac{N_{str}}{\tau^*_{str}}\right)}{\Phi_{l\rightarrow fast,NH_4}} \tag{69}$$

Should the available NH_4 be insufficient to maintain the uptake rates of plants (Eq. 73) and nitrifiers (Eq. 76), these fluxes are downregulated in proportion.

The potential immobilisation flux of phosphorus ($\Phi^*_{P,l\rightarrow fast}$) is defined in a similar manner as potential NH_4 immobilisation, but now considering the actual turnover time of the litter pools:

$$\Phi^*_{P,l\rightarrow fast} = \frac{\eta_{C,litter\rightarrow fast}}{\chi_{SOM_{fast}^{C:N}}\chi_{SOM_{fast}^{N:P}}}\left(\frac{C_{met}}{\tau_{met}} + \frac{C_{str}}{\tau_{str}}\right) - \eta_P\left(\frac{P_{met}}{\tau_{met}} + \frac{P_{str}}{\tau_{str}}\right) \tag{70a}$$

$$\Phi_{P,l\rightarrow fast} = \frac{PO_4}{max(PO_4,\, U^*_{PO_4,plant} + \Phi^*_{P,l\rightarrow fast})} \times \Phi^*_{P,l\rightarrow fast} \tag{70b}$$

Because the C:N:P stoichiometry and uptake use-efficiencies are organised such that decomposition of these pools is always leading to net mineralisation of nutrients, the $\Phi_{slow\rightarrow fast}$ values are negative and do not require special treatment to affect the carbon-use efficiency or turnover rates (i.e. $\tau_{fast} = \tau^*_{fast}$, and $\tau_{slow} = \tau^*_{slow}$). The processing of fast and slow SOM is

assumed to also include higher-order trophic levels of heterotrophic respiration Parton et al. (1993), therefore only a fraction of the respired material ($\eta_{C,fast\rightarrow slow}$ and $\eta_{C,slow\rightarrow fast}$) is assumed to enter the subsequent pool:

$$\Phi_{fast\rightarrow slow,NH_4} = \frac{\frac{\eta_{C,fast\rightarrow slow}}{\chi_{SOM^{C:N}_{slow}}} C_{fast} - N_{fast}}{\tau_{fast}} \tag{71a}$$

$$\Phi_{slow\rightarrow fast,NH_4} = \frac{\frac{\eta_{C,slow\rightarrow fast}}{\chi_{SOM^{C:N}_{fast}}} C_{slow} - N_{slow}}{\tau_{slow}} \tag{71b}$$

$$\Phi_{fast\rightarrow slow,PO_4} = \frac{\frac{\eta_{C,fast\rightarrow slow}}{\chi_{SOM^{C:N}_{slow}} \chi_{SOM^{N:P}_{slow}}} C_{fast} - P_{fast}}{\tau_{fast}} \tag{71c}$$

$$\Phi_{slow\rightarrow fast,PO_4} = \frac{\frac{\eta_{C,slow\rightarrow fast}}{\chi_{SOM^{C:N}_{fast}} \chi_{SOM^{N:P}_{fast}}} C_{slow} - P_{slow}}{\tau_{slow}} - F_{biomin,PO_4} \tag{71d}$$

M4.4 Bioturbation

Bioturbation is treated as simple diffusive flux with a rate constant D_b, as in ~~Ahrens et al. (2015)~~Koven et al. (2013), but declining with soil depth in proportion to the fraction of roots in the layer to account for reduced biological activity with increasing soil depth:

$$D_b = \frac{root_{frac}}{dz} \times \frac{k^{diff}_{org}}{\rho^{cor}_{soil}}, \; and \tag{72a}$$

$$\rho^{cor}_{soil} = MAX(\rho^{bulk}_{org}, \rho_{OM} + \rho_{soil} - \rho_{OM}\frac{\rho_{soil}}{\rho^{bulk}_{org}}) \tag{72b}$$

where $root_{frac}$ and dz are the root fraction and depth of the soil layer, ρ^{cor}_{soil} is the soil bulk density corrected with soil organic matter, ρ^{bulk}_{org} is the bulk density of organic material, ρ_{OM} is the organic matter density of the soil layer which depends on the organic matter content in the soil layer, ρ_{soil} is the bulk density of fine mineral soil, and k^{diff}_{org} is the diffusion coefficient for organic material due to bioturbation.

M4.5 Plant uptake rates

The potential uptake rates of plants for X= NH_4, NO_3, and PO_4 follow an extended Michaelis-Menten kinetics:

$$U_X^* = v_{max,X}(T_{soil},\Psi) \times X \times (K_{m1,X}(T_{soil},\Theta) + \frac{1}{K_{m2,X}(T_{soil},\Theta)+X}) \times f_{demand}^X \times C_{fine\_root},\ where \tag{73a}$$

$$v_{max,X}(T_{soil},\Psi) = v_{max,X}\frac{E_{d,uptake} \times e^{E_{a,uptake}\times T}}{E_{d,uptake} - E_{a,uptake} \times (1-e^{E_{d,uptake}\times T})} \times \frac{\Psi_{fine\_root}}{\Psi_{leaf,min}},\ with \tag{73b}$$

$$T = \frac{T_{soil} - T_{opt,uptake}}{T_{soil} \times T_{opt,uptake} \times R},\ and \tag{73c}$$

$$K_{m1,X}(T_{soil},\Theta) = K_{m1,X}/(e^{-\frac{Ea,hsc}{R}\times(\frac{1}{T_{soil}}-\frac{1}{T_{ref}^T})} \times (\frac{\Theta}{\Theta_{fc}})^{k_{hsc}}),\ and \tag{73d}$$

$$K_{m2,X}(T_{soil},\Theta) = K_{m2,X} \times e^{-\frac{Ea,hsc}{R}\times(\frac{1}{T_{soil}}-\frac{1}{T_{ref}^T})} \times (\frac{\Theta}{\Theta_{fc}})^{k_{hsc}},\ and \tag{73e}$$

$$f_{demand}^X = 1 - e^{-(\frac{\chi_{max}^{X:Y} - \chi_{labile}^{X:Y}}{\chi_{max}^{X:Y}\times(1-K_{demand}^{half,X})})^{k_{demand}}} \tag{73f}$$

where $v_{max,X}$ is the PFT-specific temperature-sensitive maximum uptake rate per unit biomass, adjusted by the current root zone moisture potential (Ψ_{fine_root}) to account for limited transport of nutrients towards the roots in dry soils, C_{fine_root} is the biomass density of fine roots ($\mathrm{mol\ C\ m^{-3}}$, see Eq. 3), T_{soil} is the soil temperature and the K_m parameters are nutrient sensitivities of the low and high affinity transporters. These affinities are assumed to be temperature sensitive and are adjusted to soil moisture to account for the difference between mass-based and soil solution concentrations (Ahrens et al., 2015). The potential uptake of nutrients can be down-regulated by plants given their internal demand f_{demand}^X, where X refers to either N or P and $X:Y$ refers to either the short-term average (τ_{mavg}^{uptake}) of the labile N:C or P:N ratios. $\chi_{max}^{X:Y}$ corresponds to the X:Y ratio of growing a unit of leaves and fine roots at the current leaf-to-root ratio (see M3.4, $K_{demand}^{half,X}$ is a parameter denoting the fraction of $\chi_{max}^{X:Y}$ at which uptake is reduced to 50% and k_{demand} is shape parameter.

M4.6 Asymbiotic biological nitrogen fixation

The asymbiotic biological nitrogen fixation (BNF) is represented as:

$$F_{BNF}^{NH_4} = v_{max,BNF} \times f(T_{soil}) \tag{74}$$

where $v_{max,BNF}$ is a parameter representing the base rate of fixation and the temperature response is calculated as above (Eq. 65). BNF is suppressed if the sum of $\mathrm{NH_4}$ and $\mathrm{NO_3}$ in any soil layer exceeds a critical threshold N_{limit}^{BNF} (Zaehle et al., 2010). The distribution of $F_{BNF}^{NH_4}$ across soil layers follows the distribution of fine roots, as indicator for C inputs into the soil. All N fixed through this mechanism is added to the mineral $\mathrm{NH_4}$ soil pool.

M4.7 Nitrification and denitrification

Calculation of nitrification and denitrification follows Xu-Ri and Prentice (2008); Zaehle et al. (2011), which relies on the separation of the soil into aerobic and anaerobic volume fractions ($anvf$):

$$anvf = e^{-(\lambda_{anvf} \times (1-afps))^{k_{anvf}}}, where \tag{75a}$$

$$afps = \frac{W_{fc} - W_{soil}}{W_{fc}} \tag{75b}$$

where λ_{anvf} and k_{anvf} are parameters, $afps$ is the air filled pore space, and the W_x are the soil moisture contents as defined in Sect. M6.3.

The potential rate of nitrification (U^*_{nit}) in the aerobic fraction of the soil is modified by temperature and soil moisture according to:

$$U^*_{nit} = v_{max,nit} \times f(T_{soil}) \times g(\Theta) \times NH_4, where \tag{76a}$$

$$f(T_{soil}) = E_{d,nit} \frac{e^{\frac{E_{a,nit} \times kt}{R_{gas}}}}{E_{d,nit} - E_{a,nit} \times (1 - e^{\frac{E_{d,nit} \times kt}{R_{gas}}})} \tag{76b}$$

$$kt = \frac{T_{soil} - T_{opt,nit}}{T_{soil} \times T_{opt,nit}} \tag{76c}$$

$$g(\Theta) = 1 - afps \tag{76d}$$

The actual rate of nitrification (U_{nit}), given the potential rate and competing demands from plant and microbial uptake (Sect. M4.3, is partitioned into its products (NO_3, NO_y, and N_2O) according to

$$F_{nit,NO_3} = (1 - f^{NO_y}_{nit} - f^{N_2O}_{nit}) \times U_{nit} \tag{77a}$$

$$F_{nit,NO_y} = f^{NO_y}_{nit} \times U_{nit} \tag{77b}$$

$$F_{nit,N_2O} = f^{N_2O}_{nit} \times U_{nit} \tag{77c}$$

where the $F_{nit,X}$ are the nitrification fluxes for NO_3, NO_y, and N_2O, respectively (Eq. 60).

The potential rate of denitrification (U^*_{denit}) in the anaerobic fraction of the soil is modified by temperature:

$$U^*_{denit} = anvf \times v_{max,denit}(T_{soil}) \times \frac{C_{fast}}{K^{fast}_{m,denit} + C_{fast}} \frac{NO_3}{K^{NO_3}_{m,denit} + NO_3}, where \tag{78a}$$

$$v_{max,denit}(T_{soil}) = v_{max,denit} \times e^{-\frac{E_{a,denit}}{R} \times (\frac{1}{T_{soil}} - \frac{1}{T^T_{ref}})} \tag{78b}$$

The actual rate of denitrification (U_{denit}), given the potential rate and competing demands from plant uptake (Sect. M4.3), is partitioned into its products (NO_y, N_2O, and N_2) according to

$$F_{denit,NO_y} = f_{denit}^{NO_y} \times U_{denit} \tag{79a}$$

$$F_{denit,N_2O} = f_{denit}^{N_2O} \times U_{denit} \tag{79b}$$

$$F_{denit,N_2} = (1 - f_{denit}^{NO_y} - f_{denit}^{NO_y}) \times U_{denit} \tag{79c}$$

where the $F_{denit,X}$ are the denitrification fluxes for NO_y, N_2O, and N_2, respectively (Eq. 60). The model currently ignores the effect of ammonia volatilisation, which is of low relevance for natural, unfertilised ecosystems.

M4.8 Phosphorus weathering and biomineralisation

Weathering is modelled following Wang et al. (2010) as:

$$F_{weath,PO_4} = f(T_{soil}) \times g(\Theta) \times f(C_{fine\_root}) \times k_{weath} \times \rho_{soil}^{cor},\ where \tag{80a}$$

$$f(T_{soil}) = e^{-\frac{Ea,hsc}{R} \times (\frac{1}{T_{soil}} - \frac{1}{T_{ref}^{T}})}, \tag{80b}$$

$$g(\Theta) = (\frac{\Theta}{\Theta_{fc}})^3, and \tag{80c}$$

$$f(C_{fine\_root}) = \frac{C_{fine\_root}}{K_{m,weath}^{root} + C_{fine\_root}} \tag{80d}$$

where k_{weath} is the rate constant for weathering, and ρ_{soil}^{cor} is the soil bulk density corrected by SOM content. The weathering rate decreases with soil depth as the fine root C decreases, given the half-saturation root density $K_{m,weath}^{root}$, and is modified by soil temperature and moisture.

The potential biomineralisation rate of PO_4 (McGill and Cole, 1981) is determined as an additional turnover of the P contained in the slow SOM pool, modified by temperature and moisture modifiers, and affected by the concentration of PO_4 and the root biomass:

$$F_{biomin,PO_4}^{*} = \frac{C_{slow}}{\chi_{SOM_{slow}^{C:N}} \times \chi_{SOM_{slow}^{N:P}} \times \tau_{biomin}} \times f(C_{fine\_root}) \times f(PO_4) \times f(T_{soil}) \times g(\Theta),\ where \tag{81a}$$

$$f(C_{fine\_root}) = \frac{C_{fine\_root}}{K_{m,biomin}^{root} + C_{fine\_root}},\ and \tag{81b}$$

$$f(PO_4) = \frac{K_{m,biomin}^{PO_4}}{K_{m,biomin}^{PO_4} + PO_4} \tag{81c}$$

where $K_{m,biomin}^{root}$ and $K_{m,biomin}^{PO_4}$ are constants constraining the biomineralisation rate under low root biomass and high PO_4 concentration, respectively; the temperature and moisture responses are calculated as those in Eq. 65. The biomineralisation

rate is further constrained so that it does not alter the stoichiometry of the fast pool.

$$F_{biomin,PO_4} = MIN(F^*_{biomin,PO_4}, \frac{\frac{\eta_{C,slow\rightarrow fast}}{\chi_{SOM^{C:N}_{slow}} \chi_{SOM^{N:P}_{slow}}} C_{slow} - P_{slow}}{\tau_{slow}}) \tag{82}$$

M4.9 Phosphorus adsorption and (ab)sorption

PO_4 desorption follows Yang et al. (2014):

$$F_{desorp,PO_4} = f(T_{soil}, E_{a,abs}) \times k_{abs} \times P_{lab} - f(T_{soil}, E_{a,des}) \times k_{des} \times P_{sorb},\ where \tag{83a}$$

$$f(T_{soil,E_a}) = e^{-\frac{E_a}{R} \times (\frac{1}{T_{soil}} - \frac{1}{T^*_{ref}})} \tag{83b}$$

where k_{abs} and k_{des} are the rate constants of (ab)sorption and desorption, and $E_{a,abs}$ and $E_{a,des}$ the respective activation energies.

The adsorption (F_{adsorp,PO_4}) flux from soil solution to the soil adsorption sites is calculated assuming constant Langmuir equilibrium (Barrow, 1978) between soluble and adsorbed P:

$$PO_4 = \frac{S_{max} \times PO_4}{K_S + PO_4},\ thus \tag{84a}$$

$$\frac{\partial P_{lab}}{\partial t} = \frac{S_{max} \times PO_4}{(K_S + PO_4)^2} \frac{\partial PO_4}{\partial t}, \tag{84b}$$

by rearranging Eq. 84b

$$\frac{\partial P_{lab}}{\partial t} = k_p \frac{\partial (P_{lab} + PO_4)}{\partial t} \tag{84c}$$

$$\frac{\partial PO_4}{\partial t} = (1 - k_p) \frac{\partial (P_{lab} + PO_4)}{\partial t},\ where \tag{84d}$$

$$k_p = \frac{S_{max} \times PO_4}{(K_S + PO_4)^2 + S_{max} PO_4}, \tag{84e}$$

where S_{max} and K_S are the maximum sorption capacity, and the half-saturation concentration coefficient of the soil, and are modified by soil moisture and SOM content as follows:

$$S_{max} = \Theta_{soil} \times (S^{max}_{om} V^{frac}_{om} \rho^{bulk}_{org} + S^{max}_{mineral} V^{frac}_{mineral} \rho_{soil}),\ and \tag{85a}$$

$$K_S = K^{sorb}_{m,om} V^{frac}_{om} \rho^{bulk}_{org} + K^{sorb}_{m,mineral} V^{frac}_{mineral} \rho_{soil} \tag{85b}$$

where V^{frac}_{om} and $V^{frac}_{mineral}$ are volumetric fractions of organic matter and fine soil minerals, respectively. S^{max}_{om} and $S^{max}_{mineral}$ are the maximum PO_4 sorption capacity of pure organic matter and pure fine soil, respectively. $K^{sorb}_{m,om}$ and $K^{sorb}_{m,mineral}$ are the half-saturation concentration coefficient of pure organic matter and pure fine soil, respectively.

Based on Eq.60f and Eq.61a, the equilibrium in Eq.84 could be solved .

$$\begin{aligned}\frac{\partial (P_{lab} + PO_4)}{\partial t} &= F_{dep,PO_4} + F_{weath,PO_4} + F_{biomin,PO_4} - U_{plant,PO_4} - F_{desorp,PO_4} \\ &\quad - \sum (\Phi_{i,PO_4}) - \frac{\partial v_{PO_4} PO_4}{\partial z} + \frac{\partial}{\partial z}(D_b \frac{\partial P_{lab}}{\partial z})\end{aligned} \tag{86}$$

M4.10 Soil in- and outfluxes

Currently, gas diffusion is not modelled explicitly. Instead, CO_2 is assumed to be directly released to the atmosphere. The carbon efflux per soil layer is described as:

$$F^{\uparrow}_{CO_2} = ((1-\eta_{C,litter\rightarrow fast})(\frac{C_{met}}{\tau_{met}}+\frac{C_{str}}{\tau_{str}})+(1-\eta_{C,wl\rightarrow met|str})\frac{C_{wl}}{\tau_{wl}}+(1-\eta_{C,fast\rightarrow slow})\frac{C_{fast}}{\tau_{fast}}+(1-\eta_{C,slow\rightarrow fast})\frac{C_{slow}}{\tau_{slow}})\Delta t, \tag{87}$$

and similar for ^{13}C and ^{14}C fluxes.

Slightly differently from that, the emission of gaseous N species is assumed to follow Xu-Ri and Prentice (2008), which considers the effect of temperature and moisture on gas loss. However, transfer between soil layers is equally not treated explicitly.

$$F^{\uparrow}_{X} = f(T_{soil}) \times afps \times X, where \tag{88a}$$

$$f(T_{soil}) = e^{-\frac{E_{a,diff}}{R}\times(\frac{1}{T_{soil}}-\frac{1}{T^{r}_{ref}})} \tag{88b}$$

and $afps$ is the air-filled pore fraction of the soil (see Eq. 75.)

M5 Isotopic composition and fractionation

The carbon (C) and nitrogen (N) flows and pool tracked in the model are comprising all major isotopes (i.e. C = ^{12}C + ^{13}C + ^{14}C, and N = ^{14}N + ^{15}N). The model explicitly tracks the mass flow of ^{13}C, ^{14}C and ^{15}N as separate entities for all biogeochemical pools and fluxes. The molar mixing ratio (R_X) of the isotope (e.g. ^{13}C) to the main element (e.g. ^{12}C) of each biogeochemical pool can be calculated as

$$R_{13C} = \frac{^{13}C}{^{12}C} = \frac{^{13}C}{C - ^{13}C} \tag{89}$$

and by convention

$$\delta_{13C} = (\frac{R_{13C}}{R_{ref,13C}} - 1) \times 1000 \tag{90}$$

where $R_{ref,13C}$ is the reference isotopic molar mixing ratio and δ_{13C} is in ‰. Similar calculations are done for the ratio of ^{15}N to ^{14}N and the reference value $R_{ref,15N}$. By convention, the delta notation of ^{14}C is dependent on the ^{13}C content, see (Levin et al., 2010), and the molar mass of ^{14}C is ignored in the calculations of ^{13}C because of the extremely low concentrations.

Biogeochemical processes discriminate against the heavier isotope, and this fractionation process is treated by calculating the mixing ratio of the isotope of the resulting flux as

$$R_{sink} = \frac{R_{source}}{\frac{\epsilon_{process}}{1000} + 1} \tag{91}$$

where R_{source} is the molar mixing ratio of the source pool of the reaction, R_{sink} is the molar mixing ratio of the resulting matter flux, and $\epsilon_{process}$ is a process and isotope specific discrimination rate.

Isotopic discrimination of ^{13}C and ^{14}C by photosynthesis is modelled according to the general equation derived by Farquhar et al. (1982); Drake (2014), so that

$$D_x = a_x + (c_x + \phi_{C4} \times b_x - a_x)\frac{c_i}{c_a} \tag{92}$$

where a_x, and b_x are isotope-specific constants (^{13}C and ^{14}C, respectively, see Table M5). c_x and ϕ_{C4} account for the additional bundle-sheath processes in C4 plants. For C3 plants, these processes do not play a role and these parameters are 0 and 1, respectively. In the model, currently only photosynthesis is assumed to result in C-isotope discrimination, ignoring the effect of the smaller and uncertain discrimination by tissue construction, storage formation and respiration (Brüggemann et al., 2011).

Isotopic discrimination for various nitrogen cycle processes (biological nitrogen fixation, ammonification, plant and microbial N uptake, and processes associated with nitrification and denitrification) are taken from (Robinson, 2001). According to (Robinson, 2001), in case of near-complete consumption of the source pool, the discrimination is reduced as

$$\epsilon^{corr}_{process} = \epsilon_{process}(f_{source} - 1)log(\frac{1 - f_{source}}{f_{source}}) \tag{93}$$

where f_{source} is the ratio of the source consumption to the source pool size.

M6 Radiation, surface energy balance and soil hydrology

M6.1 Net surface shortwave radiation budget

Canopy radiation interception is calculated with a multi-layer scheme following Spitters (1986), with radiation levels calculated at the mid-point of each canopy layer. The scheme uses up to 20 (default 10) canopy layers, with exponentially increasing layer thickness as the canopy depth increases. The original scheme, as used in OCN (Zaehle and Friend, 2010), has been extended to diagnose canopy albedo, to account for clumping (see eq. 96), and to approximate the attenuation of the shortwave radiation back-scatter from the soil to allow for a smooth transition of surface albedo from soil to vegetation values with increasing leaf coverage.

The scheme is applied separately to the visible (vis) and near-infrared (nir) radiation band, where the parameterisation of the visible radiation is based on the assumption that the radiation interception and reflection are similar to that of the photosynthetically active range (i.e. 400-700 nm). In the following, the subscripts for visible and near-infrared are omitted for readability.

~~The reflection coefficient (ρ_{rad}) of the green canopy~~ Light levels decrease exponentially in the canopy, such that the attenuation of direct (dr) and diffuse (df) top-of-the-canopy irradiance ($I_{dr\downarrow,0}$ and $I_{df\downarrow,0}$, respectively) at any cumulative leaf area index (LAI_c; from the top) is given by:

$$\rho_{rad} = \frac{1-\sqrt{1-\sigma}}{1+\sqrt{1-\sigma}} \times \frac{2}{1+\rho^{sbeta} \times cos(\gamma^*)},$$

~~where the first term on the right hand side is the reflection of a horizontally oriented canopy, and the second term empirically adjusts the reflection to a spherical distribution. σ is the PFT-specific single leaf scattering coefficient and ρ^{sbeta} is a conversion constant. Because all equations for leaf reflection and absorption coefficients are only valid for high solar elevation, the true zenith angle (γ) is constrained to values larger than 10° (γ^*). Note that Spitters (1986) use the sine of the solar elevation angle.~~

$$I_{df\downarrow} = (1-\rho_{rad}) \times I_{df\downarrow,0} \times e^{-k_{df} \times LAI_c} \tag{94a}$$

$$I_{dr\downarrow} = (1-\rho_{rad}) \times I_{dr\downarrow,0} \times e^{-\sqrt{1-\sigma} \times k_{bl} \times LAI_c} \tag{94b}$$

$$I_{dr,dr\downarrow} = I_{dr\downarrow,0} \times e^{-k_{bl} \times LAI_c} \tag{94c}$$

$$I_{dr,df\downarrow} = I_{dr\downarrow} - I_{dr,dr\downarrow} \tag{94d}$$

where $I_{dr,df\downarrow}$ is the diffuse part of the direct beam resulting from scattering of the direct beam and $I_{dr,dr\downarrow}$ is the direct beam remaining direct at the canopy depth LAI_c, and ρ_{rad} is the reflection coefficient of the green canopy, as defined in Eq. 97. For a spherical leaf angle distribution with leaves distributed randomly within the canopy volume, the extinction coefficients of the diffuse flux (k_{df}) and that of the direct component of the direct flux (k_{bl}) are approximated, respectively, by:

$$k_{df} = k_{df,0}\sqrt{1-\sigma} \times \Omega \tag{95a}$$

$$k_{bl} = \frac{k_{bl,0} \times \Omega}{cos(\gamma^*)} \tag{95b}$$

where Ω is the clumping index according to Campbell and Norman (1998), which is calculated as:

$$\Omega = \Omega_0/(\Omega_0 + (1-\Omega_0) \times e^{-k_{csf} \times acos(\gamma^*)^{\phi_{crown}}}), \tag{96}$$

where Ω_0 and ϕ_{crown} are the PFT-specific clumping factor at nadir and crown shape factor, respectively, and k_{csf} is a correction factor.

Light levels decrease exponentially in the canopy, such that the attenuation of direct (dr) and diffuse (df) top-of-the-canopy irradiance ($I_{dr\downarrow,0}$ and $I_{df\downarrow,0}$, respectively) at any cumulative leaf area index (LAI_c; from the top) The reflection coefficient (ρ_{rad}) of the green canopy is given by:

$$I_{df\downarrow} = (1 - \rho_{rad}) \times I_{df\downarrow,0} \times e^{-k_{df} \times LAI_c}$$

$$I_{dr\downarrow} = (1 - \rho_{rad}) \times I_{dr\downarrow,0} \times e^{-\sqrt{1-\sigma} \times k_{bl} \times LAI_c}$$

$$I_{dr,dr\downarrow} = I_{dr\downarrow,0} \times e^{-k_{bl} \times LAI_c}$$

$$I_{dr,df\downarrow} = I_{dr\downarrow} - I_{dr,dr\downarrow}$$

$$\rho_{rad} = \frac{1 - \sqrt{1-\sigma}}{1 + \sqrt{1-\sigma}} \times \frac{2}{1 + \rho^{sbeta} \times cos(\gamma^*)}, \tag{97}$$

where $I_{dr,df\downarrow}$ is the diffuse part of the direct beam resulting from scattering of the direct beam and $I_{dr,dr\downarrow}$ is the direct beam remaining direct at the canopy depth $LAI_c$the first term on the right hand side is the reflection of a horizontally oriented canopy, and the second term empirically adjusts the reflection to a spherical distribution. σ is the PFT-specific single leaf scattering coefficient and ρ^{sbeta} is a conversion constant. Because all equations for leaf reflection and absorption coefficients are only valid for high solar elevation, the true zenith angle (γ) is constrained to values larger than 10° (γ^*). Note that Spitters (1986) use the sine of the solar elevation angle.

Below the canopy (bc), i.e. at the soil surface, the downwelling energy flux ($I_{bc\downarrow}$) is divided into a part that is absorbed by the soil ($I_{a,soil}$) and a part that is backscattered as diffuse radiation ($I_{bc\uparrow}$), depending on the soil's albedo (alb_{soil}):

$$I_{bc\downarrow} = (1 - \rho_{rad}) \times (I_{df\downarrow,0} \times e^{-k_{df} \times LAI} + I_{dr\downarrow,0} \times e^{-\sqrt{1-\sigma} \times k_{bl} \times LAI}) \tag{98a}$$

$$I_{a,soil} = (1 - alb_{soil}) \times I_{bc\downarrow} \tag{98b}$$

$$I_{bc\uparrow} = alb_{soil} \times I_{bc\downarrow} \tag{98c}$$

To first-order, the diffuse light profile of the canopy accounting for the backscatter of diffuse radiation from the soil can be approximated as

$$I_{df\downarrow\uparrow} = (1 - \rho_{rad}) \times (I_{df\downarrow,0} \times e^{-k_{df} \times LAI_c} + \times I_{bc\uparrow} \times e^{-k_{df} \times (LAI - LAI_c))} \tag{99}$$

Absorption (A^{rad}) is taken to be complementary to transmission, therefore the absorbed diffuse and direct energy flux at a cumulative leaf area LAI_c can be written as:

$$A^{rad}_{df} = k_{df} \times I_{df\downarrow\uparrow} \tag{100a}$$

$$A^{rad}_{dr} = (1-\sigma) \times k_{bl} \times I_{dr} \tag{100b}$$

$$A^{rad}_{dr,dr} = (1-\sigma) \times k_{bl} \times I_{dr\downarrow,0} \times e^{-k_{bl} \times LAI_c} \tag{100c}$$

$$A^{rad}_{dr,df} = A^{rad}_{dr} - A^{rad}_{dr,dr} \tag{100d}$$

The canopy is then split into a sunlit and a shaded part, with the sunlit fraction defined as:

$$f_{sunlit} = e^{-k_{bl} \times LAI_c} \tag{101}$$

following eq. 94c. The sunlit part receives both diffuse and direct radiation, whereas the shaded part only received diffuse radiation. Thus,

$$A^{rad}_{shaded} = A^{rad}_{df} + A^{rad}_{dr,df} \tag{102a}$$

$$A^{rad}_{sunlit} = A^{rad}_{shaded} + (1-\sigma) \times k_{bl} \times I_{dr\downarrow,0} \tag{102b}$$

The canopy albedo is diagnosed (rather than simply taken as ρ_{rad}) as:

$$alb_{can} = 1 - \frac{I_{bc\downarrow} + (1-f_{sunlit}) \times A^{rad}_{shaded} + f_{sunlit} \times A^{rad}_{sunlit}}{I_{df\downarrow,0} + I_{dr\downarrow,0}} \tag{103}$$

The total shortwave upward flux is diffuse and calculated as the backscattered flux of the canopy plus the backscattered flux from the soil, which is transmitted diffusely through the canopy:

$$I_{df\uparrow} = alb_{can} \times (I_{df\downarrow,0} + I_{dr\downarrow,0} - I_{bc\downarrow}) + (1-\rho_{rad}) \times I_{bc\uparrow} \times e^{-k_{df} \times LAI} \tag{104}$$

Based on this, the total surface albedo alb_{surf} (i.e. the albedo derived from vegetation and soil radiation transfer, absorption, and reflection) and net shortwave flux I_{net} can be calculated as:

$$alb_{surf} = \frac{I_{df\uparrow}}{I_{df\downarrow,0} + I_{dr\downarrow,0}} \tag{105a}$$

$$I_{net} = (1 - alb_{surf}) \times (I_{df\downarrow,0} + I_{dr\downarrow,0}) \tag{105b}$$

M6.2 Surface energy balance

The representation of the surface energy balance including the turbulent momentum and heat exchanges, surface, and soil temperature calculations follows largely the scheme of JSBACH 3, as described by Roeckner et al. (2003). The net radiation

(R_{net}) at the surface consists of the following components:

$$R_{net} = (1 - \alpha_s) R_{sd} + R_{ld} - \epsilon \sigma_{SB} {T_s}^4 \tag{106}$$

where the term $\alpha_s \times R_{sd}$ is the net surface shortwave balance, denoted as I_{net} in Eq. 105, R_{ld} the downwelling longwave radiation, ϵ the surface emissivity, σ_{SB} the Stefan-Boltzmann constant, and T_s is the surface temperature.

The surface energy balance can then be written as

$$C_{s,l} \frac{\partial T_s}{\partial t} = R_{net} + LE + H + G \tag{107}$$

where $C_{s,l}$ is the heat capacity of the surface layer, H is the sensible heat flux, LE the latent heat flux, composed of interception loss E_i, soil evaporation E_s and transpiration E_v, as described in Section M6.3. G is the ground heat flux, which is obtained from the solution of the thermal diffusion equation, which is used to diagnose the temperature profile within the soil

$$C_s \frac{\partial T}{\partial t} = -\frac{\partial G}{\partial z} = -\frac{\partial}{\partial z} \left(-\lambda_s \frac{\partial T}{\partial z} \right) \tag{108}$$

where C_s is the volumetric heat capacity of the soil, G is the thermal heat flux (positive downward), $\lambda_s = C_s \kappa_s$ is the thermal conductivity, κ_s the thermal diffusivity, both derived from soil texture, and z the depth. This equation is solved down to a prescribed depth assuming zero flux conditions at the bottom and surface temperature T_s at the top as obtained from Eq. 107.

The sensible heat flux H is obtained from the temperature gradient according to

$$H = \rho_{air} C_p \frac{T_{air} - T_s}{r_a} \tag{109}$$

where ρ_{air} and C_p are density and heat capacity of the surface atmospheric layer, and T_{air} and T_s are air and surface temperature. r_a is the aerodynamic resistance:

$$r_a = (C_h \, |v_h|)^{-1} \tag{110}$$

and depends on the transfer coefficient for heat C_h Roeckner et al. (2003). and the absolute value of horizontal wind velocity v_h.

M6.3 Surface and soil hydrology

~~The soil model keeps track of water in terms of amount of water ($W_{skin|soil}$; m), which in the soil can be converted to the layers fractional water content (Θ) as:~~

~~$\Theta_{soil,sl} = \frac{W_{soil,sl}}{dz_{sl}}$~~

with a soil water matrix potential ($\Psi_{soil,sl}$) derived from a pedotransfer function Saxton and Rawls (2006) as follows:

$$\Psi_{soil,sl} = k_A^{\Psi} \Theta_{soil,sl}^{k_B^{\Psi}}$$

where k_A^{Ψ}, and k_B^{Ψ} are soil texture dependent parameters Saxton and Rawls (2006). Surface hydrology is represented in very simple terms in QUINCY, because it is meant to be replaced by the JSBACH 4 hydrology in a future version. The model largely follows JSBACH 3 Roeckner et al. (2003), with some modifications. The model represents surface hydrology for a number of soil layers (see Section M1) and including a canopy skin layer (hereafter referred to as skin). It represents interception (F_{inter}) by and interception loss (E_i) from the canopy, infiltration (F_{inf}), bare soil evaporation (E_a), and surface runoff generation (F_{runoff}) at the soil surface, water movement in the soil (F_{diff}, F_{pref}), as well as deep drainage, and transpiration by vegetation (E_v) distributed across the rooting zone. The water budget can be described as follows

$$\frac{W_{skin}}{dt} = F_{inter} - E_i \tag{111a}$$

$$\frac{W_{soil,sl=1}}{dt} = F_{inf} - E_a - f_{frans,sl=1} E_v - F_{diff,sl=1 \rightarrow sl=2} \tag{111b}$$

$$\frac{W_{soil,sl=2,n}}{dt} = (1 - \frac{k_{pref}}{dz_{sl}}) F_{pref,sl-1} - f_{frans,sl} F_{trans} + F_{diff,sl-1 \rightarrow sl} - F_{diff,sl \rightarrow sl+1} \tag{111c}$$

(111d)

Precipitation ($Precip$) becomes partially intercepted by the canopy before reaching the soil:

$$F_{inter} = MIN(k_{eff,inter} \times Precip, \frac{w_{skin,max} \times LAI - W_{skin}}{dt})$$

within the limit (F_{inter}), within the limits of the maximum size of this reservoir, the canopy skin reservoir(W_{skin}), with the remaining throughfall ($F_{through}$) reaching the first soil layer.

$$F_{inter} = MIN(k_{eff,inter} \times Precip, \frac{w_{skin,max} \times LAI - W_{skin}}{dt}) \tag{112a}$$

$$F_{through} = Precip - F_{inter} \tag{112b}$$

where $w_{skin,max}$ is a parameter. Different from Roeckner et al. (2003), the remaining throughfall is partitioned in $F_{through}$ is infiltrating into the first soil layer into infiltration (F_{inf}) , within the limits of its water content at field capacity (Θ_{fc}), surface runoff (F_{runoff}), and a fraction that is leaked $W_{fc,sl=1}$), but –different to Roeckner et al. (2003) – reduced by a constant fraction (k_{pref}), which is assumed to be leaked preferentially to the next layer along preferential flow pathways (F_{pref}): lower layer. The difference between $F_{through}$ and F_{inf}, i.e. the excess water unable to remain in the surface layer, is partitioned into surface runoff (F_{runoff}) and preferential flow to the second layer ($F_{pref,sl=1}$).

$$F_{input} = MIN(Precip - F_{inter}, \frac{W_{fc,sl=1} - W_{act,sl=1}}{dt}), F_{inf} = (1 - \frac{k_{pref}}{dz_{sl}}) \times MIN(F_{input through}, \frac{W_{fc,sl=1} - W_{act,sl=1}}{dt}) \quad (113a)$$

$$F_{runoff} = (1 - k_{pref,runoff})(F_{through} - F_{input inf}), and \quad (113b)$$

$$F_{pref,sl=1} = \frac{k_{pref}}{dz_{sl}} F_{inf} + k_{pref,runoff}(F_{through} - F_{input inf}) \quad (113c)$$

Preferential flow to the lower layers is assumed to occur for any water leakage following infiltration according to

$$F_{inf,sl} = (1 - \frac{k_{pref}}{dz_{sl}}) \times F_{pref,sl-1} \quad (114a)$$

$$F_{pref,sl} = \frac{k_{pref}}{dz_{sl}} F_{inf,sl} \times F_{pref,sl-1} \quad (114b)$$

Different from Roeckner et al. (2003), the diffusive flux between two layers of depth dz is given by the Richards-equation:

$$F_{diff,sl-1 \to sl} = \frac{\bar{K}_{diff,sl-1 \to sl}}{0.5 \times (dz_{sl-1} + dz_{sl})} (\Psi_{soil,sl} - \Psi_{soil,sl-1}), where \quad (115a)$$

$$\bar{K}_{diff,sl-1 \to sl} = \frac{dz_{sl-1} K_{diff,sat,sl-1} (\frac{\Theta_{act,sl-1}}{\Theta_{sat,sl-1}})^{k_{C,sl}^{diff}} + dz_{sl} K_{diff,sat,sl} (\frac{\Theta_{act,sl}}{\Theta_{sat,sl}})^{k_{C,sl}^{diff}}}{dz_{sl-1} + dz_{sl}} \quad (115b)$$

where $K_{diff,sat,sl}$ and $k_{C,sl}^{diff}$ are derived from soil texture according to Saxton and Rawls (2006), Θ_{sl} is the volumentric water content given by Eq. 120, and $\Psi_{soil,sl}$ is the soil water matrix potential given by Eq. 121. Saturation of a soil layer leads to increased percolation to the next lower layer. The lower boundary layer in the soil is modelled as a zero gradient boundary, i.e. only percolation flow leads to drainage from the soil column.

Interception loss (E_i) is calculated from the filled fraction of canopy skin reservoir (W_{skin}), i.e. the ratio of the actual to the maximum size of the canopy water storage

$$E_i = \rho_{air} \frac{q_a - q_s(T_s, p_s)}{r_a} \frac{W_{skin}}{w_{skin,max} \times LAI}, \quad (116)$$

where ρ_{air} is air density, q_a specific humidity in lowest atmospheric level, q_s saturation specific humidity at surface temperature T_s and pressure p_s, ~~and ratio of the size of the canopy water storage (W_{skin}) and the maximum size of this reservoir, where $w_{skin,max}$ is a parameter~~ r_a is the aerodynamic resistance, and LAI is the current leaf area index of the vegetation.

Evaporation from the soil surface (E_s) is calculated as:

$$E_s = \rho_{air} \frac{q_a - q_s(T_s, p_s)}{r_a^*} \Theta_{soil,1} (1 - exp(k_{fpc} \times LAI)) \quad (117)$$

where $\Theta_{soil,1}$ the fractional soil water content of the first soil layer. The term $(1 - exp(k_{fpc} \times LAI))$ has been added to the model of Roeckner et al. (2003) to account for the reduced energy available for evaporation underneath a closed canopy.

Transpiration from the dry vegetation surfaces (E_v) is

$$E_v = \rho_{air} \frac{q_a - q_s(T_s, p_s)}{r_a + r} \tag{118}$$

where stomatal resistance r of the canopy is the inverse of the stomatal conductance of the canopy (see Eq. 17).

The partitioning of the transpiration flux across soil layers $f_{trans,sl}$ is calculated based on the layered soil water potential ($\Psi_{soil,sl}$), the fractional root distribution ($f_{root,sl}$), as well as a PFT-specific minimum soil water potential,

$$f_{trans,sl} = \frac{f_{root,sl} \times \beta_{gs,soil,sl}}{\sum_{i=1}^{n} f_{root,i} \times \beta_{gs,soil,i}}, where \tag{119a}$$

$$\beta_{gs,soil,sl} = \Psi_{soil,sl} / \Psi_{soil,min} \tag{119b}$$

~~Based on these fluxes, the water budget can be described asfollows~~ The soil model keeps track of water in terms of amount of water ($W_{skin|soil}$; m), which in the soil can be converted to the layers fractional water content (Θ) as:

$$\Theta_{soil,sl} = \frac{W_{soil,sl}}{dz_{sl}} \tag{120}$$

$$\begin{aligned}
\frac{W_{skin}}{dt} &= F_{inter} - E_i \\
\frac{W_{soil,sl=1}}{dt} &= F_{inf} - E_a - f_{frans,sl=1} E_v - F_{diff,sl=1 \to sl=2} \\
\frac{W_{soil,sl=2,n}}{dt} &= (1 - \tfrac{k_{pref}}{dz_{sl}}) F_{pref,sl-1} - f_{frans,sl} F_{trans} + F_{diff,sl-1 \to sl} - F_{diff,sl \to sl+1}
\end{aligned}$$

with a soil water matrix potential ($\Psi_{soil,sl}$) derived from a pedotransfer function Saxton and Rawls (2006) as follows:

$$\Psi_{soil,sl} = k_A^{\Psi} \Theta_{soil,sl}^{k_B^{\Psi}} \tag{121}$$

where k_A^{Ψ}, and k_B^{Ψ} are soil texture dependent parameters Saxton and Rawls (2006).

~~Saturation of a soil layer leads to increased percolation to the next lower layer. The lower boundary layer in the soil is modelled as a zero gradient boundary, i.e. only percolation flow leads to drainage from the soil column.~~ The net water transport between layers is used as input to the vertical flow of soluable biogeochemical pools.

Table M1. Memory time scale for processes

Symbol	Description	Value	Unit	Eq.
τ_{mavg}^{jmax}	Acclimation of temperature optimum for photosynthesis	7	days	9
τ_{mavg}^{resp}	Acclimation of temperature response of maintenance respiration	30	days	23
τ_{mavg}^{soa}	Frost response of photosynthesis (state-of-acclimation)	2	days	46
τ_{mavg}^{labile}	Labile pool dynamics	7	days	20
τ_{mavg}^{uptake}	Demand for nutrient uptake	3	days	73
τ_{mavg}^{χ}	Response of foliar stoichiometry	20	days	37
τ_{mavg}^{pheno}	Phenological processes	7	days	45
τ_{mavg}^{alloc}	Allometric responses	30	years	34
$\tau_{mavg}^{dynamics}$	Vegetation dynamics processes	365	days	56

Table M2. Photosynthesis parameters

Symbol	Description	Value	Unit	Equation	Citation
j_{max}^{n}	electron-transport limited carboxylation rate per unit N	4.4	$\frac{\mu mol\, CO_2}{mmol\, N}$	7	Niinemets and Tenhunen (1997)
v_{cmax}^{n}	Rubisco limited carboxylation rate per unit N	1.8	$\frac{\mu mol\, CO_2}{mmol\, N}$	10	Niinemets and Tenhunen (1997)
v_{pepc}^{n}	PePC limited carboxylation rate per unit N	98777.97	$\frac{\mu mol\, CO_2}{mmol\, N}$	12	Tazoe et al. (2006)
fN_{pep}	Fraction of N in PEP and PPKD (C4 plants only)	0.045	-	Sect. M2.1	Makino et al. (2003)
r_{J2V}	Jmax25/Vcmax25 (C3/C4) plants	1.97 / 1.4	-	Sect. M2.1	Wullschleger (1993)
a_{chl}^{n}	Chlorophyll N content	25.12	$\frac{mol}{mmol}$	15	Evans (1989)
α_i	Intrinsic quantum efficiency	0.0561	$\frac{\mu mol\, CO_2}{mol\ quanta}$	15	Kull and Kruijt (1998)
k_a	Extinction coefficient for PAR on chlorophyll	0.005	mol^{-1}	15	Kull and Kruijt (1998)
k_n	Extinction coefficient to describe decline of N within the canopy	0.11	-	2	Zaehle and Friend (2010)
k_1^{struc}	Slope of structural leaf N with total N	7.14×10^3	$g^{-1}N$	4	Friend et al. (1997)
k_0^{chl}	Chlorophyll distribution with canopy depth for C3/C4 plants	6.0 / 15.0	-	5	Zaehle and Friend (2010)
k_1^{chl}	Chlorophyll distribution with canopy depth for C3/C4 plants	3.6 / 4.4	-	5	Zaehle and Friend (2010)
k_{fn}^{chl}	Chlorophyll distribution with canopy depth	0.7	-	5	Friend (2001)

Table M2. Photosynthesis parameters (ctnd.)

Symbol	Description	Value	Unit	Equation	Citation
E_0^{kc}	Scaling constant of k_c	38.05	-	6	Bernacchi et al. (2001)
E_1^{kc}	Activation energy of k_c	79.43	$\frac{\mathrm{kJ}}{\mathrm{mol}}$	6	Bernacchi et al. (2001)
E_0^{ko}	Scaling constant of k_o	20.3	-	6	Bernacchi et al. (2001)
E_1^{ko}	Activation energy of k_o	36.38	$\frac{\mathrm{kJ}}{\mathrm{mol}}$	6	Bernacchi et al. (2001)
$E_0^{\Gamma^*}$	Scaling constant of photosynthetic compensation point	19.02	-	6	Bernacchi et al. (2001)
$E_1^{\Gamma^*}$	Activation energy of photosynthetic compensation point	37.83	$\frac{\mathrm{kJ}}{\mathrm{mol}}$	6	Bernacchi et al. (2001)
E_0^{vcmax}	Scaling constant of of Rubisco	26.35	-	6	Bernacchi et al. (2001)
E_1^{vcmax}	Temperature sensitivity of Rubisco	65.33	$\frac{\mathrm{kJ}}{\mathrm{mol}}$	6	Bernacchi et al. (2001)
$k0_{jmax}^{topt}$	Offset of the T_{jmax}^{opt} to T_{air} relationship	17.0	$^\circ\mathrm{C}$	9	Friend (2010)
$k1_{jmax}^{topt}$	Slope of the T_{jmax}^{opt} to T_{air} relationship	0.35	-	9	Friend (2010)
$T_{jmax,min}^{opt}$	Minimum of T_{jmax}^{opt}	17.0	$^\circ\mathrm{C}$	9	Friend (2010)
$T_{jmax,max}^{opt}$	Maximum of T_{jmax}^{opt}	38.0	$^\circ\mathrm{C}$	9	Friend (2010)
T_{ref}^{pepc}	Reference temperature of PePC C4 photosynthesis	25.0	$^\circ C$	13	Friend et al. (2009)
T_{base}^{pepc}	Base temperature of PePC C4 photosynthesis	10.0	$^\circ C$	13	Friend et al. (2009)
D_{air}^{wv2co2}	Ratio of diffusion coefficient for H_2O and CO_2 in air	1.6	-	17	Monteith and Unsworth (2013)
D_{turb}^{wv2co2}	Ratio of diffusion coefficient for H_2O and CO_2 in turbulent air	1.37	-	17	Monteith and Unsworth (2013)
O_i	Partial Pressure of O_2	20.9	kPa	10	-
$c_{i,max}$	Saturating Ci in C4 plants	7800.0	Pa		Friend et al. (2009)

Table M3. Vegetation growth and dynamics parameters

Symbol	Description	Value	Unit	Equation	Citation
Respiration					
$f_{resp,growth}$	Growth respiration fraction per unit new biomass	0.25	$\frac{\mathrm{molC}}{\mathrm{molC}}$	20	Sprugel et al. (1995)
$f_{resp,maint}^{non-woody}$	Maintenance respiration rate for fine roots and leaves	1.0	$\frac{\mu\mathrm{molCO_2}}{\mathrm{mmolN\ s}}$	21	Sprugel et al. (1995)
$f_{resp,maint}^{woody}$	Maintenance respiration rate for wood	0.25	$\frac{\mu\mathrm{molCO_2}}{\mathrm{mmolN\ s}}$	21	Sprugel et al. (1995)
t_{k1}	Coefficient for temperature sensitivity of respiration	308.56	K	22	Lloyd and Taylor (1994)
t_{k2}	Coefficient for temperature sensitivity of respiration	56.02	K	22	Lloyd and Taylor (1994)
t_{k3}	Coefficient for temperature sensitivity of respiration	227.13	K	22	Lloyd and Taylor (1994)
$T_{acclim,ref}$	Base temperature for respiration acclimation	283.15	K	23	Atkin et al. (2014)
f_{resp_acclim}	Respiration temperature acclimation factor	-0.008	K^{-1}	23	Atkin et al. (2014)
$cost_{NH4}$	Transformation and uptake cost for plant uptake of $\mathrm{NH_4}$	1.7	$\mathrm{gCg}^{-1}\mathrm{N}$	24	Zerihun et al. (1998)
$cost_{NO3}$	Transformation and uptake cost for plant uptake of $\mathrm{NO_3}$	2.3	$\mathrm{gCg}^{-1}\mathrm{N}$	24	Zerihun et al. (1998)
Labile Pool					
τ_{labile}	Turnover time of the labile pool	5	days	25	This study
λ_{temp}^{labile}	Temperature response function of labile pool	0.5	K^{-1}	25	This study
k_{temp}^{labile}	Shape parameter of the labile pool's temperature response	2.0	-	25	This study
$\lambda_{\theta}^{labile}$	Moisture response function of labile pool	10.0	-	25	This study
k_{θ}^{labile}	Moisture response function of labile pool	2.0	-	25	This study
k_{labile}^{nut}	Rate at which N/P can be quicker retrieved than C	1.2	-	28	This study
Allometry and allocation					
$k1_{alloc}^{fruit}$	Minimum fraction of allocation going to fruit	0.01	-	29	This study
$k3_{alloc}^{fruit}$	Reserve usage rate below which fruit growth starts	0.1	$\frac{\mu\mathrm{molC}}{\mathrm{m^2\ s}}$	29	This study
λ_{alloc}^{fruit}	Shape parameter in the fruit allocation response to reserve changes	10.0	-	29	This study
$k4_{alloc}^{fruit}$	Shape parameter in the fruit allocation response to reserve changes	2.0	-	29	This study
$W_{soil,crit}^{alloc}$	Fraction of root zone water at field capacity below which root allocation starts responding	0.8	-	35	This study
k_{htol}	Stem mass to leaf mass ratio of grasses	0.05	-	30	Zaehle and Friend (2010)

Table M3. Vegetation growth and dynamics parameters (ctnd.)

Symbol	Description	Value	Unit	Equation	Citation
Stoichiometry					
C_m	Carbon mass per unit dry weight of leaves	0.48	$\frac{\mathrm{gC}}{\mathrm{gDW}}$	-	Kattge et al. (2011)
$\chi_{root}^{C:N}$	Relative C:N of fine roots compared to leaves	0.85	-	Sect. M3.5	Zaehle and Friend (2010)
$\chi_{wood}^{C:N}$	Relative C:N of woody biomass compared to leaves	0.145	-	Sect. M3.5	Zaehle and Friend (2010)
$\chi_{root}^{N:P}$	Relative N:P of fine roots compared to leaves	1.0	-	Sect. M3.5	This study
$\chi_{wood}^{N:P}$	Relative N:P of woody biomass compared to leaves	1.0	-	Sect. M3.5	This study
δ_{leaf}^{χ}	Maximum rate of foliar stoichiometry change	0.0048	day^{-1}	36	(Zaehle and Friend, 2010)
λ_{leaf}^{χ}	Shape parameter in leaf stoichiometry nutrient response	2.0	-	37	(Zaehle and Friend, 2010)
k_{leaf}^{χ}	Shape parameter in leaf stoichiometry nutrient response	8.0	-	37	(Zaehle and Friend, 2010)
Reserve dynamics					
LAI_{max}^{target}	Maximum LAI target for reserve use calculations	5.0	$\frac{\mathrm{m}^2}{\mathrm{m}^2}$	39	This study
$\lambda_{maint,C}^{\Phi}$	Shape parameter for pull from reserve C to labile C pools	4.0	-	40	This study
$k_{maint,C}^{\Phi}$	Shape parameter for pull from reserve C to labile C pools	1.2	-	40	This study
$k_{maint,NP}^{\Phi}$	Shape parameter for pull from reserve N|P to labile N|P pools	1.6	-	40	This study
$\lambda_{maint,NP}^{\Phi}$	Shape parameter for pull from reserve N|P to labile N|P pools	3.0	-	40	This study
λ_{store}^{Φ}	Shape parameter for pull from labile to reserve pool	2.0	-	40	This study
k_{store}^{Φ}	Shape parameter for pull from labile to reserve pool	3.0		40	This study
λ_{phen}^{Φ}	Shape parameter in storage response function to phenology	1.3	-	42	This study
k_{phen}^{Φ}	Shape parameter in storage response function to phenology	8.0	-	42	This study
$\lambda_{sinklim}^{ps}$	Photosynthetic sink limitation with labile C accumulation	0.1	-	43	This study
$k_{sinklim}^{ps}$	Photosynthetic sink limitation with labile C accumulation	2.0	-	43	This study
$k_{sinklim}^{CNP}$	Photosynthetic sink limitation with nutrient limitation	4.0	-	44	This study
$\beta_{sinklim,min}^{ps}$	Lower bound of photosynthetic sink limitation	0.25	-	43	This study
$f_{store,max}^{leaf}$	Maximum reserve storage in leaves relative to leaf mass	0.02	-	Sect. M3.6	This study
$f_{store,max}^{root}$	Maximum reserve storage in fine roots relative to fine root mass	0.2	-	Sect. M3.6	This study
$f_{store,max}^{wood}$	Maximum reserve storage in sap wood relative to sap wood mass	0.15	-	Sect. M3.6	This study
k_{Φ}^{inter}	Threshold value of Φ_{maint}^{X} beyond which Φ_{store}^{X} is reduced	0.75	-	41	This study

Table M3. Vegetation growth and dynamics parameters (ctnd.)

Symbol	Description	Value	Unit	Equation	Citation
Phenology					
t_{air}^{GDD}	Temperature threshold for the accumulation of growing degree days		°C	5	-	by convention
τ_{soa}	Time constant in calculation state of acclimation	114	hours	46	This study
T_{min}^{soa}	Min temp. in β_{soa} calculation	-3	°C	47	This study
T_{max}^{soa}	Max temp. in β_{soa} calculation	17	°C	47	This study
Turnover					
$\tau_{nut\_recycle}$	Time scale of foliar and fine root nutrient turnover	10.0	days	48	Zaehle and Friend (2010)
$f_{shed,max}$	Maximum rate of leaf shedding	0.05	days	49	This study
k_{resorb}^{leaf}	Fraction of nutrient resorption before leaf shedding	0.5	-	50	This study
k_{resorb}^{wood}	Fraction of nutrient resorption before wood death	0.2	-	50	This study
Vegetation dynamics					
k_{CA}	Scaling parameter in crown area to diameter relationship	100.0	-	51	Sitch et al. (2003)
k_{rp}	Scaling exponent in crown area to diameter relationship	1.6	-	51	Sitch et al. (2003)
CA_{max}	Maximum crown area	15.0	m^2	51	Sitch et al. (2003)
k_{fpc}	Light-extinction coefficient	0.5	-	52	Sitch et al. (2003)
λ_{est}^{T}	Shape parameter for temperature effect on establishment	0.075	-	Sect. M3.10	This study
k_{est}^{T}	Shape parameter for temperature effect on establishment	4.0	-	Sect. M3.10	This study
$\lambda_{est}^{\Theta_1}$	Shape parameter for moisture effect on establishment	10.0	-	Sect. M3.10	This study
$k_{est}^{\Theta_1}$	Shape parameter for moisture effect on establishment	2.0	-	Sect. M3.10	This study
FPC_{max}	Maximum foliage projective cover	0.95	-	54, 57	Sitch et al. (2003)
$k1_{mort\_greff}$	Asymptotic growth efficiency mortality rate	0.05	year^{-1}	56	Sitch et al. (2003)
$k2_{mort\_greff}$	Scaling coefficient for growth efficiency mortality rate	0.3	$\frac{\text{m}^2\ \text{yr}}{\text{molC}}$	56	Sitch et al. (2003)

Table M4. Soil biogeochemistry parameters

Symbol	Description	Value	Unit	Equation	Citation
Litter partitioning					
$f_{met,max,C}$	Maximum fraction of metabolic litter formation	0.85	-	62	Parton et al. (1993)
$k_{met,C}$	Slope of metabolic fraction with lignin to N ratio	0.018	-	62	Parton et al. (1993)
LC_{fine_root}	Lignin content of fine root	0.2565592	mol^{-1}	62	White et al. (2000)
LC_{coarse_root}	Lignin content of coarse roots	0.8163248	mol^{-1}	62	assuming woody values
LC_{woody_litter}	Lignin content of woody litter	0.8163248	mol^{-1}	62	White et al. (2000)
LC_{fruit}	Lignin content of seed bed	0.2565592	mol^{-1}	62	set to fine-roots
LC_{seed_bed}	Lignin content of fine root	0.2565592	mol^{-1}	62	set to fine-roots
$LC_{leaf,max}$	Maximum lignin content of leaves	0.3440226	mol^{-1}	63	White et al. (2000)
$k_{leaf2sla}$	Slope of lignin to sla relationship	-0.4328854	m^{-2}	63	White et al. (2000)
$k_{met,vp,N}$	Proportionality factor controlling C:N of metabolic vs. structural pool	5.0	-	64	Parton et al. (1993)
$k_{met,vp,P}$	Proportionality factor controlling C:P of metabolic vs. structural pool	5.0	-	64	Parton et al. (1993)
$\eta_{C,wl\rightarrow met,str}$	Fraction of woody litter C transformed into metabolic or structural litter	0.3	-	Sect. M4.1	following Parton et al. (1993)
Turnover times and their rate modifiers					
τ_{met}^{base}	Turnover time of metabolic litter	0.033	years	65	Parton et al. (1993)
τ_{str}^{base}	Turnover time of structural litter	0.124	years	65	Parton et al. (1993)
τ_{wl}^{base}	Turnover time of woody litter	2.5	years	65	This study
τ_{fast}^{base}	Turnover time of fast SOM pool	2.0	years	65	This study
τ_{slow}^{base}	Turnover time of slow SOM pool	100.0	years	65	This study
$T_{opt,decomp}$	Temperature of peak decomposition rate	313.15	K	65	This study
$E_{a,decomp}$	Activation energy for decomposition	53000.0	Jmol^{-1}	65	Ahrens et al. (2015)
$E_{d,decomp}$	De-activation energy for decomposition	100000.0	Jmol^{-1}	65	Ahrens et al. (2015)
$\Psi_{dec,min}$	Minimum water potential for decomposition	-2.0	MPa	65	This study

Table M4. Soil biogeochemistry parameters (ctnd.)

Symbol	Description	Value	Unit	Equation	Citation
SOM dynamics					
$\chi_{SOM^{C:N}_{fast,max}}$	Maximum C:N ratio of fast SOM	15.27693	$\frac{mol}{mol}$	66	Manzoni et al. (2008)
$\chi_{SOM^{C:N}_{fast,min}}$	Minimum C:N ratio of fast SOM	5.830891	$\frac{mol}{mol}$	66	Manzoni et al. (2008)
f_χ	Slope of fast SOM C:N to mineral soil N	51000.0	$\frac{\mathrm{kg}}{\mathrm{mol}}$	66	Parton et al. (1993)
$\chi_{SOM^{C:N}_{slow}}$	C:N ratio of slow SOM pool	10.4956	$\frac{mol}{mol}$	71	Parton et al. (1993)
$\chi_{SOM^{N:P}_{slow}}$	N:P ratio of slow SOM pool	30.98107	$\frac{mol}{mol}$	71	This study
$\chi_{SOM^{N:P}_{fast}}$	N:P ratio of fast SOM pool	30.98107	$\frac{mol}{mol}$	70	This study
η_N	Microbial nitrogen-use efficiency	0.8	$\frac{mol}{mol}$	67	Manzoni et al. (2008)
η_P	Microbial phosphorus-use efficiency	0.8	$\frac{mol}{mol}$	70	Manzoni et al. (2008)
$\eta_{C,litter\rightarrow fast}$	Fraction of litter transformed into fast SOM	0.45	-	70	Parton et al. (1993)
$\eta_{C,fast\rightarrow slow}$	Fraction of fast SOM transformed into slow SOM	0.15	-	71	Parton et al. (1993)
$\eta_{C,slow\rightarrow fast}$	Fraction of slow SOM transformed into fast SOM	0.3	-	71	Parton et al. (1993)
k^{diff}_{org}	Diffusion velocity due to bioturbation	0.15	$\frac{m^2\ kg}{m^3\ yr}$	72	Koven et al. (2013)
ρ^{bulk}_{org}	Bulk density of organic material	150.3935	$\frac{\mathrm{kg}}{\mathrm{m}^3}$	72	Ahrens et al. (2015)
Nutrient uptake kinetics					
$T_{opt,uptake}$	Temperature of peak uptake rate	313.15	K	73	??
$E_{a,uptake}$	Activation energy for uptake	53000.0	Jmol^{-1}	73	Ahrens et al. (2015)
$E_{d,uptake}$	De-activation energy for uptake	100000.0	Jmol^{-1}	73	Ahrens et al. (2015)
K_{m1,NH_4}	Low-affinity NH_4 uptake	0.0416	$\frac{\mathrm{m}^3}{\mathrm{mol}}$	73	Kronzucker et al. (1996)
K_{m1,NO_3}	Low-affinity parameter for plant uptake	0.0416	$\frac{\mathrm{m}^3}{\mathrm{mol}}$	73	Kronzucker et al. (1995)
K_{m1,PO_4}	Low-affinity parameter for plant uptake	229.6667	$\frac{\mathrm{L}}{\mathrm{mol}}$	73	Kavka and Polle (2016)
K_{m2,NH_4}	High-affinity parameter for plant uptake	1.0	$\frac{\mathrm{mol}}{\mathrm{m}^3}$	73	Kronzucker et al. (1996)
K_{m2,NO_3}	High-affinity parameter for plant uptake	1.0	$\frac{\mathrm{mol}}{\mathrm{m}^3}$	73	Kronzucker et al. (1995)
K_{m2,PO_4}	High-affinity parameter for plant uptake	0.000022	$\frac{\mathrm{mol}}{\mathrm{L}}$	73	Kavka and Polle (2016)
$E_{a,hsc}$	Activation energy of half-saturation point	30000.0	$\frac{J}{mol}$	73	Ahrens p. com. 2016
k_{hsc}	Scaling factor for the sensitivity of half-saturation constant to moisture limitation	0.001	-	73	Davidson et al. (2012)
$K^{half,N}_{demand}$	Fraction of target labile N at which uptake is reduced to 50%	0.75	-	73	This study
$K^{half,P}_{demand}$	Fraction of target labile P at which uptake is reduced to 50%	0.9	-	73	This study
k_{demand}	Nutrient uptake response function to labile nutrient concentration	2.0	-	73	This study
N^{BNF}_{limit}	Maximum sum of NH_4 and NO_3 at which BNF occurs	0.05	$\frac{\mathrm{molN}}{\mathrm{m}^2}$	Sect. M4.6	Zaehle and Friend (2010)
$v_{max,BNF}$	Maximum rate of BNF	0.005	$\frac{\mathrm{molN}}{\mathrm{m}^2\ \mathrm{s}}$	74	Zaehle and Friend (2010)

Table M4. Soil biogeochemistry parameters (ctnd.)

Symbol	Description	Value	Unit	Equation	Citation
Nitrification, denitrification, and BNF parameters					
λ_{anvf}	Weibull function to relate anaerobic volume fraction to soil moisture	1.3	-	75	Zaehle and Friend (2010)
k_{anvf}	Weibull function to relate anaerobic volume fraction to soil moisture	3.0	-	75	Zaehle and Friend (2010)
$v_{max,nit}$	Maximum nitrification rate	0.4	day^{-1}	76	Xu-Ri and Prentice (2008)
$E_{a,nit}$	Activation energy of nitrification	80000	$\frac{J}{mol}$	76	Xu-Ri and Prentice (2008)
$E_{d,nit}$	De-activation energy of nitrification	200000	$\frac{J}{mol}$	76	Xu-Ri and Prentice (2008)
$T_{opt,nit}$	Optimum temperature for nitrification	311.15	K	76	Xu-Ri and Prentice (2008)
$f_{nit}^{NO_y}$	Fraction of nitrification lost to NO_y	0.02	-	77	Xu-Ri and Prentice (2008)
$f_{nit}^{N_2O}$	Fraction of nitrification lost to N_2O	0.002	-	77	Xu-Ri and Prentice (2008)
$E_{a,denit}$	Activation energy of denitrification	47000	$\frac{J}{mol}$	78	Xu-Ri and Prentice (2008)
$v_{max,denit}$	Maximum denitrification rate	0.1	day^{-1}	78	Xu-Ri and Prentice (2008)
$K_{m,denit}^{fast}$	Half-saturation constant C of denitrification	20.0	$\frac{\mathrm{mol}}{\mathrm{m}^3}$	78	Xu-Ri and Prentice (2008)
$K_{m,denit}^{NO_3}$	Half-saturation constant NO_3 of denitrification	1162.598	$\frac{\mathrm{mol}}{\mathrm{m}^3}$	78	Xu-Ri and Prentice (2008)
$f_{denit}^{NO_y}$	Fraction of denitrification lost to NO_y	0.002	-	79	Xu-Ri and Prentice (2008)
$f_{denit}^{N_2O}$	Fraction of denitrification lost to N_2O	0.02	-	79	Xu-Ri and Prentice (2008)
$E_{a,diff}$	Activation energy of gas diffusion	47000	$\frac{J}{mol}$	88	Xu-Ri and Prentice (2008)

Table M4. Soil biogeochemistry parameters (ctnd.)

Symbol	Description	Value	Unit	Equation	Citation
Soil P fluxes					
k_{ocl}	Occlusion coefficient of sorbed PO_4	3.86	$10^{-13}\mathrm{s}^{-1}$	61	Yang et al. (2014)
k_{weath}	Weathering rate constant of mineral soil	8.16208	$10^{-14}\ \frac{\mathrm{molP}}{\mathrm{m}^3\ \mathrm{s}}$	80	Wang et al. (2010)
$K^{root}_{m,weath}$	Half-saturation root biomass for PO_4 weathering	10.0	$\frac{\mathrm{molC}}{\mathrm{m}^3}$	80	calibrated
$K^{PO_4}_{m,biomin}$	Half-saturation solute P concentration for PO_4 biochemical mineralization	0.001	$\frac{\mathrm{molP}}{\mathrm{m}^3}$	81	estimated
$K^{root}_{m,biomin}$	Half-saturation root C biomass for PO_4 biochemical mineralization	20.0	$\frac{\mathrm{molC}}{\mathrm{m}^3}$	81	calibrated
k_{abs}	PO_4 (ab)sorption rate from P_{lab} to P_{sorb}	651.8519	$\frac{\mu\mathrm{mol}}{\mathrm{kg\,soil\,s}}$	83	Yang et al. (2014)
$E_{a,abs}$	Activation energy for sorption to mineral surfaces	5000.0	$\frac{\mathrm{J}}{\mathrm{mol}}$	83	Ahrens p. com. 2016
k_{des}	PO_4 desorption rate from P_{sorb} to P_{lab}	0.000733	$\frac{mol}{kg\,soil\,s}$	83	Yang et al. (2014)
$E_{a,des}$	Activation energy for desorption from mineral surfaces	20000.0	$\frac{\mathrm{J}}{\mathrm{mol}}$	83	Ahrens p. com. 2016
S^{max}_{om}	PO_4 sorption capacity of organic matter	0.4	$\frac{\mathrm{mmolP}}{\mathrm{kg\,OM}}$	85	This study[1]
$S^{max}_{mineral}$	PO_4 sorption capacity of mineral soil	0.0387	$\frac{\mathrm{molP}}{\mathrm{kg\,soil}}$	85	This study[1]
$K^{sorb}_{m,om}$	Half-saturation concentration for PO_4 adsorption to OM	0.045	$\frac{\mathrm{mmolP}}{\mathrm{kg\,OM}}$	85	This study[1]
$K^{sorb}_{m,mineral}$	Half-saturation concentration for PO_4 adsorption to soil mineral	0.00225	$\frac{\mathrm{mmolP}}{\mathrm{kg\,soil}}$	85	This study[1]

[1]: Based on a literature review including Abekoe and Sahrawat (2001); Ahmed et al. (2008); Chakraborty et al. (2012); Debicka et al. (2015); Dossa et al. (2008); Fan et al. (2014); Guedes et al. (2016); Harrell and Wang (2006); Hartono et al. (2005); Herlihy and McCarthy (2006); Holford et al. (1974); Horta et al. (2013); Huang et al. (2005); Janardhanan and Daroub (2010); Kolahchi and Jalali (2013); Olander and Vitousek (2005); Pal (2011); Sakadevan and Bavor (1998); Sanyal et al. (1993); Sato and Comerford (2005); Shirvani et al. (2010); Singh et al. (2005); Singh et al. (2006); Villapando and Graetz (2001); Wisawapipat et al. (2009); Xu et al. (2006); Zafar et al. (2016); Zhou and Li (2001); Zou et al. (2011)

Table M5. Parameters for the calculation of isotopic fractionation and mixing ratios calculation

Symbol	Description	Value	Unit	Equation	Citation
a_{13C}	Discrimination of ^{13}C due to stomatal diffusion	4.4	‰	92	Drake (2014)
b_{13C}	Discrimination of ^{13}C due to Rubisco	27.0	‰	92	Drake (2014)
c_{13C}	Discrimination of ^{13}C due to PEP C	5.7	‰	92	Drake (2014)
a_{14C}	Discrimination of ^{14}C due to stomatal diffusion	8.668	‰	92	Drake (2014)
b_{14C}	Discrimination of ^{14}C due to Rubisco	51.03	‰	92	Drake (2014)
c_{14C}	Discrimination of ^{14}C due to PEP C	10.773	‰	92	Drake (2014)
ϕ_{C4}	Leakage rate of bundle sheath cells	0.16	-	92	Drake (2014)
$R_{ref,C13}$	Reference isotopic mixing ratio of $^{13}\mathrm{C}/^{12}\mathrm{C}$; PDB standard	0.0112372	$\frac{mol}{mol}$	90	-
$R_{ref,C13}$	Reference isotopic mixing ratio of $^{15}\mathrm{N}/^{14}\mathrm{N}$	0.0036765	$\frac{mol}{mol}$	90	Robinson (2001)
$\epsilon^{mic}_{uptake,NH_4}$	Discrimination due to microbial NH_4 uptake	17.0	‰	91	Robinson (2001)
$\epsilon^{plant}_{uptake,NH_4}$	Discrimination due to plant NH_4 uptake	13.5	‰	91	Robinson (2001)
$\epsilon^{plant}_{uptake,NO_3}$	Discrimination due to plant NO_3 uptake	9.5	‰	91	Robinson (2001)
ϵ_{nit}	Discrimination due to nitrification	47.5	‰	91	Robinson (2001)
$\epsilon_{nitrate,production}$	Discrimination due to NO_3 production	25.0	‰	91	Robinson (2001)
ϵ_{denit}	Discrimination due to denitrification	31.0	‰	91	Robinson (2001)
$\epsilon_{ammonification}$	Discrimination due to NH_4 production	2.5	‰	91	Robinson (2001)

Table M6. Parameters for the albedo, fAPAR and surface energy and water calculation

Albedo and fAPAR					
Symbol	Description	Value	Unit	Equation	Citation
ρ^{sbeta}	Scaling factor of solar angle in reflection calculation	1.6	-	97	Spitters (1986)
$k^{vis}_{bl,0}$	Extinction coefficient over black leaves (VIS range)	0.5	-	95	Spitters (1986)
$k^{vis}_{df,0}$	Extinction coefficient for diffuse radiation (VIS range)	0.8	-	95	Spitters (1986)
$k^{nir}_{bl,0}$	Extinction coefficient over black leaves (NIR range)	0.5	-	95	Spitters (1986)
$k^{nir}_{df,0}$	Extinction coefficient for diffuse radiation (NIR range)	0.8	-	95	Spitters (1986)
k_{csf}	Crown shape correction parameter	2.2	-	96	(Campbell and Norman, 1998)
alb^{vis}_{soil}	Soil albedo (VIS range)	0.15	-	98	Bonan (2015)
alb^{nir}_{soil}	Soil albedo (NIR range)	0.30	-	98	Bonan (2015)
Surface energy and water balance					
$k_{eff,inter}$	Efficiency of interception of precipitation as rain	0.25	-	112	Raddatz et al. (2007)
$w_{skin,max}$	Maximum water storage per unit LAI	0.0002	m	112	Raddatz et al. (2007)
k_{pref}	Preferential flow fraction of infiltrating water	0.01	m^{-1}	113	This study
$k_{pref,runoff}$	Infiltrating fraction of surface runoff	0.95	-	113	Krinner et al. (2005)

Table M7. PFT-specific parameters

Symbol	Description	Unit	Equation	Citation
σ_{vis}	Single leaf scattering albedo (VIS range)	-	97	Otto et al. (2014); Spitters (1986)
σ_{nir}	Single leaf scattering albedo (NIR range)	-	97	Otto et al. (2014); Spitters (1986)
Ω_0	Canopy clumping factor	-	96	Campbell and Norman (1998)
ϕ_{crown}	Crown shape factor	-	96	Campbell and Norman (1998)
sla	Specific leaf area	$\frac{\mathrm{m}^2}{\mathrm{molC}}$	-	Kattge et al. (2011)
$\chi_{leaf}^{C:N}$	Default foliar C:N	$\frac{\mathrm{gC}}{\mathrm{gN}}$	Sect. M3.5	Kattge et al. (2011)
$\chi_{leaf,min}^{C:N}$	Minimum foliar C:N	$\frac{\mathrm{gC}}{\mathrm{gN}}$	37	Kattge et al. (2011)
$\chi_{leaf,max}^{C:N}$	Maximum foliar C:N	$\frac{\mathrm{gC}}{\mathrm{gN}}$	37	Kattge et al. (2011)
$\chi_{leaf}^{N:P}$	Default foliar N:P	$\frac{\mathrm{gN}}{\mathrm{gP}}$	Sect. M3.5	Kattge et al. (2011)
$\chi_{leaf,min}^{N:P}$	Minimum foliar N:P	$\frac{\mathrm{gN}}{\mathrm{gP}}$	37	Kattge et al. (2011)
$\chi_{leaf,min}^{N:P}$	Maximum foliar N:P	$\frac{\mathrm{gN}}{\mathrm{gP}}$	37	Kattge et al. (2011)
k_0^{struc}	Maximum fraction of structural foliar N	-	4	Friend et al. (1997); Kattge et al. (2011)
$fN_{struc,cl}^{min}$	Minimum fraction of structural foliar N	-	4	This study
T_Ω	Shape parameter of J_{max} temperature response	K	9	Friend (2010)
g_0	Intercept of the A_n g_s relationship	-	17	Lin et al. (2015)
g_1	Slope of the A_n g_s relationship	-	17	Lin et al. (2015)
g_{min}	Minimum stomatal conductance	$\frac{\mathrm{m}}{\mathrm{s}}$	17	This study
τ_{leaf}	Turnover time of leaves	years	Sect. M3.9	Kattge et al. (2011)
τ_{fine_root}	Turnover time of fine roots	years	Sect. M3.9	Ahrens et al. (2014)
τ_{coarse_root}	Turnover time of coarse roots	years	Sect. M3.9	Ahrens et al. (2014)
τ_{branch}	Turnover time of branches	years	Sect. M3.9	This study
τ_{sap_wood}	Turnover time of the sapwood	years	Sect. M3.9	Sitch et al. (2003)
τ_{fruit}	Turnover time of the fruit	years	Sect. M3.9	This study
τ_{seed_litter}	Turnover time of the seed bed to litter	years	M3.9	This study
$\tau_{seed,est}$	Turnover time of the seed bed to establishment	years	53	This study
$v_{max,NH_4\|NO_3}$	Maximum plant N uptake rate	$\frac{\mu\mathrm{mol\,N}}{\mathrm{mol\,C\,s}}$	73	Zaehle et al. (2010)
v_{max,PO_4}	Maximum plant P uptake rate	$\frac{\mu\mathrm{mol\,P}}{\mathrm{mol\,C\,s}}$	73	Kavka and Polle (2016)

Table M7. PFT-specific parameters (ctnd.)

Symbol	Description	Unit	Equation	Citation
GDD_{req}^{max}	Maximum GDD requirement in the absence of chilling	$^{\circ}\mathrm{C\,days}$	45	This study
$k_{dormance}^{GDD}$	Response of GDD to number of dormant days	days^{-1}	45	This study
β_{soil}^{flush}	Soil water level inducing leaf flushing	-	Sect. M3.8	This study
β_{soil}^{sen}	Soil water stress inducing leaf senescence	-	Sect. M3.8	This study
t_{air}^{sen}	Air temperature threshold inducing leaf senescence	$^{\circ}\mathrm{C}$	Sect. M3.8	This study
age_{min}^{leaf}	Minimum leaf age before senescence	days	Sect. M3.8	This study
$f_{sap\_wood}^{branch}$	Fraction of sapwood in branches	-	Sect. M4.2	This study
ρ_{wood}	Wood density	$\frac{\mathrm{g\,C}}{\mathrm{cm}^3}$	31	Chave et al. (2009); Zanne et al. (2009)
k_{latosa}	Leaf area to sapwood area ratio	-	31	Zaehle et al. (2010)
k_{ctos}	Coarse root to sapwood mass ratio	-	33	This study
k_{rtos}	Trade-off parameter for hydraulic investment into sapwood or fine roots	-	34	This study
$k2_{alloc}^{fruit}$	Maximum fraction of growth allocated to fruit	-	29	This study
$k1_{allom}$	Parameter in height diameter relationship	-	32	Zaehle et al. (2010)
$k2_{allom}$	Parameter in height diameter relationship	-	32	Zaehle et al. (2010)
Ψ_{leaf}^{min}	Minimum leaf water potential	MPa	18	Hickler et al. (2006)
$k_{reserve}^{target}$	Target size of the long-term reserve pool	-	39	This study
k_{root_dist}	Exponent describing the vertical root profile	-	3	Jackson et al. (1996)
k_{seed}	Seed size	molC	58	This study
$mort_{bg,PFT}$	Background mortality rate	year^{-1}	56	Sitch et al. (2003)

Table M8. PFT-specific parameter values

Parameter	TrBE	TeBE	TrBR	TeBS	BNE	BNS	TeH	TrH
PS pathway	C3	C3	C3	C3	C3	C3	C3	C4
σ_{vis}	0.17	0.17	0.17	0.17	0.15	0.15	0.2	0.2
σ_{nir}	0.76	0.76	0.76	0.76	0.73	0.73	0.8	0.8
Ω_0	0.9	0.9	0.9	0.9	0.5	0.7	1.0	1.0
ϕ_{crown}	3.34	3.34	3.34	3.34	2.19	2.88	3.34	3.34
sla	0.24	0.22	0.39	0.39	0.13	0.25	0.50	0.48
$\chi_{leaf}^{C:N}$	28.4	35.0	22.5	22.5	39.7	24.8	26.9	33.9
$\chi_{leaf,min}^{C:N}$	14.0	14.0	14.0	14.0	24.0	16.0	13.7	17.1
$\chi_{leaf,max}^{C:N}$	38.7	38.7	38.7	38.7	64.9	31.0	40.0	48.0
$\chi_{leaf}^{N:P}$	16.8	14.0	12.7	12.7	8.4	9.1	10.7	8.9
$\chi_{leaf,min}^{N:P}$	8.4	7.0	6.3	6.3	4.2	4.5	5.3	4.4
$\chi_{leaf,min}^{N:P}$	25.3	21.0	19.0	19.0	12.6	13.6	16.0	13.3
k_0^{struc}	0.75	0.70	0.63	0.63	0.83	0.79	0.3	0.3
$fN_{struc,cl}^{min}$	0.57	0.52	0.45	0.45	0.65	0.61	0.12	0.12
T_Ω	18.0	18.0	18.0	18.0	18.0	18.0	18.0	18.0
g_0	0.01	0.01	0.01	0.01	0.01	0.01	0.03	0.03
g_1	9.3	8.3	7.0	10.9	5.5	7.0	9.3	2.0
g_{min}	0.00006	0.00006	0.00006	0.00006	0.00003	0.00003	0.00006	0.00006
τ_{leaf}	1.4	1.32	0.48	0.48	3.31	0.51	0.32	0.32
τ_{fine_root}	0.7	0.7	0.7	0.7	0.7	0.7	0.7	0.7
τ_{coarse_root}	8.0	8.0	8.0	8.0	8.0	8.0	8.0	8.0
τ_{branch}	10.0	10.0	10.0	10.0	10.0	10.0	10.0	10.0
τ_{sap_wood}	40.0	40.0	40.0	40.0	40.0	40.0	40.0	40.0
τ_{fruit}	1.0	1.0	1.0	1.0	1.0	1.0	1.0	1.0
τ_{seed_litter}	2.0	2.0	2.0	2.0	2.0	2.0	2.0	2.0
τ_{seed_est}	20.0	20.0	20.0	20.0	20.0	20.0	20.0	20.0
$v_{max,N}$	0.42	0.42	0.42	0.42	0.42	0.42	0.42	0.42
$v_{max,P}$	0.0044	0.0044	0.0044	0.0044	0.0044	0.0044	0.0044	0.0044

Table M8. Lctlib Parameter Values per PFT (ctnd.)

Parameter	TrBE	TeBE	TrBR	TeBS	BNE	BNS	TeH	TrH
Phenotype	evergreen	evergreen	raingreen	summergreen	evergreen	summergreen	perennial	perennial
GDD_{req}^{max}	0.0	0.0	0.0	800.0	0.0	800.0	10.0	10.0
$k_{dormance}^{GDD}$	0.0	0.0	0.0	0.007	0.0	0.0098	0.1	0.1
β_{soil}^{flush}	0.0	0.0	0.98	0.0	0.0	0.0	0.9	0.9
β_{soil}^{sen}	0.0	0.0	0.5	0.0	0.0	0.0	0.01	0.01
t_{air}^{sen}	0.0	0.0	0.0	8.5	0.0	5.0	0.0	0.0
age_{min}^{leaf}	10	10	10	50	10	10	10	10
Growthform	tree	tree	tree	tree	tree	tree	herb.	herb.
$f_{sap\_wood}^{branch}$	0.05	0.05	0.05	0.05	0.05	0.05	n.a.	n.a.
ρ_{wood}	0.3	0.3	0.3	0.3	0.3	0.3	n.a.	n.a.
k_{latosa}	4000.0	4000.0	4000.0	4000.0	4000.0	4000.0	n.a.	n.a.
k_{crtos}	0.1	0.1	0.1	0.1	0.1	0.1	n.a.	n.a.
k_{rtos}	4.21	4.21	4.21	4.21	4.21	4.21	10.0	10.0
$k2_{alloc}^{fruit}$	0.1	0.1	0.1	0.1	0.1	0.1	0.2	0.2
$k1_{allom}$	55.0	55.0	55.0	55.0	55.0	55.0	n.a.	n.a.
$k2_{allom}$	0.65	0.65	0.65	0.65	0.65	0.65	n.a.	n.a.
Ψ_{leaf}^{min}	-2.0	-2.0	-2.0	-2.0	-2.0	-2.0	-1.5	-1.5
$k_{reserve}^{target}$	1.0	1.2	1.0	1.0	0.5	1.0	1.0	1.0
k_{root_dist}	3.5	2.8	2.5	3.5	3.5	3.5	5.5	5.5
k_{seed}	0.5	0.5	0.5	0.5	0.5	0.5	0.1	0.1
$mort_{bg,PFT}$	0.1	0.1	0.1	0.1	0.1	0.1	0.05	0.05

References

Abekoe, M. K. and Sahrawat, K. L.: Phosphate retention and extractability in soils of the humid zone in West Africa, Geoderma, 102, 175–187, https://doi.org/10.1016/S0016-7061(00)00110-5, http://linkinghub.elsevier.com/retrieve/pii/S0016706100001105, 2001.

Ahmed, M. F., Kennedy, I. R., Choudhury, a. T. M. a., Kecskes, M. L., and Deaker, R.: Phosphorus adsorption in some Australian soils and influence of bacteria on the desorption of phosphorus, Communications in Soil Science and Plant Analysis, 39, 1269–1294, https://doi.org/10.1080/00103620802003963, http://www.tandfonline.com/doi/abs/10.1080/00103620802003963, 2008.

Ahrens, B., Hansson, K., Solly, E. F., and Schrumpf, M.: Reconcilable differences: a joint calibration of fine-root turnover times with radiocarbon and minirhizotrons, New Phytologist, 204, 932–942, 2014.

Ahrens, B., Braakhekke, M. C., Guggenberger, G., Schrumpf, M., and Reichstein, M.: Contribution of sorption, DOC transport and microbial interactions to the 14C age of a soil organic carbon profile: Insights from a calibrated process model, Soil Biology and Biochemistry, 88, 390–402, 2015.

Atkin, O. K., Meir, P., and Turnbull, M. H.: Improving representation of leaf respiration in large-scale predictive climate–vegetation models, New Phytologist, 202, 743–748, https://doi.org/10.1111/nph.12686, https://nph.onlinelibrary.wiley.com/doi/abs/10.1111/nph.12686, 2014.

Ball, J., Wooddrow, I., and Berry, J. A.: A model predicting stomatal conductance and its contribution to the control of photosynthesis under different environmental conditions, in: Progress in Photosynthesis Research, edited by Biggens, J., pp. 1–4, Dordrecht, The Netherlands, 1987.

Barrow, N. J.: The description of phosphate adsorption curves, Journal of Soil Science, 29, 447–462, 1978.

Bernacchi, C. J., Singsaas, E. L., Pimentel, C., Protis JR, A. R., and Long, S. P.: Improved temperature response functions for models of Rubisco-limited photosynthesis, Plant, Cell & Environment, 24, 253–259, 2001.

Bonan, G.: Ecological Climatology: Concepts and Applications, Cambridge University Press, 3 edn., https://doi.org/10.1017/CBO9781107339200, 2015.

Brüggemann, N., Gessler, A., Kayler, Z., Keel, S. G., Badeck, F., Barthel, M., Boeckx, P., Buchmann, N., Brugnoli, E., Esperschütz, J., Gavrichkova, O., Ghashghaie, J., Gomez-Casanovas, N., Keitel, C., Knohl, A., Kuptz, D., Palacio, S., Salmon, Y., Uchida, Y., and Bahn, M.: Carbon allocation and carbon isotope fluxes in the plant-soil-atmosphere continuum: a review, Biogeosciences, 8, 3457–3489, 2011.

Campbell, G. S. and Norman, J. M.: An Introduction to Environmental Biophysics, Springer, 1998.

Chakraborty, D., Nair, V. D., and Harris, W. G.: Compositional Differences Between Alaquods and Paleudults Affecting Phosphorus Sorption-Desorption Behavior, Soil Science, 177, 188–197, https://doi.org/10.1097/SS.0b013e31824329ca, http://content.wkhealth.com/linkback/openurl?sid=WKPTLP:landingpage&an=00010694-201203000-00006, 2012.

Chave, J., Coomes, D., Jansen, S., Lewis, S. L., Swenson, N. G., and Zanne, A. E.: Towards a worldwide wood economics spectrum, Ecology letters, 12, 351–366, https://doi.org/10.1111/j.1461-0248.2009.01285.x, http://dx.doi.org/10.1111/j.1461-0248.2009.01285.x, 2009.

Collatz, G. J., Ribas-Carbo, M., and Berry, J. A.: Coupled photosynthesis-stomatal conductance model for leaves of C4 plants, Australian Journal of Plant Physiology, 19, 519–538, 1992.

Davidson, E. A., Samanta, S., Caramori, S. S., and Savage, K.: The Dual Arrhenius and Michaelis-Menten kinetics model for decomposition of soil organic matter at hourly to seasonal time scales, Glob. Change Biol., 18, 371–384, 2012.

Debicka, M., Kocowicz, A., Weber, J., and Jamroz, E.: Organic matter effects on phosphorus sorption in sandy soils, Archives of Agronomy and Soil Science, 62, 840–855, https://doi.org/10.1080/03650340.2015.1083981, 2015.

Dossa, E. L., Baham, J., Khouma, M., Sene, M., Kizito, F., and Dick, R. P.: Phosphorus Sorption and Desorption in Semiarid Soils of Senegal Amended With Native Shrub Residues, Soil Science, 173, 669–682, https://doi.org/10.1097/SS.0b013e3181893999, http://content.wkhealth.com/linkback/openurl?sid=WKPTLP:landingpage&an=00010694-200810000-00001, 2008.

Drake, B. L.: Using Models of Carbon Isotope Fractionation during Photosynthesis to Understand the Natural Fractionation Ratio, Radiocarbon, 56, 29–38, 2014.

Evans, J. R.: Photosynthesis and nitrogen relationships in leaves of C3 plants, Oecologia, 78, 9–19, 1989.

Fan, H., Huang, D., Zhou, L., and Jia, Y.: Effects of freeze–thaw cycles on phosphorus adsorption and desorption in the black soil of northeastern China, Acta Agriculturae Scandinavica, Section B — Soil & Plant Science, 64, 24–32, https://doi.org/10.1080/09064710.2014.882401, 2014.

Farquhar, G. D., OLeary, M. H., and Berry, J. A.: On the Relationship Between Carbon Isotope Discrimination and the Intercellular Carbon Dioxide Concentration in Leaves, Functional Plant Biology, 9, 121–137, 1982.

Friend, A. D.: Modelling canopy CO2 fluxes: are 'big-leaf'simplifications justified?, Global ecology and biogeography: a journal of macroecology, 10, 603–619, https://nph.onlinelibrary.wiley.com/doi/abs/10.1046/j.1466-822x.2001.00268.x, 2001.

Friend, A. D.: Terrestrial plant production and climate change, Journal of Experimental Botany, 61, 1293–1309, 2010.

Friend, A. D., Stevens, A. K., Knox, R. G., and Cannell, M. G. R.: A process-based, terrestrial biosphere model of ecosystem dynamics (Hybrid v3.0), Ecological modelling, 95, 249–287, 1997.

Friend, A. D., Geider, R. J., Behrenfeld, M. J., and Still, C. J.: Photosynthesis in Global-Scale Models, in: Photosynthesis in silico: Understanding complexity from molecules to ecosystems, edited by Laisk, A., Nedbal, L., and Govindjee, pp. 465–497, Springer, 2009.

Guedes, R. S., Melo, L. C. A., Vergütz, L., Rodríguez-Vila, A., Covelo, E. F., and Fernandes, A. R.: Adsorption and desorption kinetics and phosphorus hysteresis in highly weathered soil by stirred flow chamber experiments, Soil and Tillage Research, 162, 46–54, https://doi.org/10.1016/j.still.2016.04.018, 2016.

Harrell, D. L. and Wang, J. J.: Fractionation and Sorption of Inorganic Phosphorus in Louisiana Calcareous Soils, Soil Science, 171, 39–51, https://doi.org/10.1097/01.ss.0000187347.37825.46, http://content.wkhealth.com/linkback/openurl?sid=WKPTLP:landingpage&an=00010694-200601000-00006, 2006.

Hartmann, H., Adams, H. D., Hammond, W. M., Hoch, G., Landhäusser, S. M., Wiley, E., and Zaehle, S.: Identifying differences in carbohydrate dynamics of seedlings and mature trees to improve carbon allocation in models for trees and forests, Environmental and Experimental Botany, 152, 7–18, 2018.

Hartono, A., Funakawa, S., and Kosaki, T.: Phosphorus sorption-desorption characteristics of selected acid upland soils in Indonesia, Soil Science and Plant Nutrition, 51, 787–799, https://doi.org/10.1111/j.1747-0765.2005.tb00113.x, http://www.tandfonline.com/doi/abs/10.1111/j.1747-0765.2005.tb00113.x, 2005.

Herlihy, M. and McCarthy, J.: Association of soil-test phosphorus with phosphorus fractions and adsorption characteristics, Nutrient Cycling in Agroecosystems, 75, 79–90, https://doi.org/10.1007/s10705-006-9013-2, http://link.springer.com/10.1007/s10705-006-9013-2, 2006.

Hickler, T., Prentice, I. C., Smith, B., SYKES, M. T., and Zaehle, S.: Implementing plant hydraulic architecture within the LPJ Dynamic Global Vegetation Model, Global Ecology and Biogeography, 15, 567–577, 2006.

Holford, i. C. R., Wedderburn, r. W. M., and Mattingly, g. E. G.: A langmuir two-surface equation as a model for phosphate adsorption by soils, Journal of Soil Science, 25, 242–255, https://doi.org/doi:10.1111/j.1365-2389.1974.tb01121.x, https://onlinelibrary.wiley.com/doi/abs/10.1111/j.1365-2389.1974.tb01121.x, 1974.

Horta, C., Monteiro, F., Madeira, M., and Torrent, J.: Phosphorus sorption and desorption properties of soils developed on basic rocks under a subhumid Mediterranean climate, Soil Use and Management, 29, 15–23, https://doi.org/10.1111/j.1475-2743.2012.00405.x, 2013.

Huang, Q., Liang, W., and Cai, P.: Adsorption, desorption and activities of acid phosphatase on various colloidal particles from an Ultisol, Colloids and surfaces B: Biointerfaces, 45, 209–214, https://doi.org/10.1016/j.colsurfb.2005.08.011, http://www.ncbi.nlm.nih.gov/pubmed/16198547, 2005.

Jackson, R. B., Canadell, J., Ehleringer, J. R., Mooney, H. A., Sala, O. E., and Schulze, E. D.: A global analysis of root distributions for terrestrial biomes, Oecologia, 108, 389–411, 1996.

Janardhanan, L. and Daroub, S. H.: Phosphorus Sorption in Organic Soils in South Florida, Soil Science Society of America Journal, 74, 1597–1597, https://doi.org/10.2136/sssaj2009.0137, https://www.soils.org/publications/sssaj/abstracts/74/5/1597, 2010.

June, T., Evans, J. R., and Farquhar, G. D.: A simple new equation for the reversible temperature dependence of photosynthetic electron transport: a study on soybean leaf, Functional Plant Biology, 31, 275, 2004.

Kattge, J., Díaz, S., Lavorel, S., Prentice, I. C., Leadley, P., Bönisch, G., Garnier, E., Westoby, M., Reich, P. B., Wright, I. J., Cornelissen, J. H. C., Violle, C., Harrison, S. P., Van Bodegom, P. M., Reichstein, M., Enquist, B. J., Soudzilovskaia, N. A., Ackerly, D. D., Anand, M., Atkin, O., Bahn, M., Baker, T. R., Baldocchi, D., Bekker, R., Blanco, C. C., Blonder, B., Bond, W. J., Bradstock, R., Bunker, D. E., Casanoves, F., Caverner-Bares, J., Chambers, J. Q., Chapin III, F. S., Chave, J., Coomes, D., Cornwell, W. K., Craine, J. M., Dobrin, B. H., Duarte, L., Durka, W., Elser, J., Esser, G., Estiarte, M., Fagan, W. F., Fand, J., Fernández-Méndez, F., Fidelis, A., Finegan, B., Flores, O., Ford, H., Frank, D., Freschet, G. T., Fyllas, N. M., Gallagher, R. V., Green, W. A., Gutierrez, A. G., Thomas, H., Higgins, S. I., Hodgson, J. G., Jalili, A., Jansen, S., Joly, C. A., Kerkhoff, A. J., Kirkup, D., Kitajima, K., Kleyer, M., Klotz, S., Knops, J. M. H., Kramer, K., Kühn, I., Kurokawa, H., Laughlin, D., Lee, T. D., Leishman, M., Lens, F., Lenz, T., Lewis, S. L., Lloyd, J., Llusià, J., Louault, F., Ma, S., Mahecha, M. D., Manning, P., Massad, T., Medlyn, B. E., Messier, J., Moles, A. T., Müller, S. C., Nadrowski, K., Naeem, S., Niinemets, Ü., Nöllert, S., Nüske, A., Ogaya, R., Oleksyn, J., Onipchenko, V. G., Onoda, Y., Ordoñez, J., Overbeck, G., Ozinga, W. A., Patino, S., Paula, S., Pausas, J. G., Peñuelas, J., Phillips, O. L., Pillar, V., Poorter, H., Poorter, L., Poschlod, P., Prinzing, A., Proulx, R., Rammig, A., Reinsch, S., Reu, B., Sack, L., Salgado-Negret, B., Sardans, J., Shiodera, S., Shipley, B., Siefert, A., Sosinski, E., Soussana, J. F., Swaine, E., Swenson, N., Thompson, K., Thornton, P., Waldram, M., Weiher, E., White, M., White, S., Wright, S. J., Yguel, B., Zaehle, S., Zanne, A. E., and Wirth, C.: TRY - a global database of plant traits, Global Change Biology, 17, 2905–2935, 2011.

Kavka, M. and Polle, A.: Phosphate uptake kinetics and tissue-specific transporter expression profiles in poplar (Populus × canescens) at different phosphorus availabilities, BMC Plant Biology, 16, 206, https://doi.org/10.1186/s12870-016-0892-3, https://doi.org/10.1186/s12870-016-0892-3, 2016.

Knauer, J., Werner, C., and Zaehle, S.: Evaluating stomatal models and their atmospheric drought response in a land surface scheme: A multibiome analysis, Journal of Geophysical Research: Biogeosciences, 120, 1894–1911, 2015.

Kolahchi, Z. and Jalali, M.: Phosphorus Movement and Retention by Two Calcareous Soils, Soil and Sediment Contamination: An International Journal, 22, 21–38, https://doi.org/10.1080/15320383.2012.697939, 2013.

Koven, C. D., Riley, W. J., Subin, Z. M., Tang, J. Y., Torn, M. S., Collins, W. D., Bonan, G. B., Lawrence, D. M., and Swenson, S. C.: The effect of vertically resolved soil biogeochemistry and alternate soil C and N models on C dynamics of CLM4, Biogeosciences, 10, 7109–7131, 2013.

Krinner, G., Viovy, N., de Noblet-Ducoudré, N., Ogée, J., Polcher, J., Friedlingstein, P., Ciais, P., Sitch, S. A., and Prentice, I. C.: A dynamic global vegetation model for studies of the coupled atmosphere-biosphere system, Global Biogeochemical Cycles, 19, GB1015, 2005.

Kronzucker, H. J., Siddiqi, M. Y., and Glass, A. D. M.: Kinetics Of NO3-Influx In Spruce, Plant Physiology, 109, 319–326, 1995.

Kronzucker, H. J., Siddiqi, M. Y., and Glass, A. D. M.: Kinetics of NH4+ influx in spruce, Plant Physiology, 110, 773–779, 1996.

Kull, O. and Kruijt, B.: Leaf photosynthetic light response: a mechanistic model for scaling photosynthesis to leaves and canopies, Functional Ecology, 12, 767–777, 1998.

Levin, I., Naegler, T., Kromer, B., Diehl, M., Francey, R., Gomez-Pelaez, A., Steele, P., Wagenbach, D., Weller, R., and Worthy, D.: Observations and modelling of the global distribution and long-term trend of atmospheric $^{14}CO_2$, Tellus Series B-Chemical and Physical Meteorology, 62, 26–46, 2010.

Lin, Y.-S., Medlyn, B. E., Duursma, R. A., Prentice, I. C., Wang, H., Baig, S., Eamus, D., de Dios, V. R., Mitchell, P., Ellsworth, D. S., de Beeck, M. O., Wallin, G., Uddling, J., Tarvainen, L., Linderson, M.-L., Cernusak, L. A., Nippert, J. B., Ocheltree, T. W., Tissue, D. T., Martin-StPaul, N. K., Rogers, A., Warren, J. M., De Angelis, P., Hikosaka, K., Han, Q., Onoda, Y., Gimeno, T. E., Barton, C. V. M., Bennie, J., Bonal, D., Bosc, A., Low, M., Macinins-Ng, C., Rey, A., Rowland, L., Setterfield, S. A., Tausz-Posch, S., Zaragoza-Castells, J., Broadmeadow, M. S. J., Drake, J. E., Freeman, M., Ghannoum, O., Hutley, L. B., Kelly, J. W., Kikuzawa, K., Kolari, P., Koyama, K., Limousin, J. M., Meir, P., Lola da Costa, A. C., Mikkelsen, T. N., Salinas, N., Sun, W., and Wingate, L.: Optimal stomatal behaviour around the world, Nature Climate Change, 5, 459–464, 2015.

Lloyd, J. and Taylor, J. A.: On the temperature dependence of soil respiration, Functional ecology, pp. 315–323, https://www.jstor.org/stable/2389824, 1994.

Makino, A., Sakuma, H., Sudo, E., and Mae, T.: Differences between maize and rice in N-use efficiency for photosynthesis and protein allocation, Plant & cell physiology, 44, 952–956, https://www.ncbi.nlm.nih.gov/pubmed/14519777, 2003.

Manzoni, S., Porporato, A., and Schimel, J. P.: Soil heterogeneity in lumped mineralization–immobilization models, Soil Biology and Biochemistry, 40, 1137–1148, 2008.

McGill, W. B. and Cole, C. V.: Comparative aspects of cycling of organic C, N, S and P through soil organic matter, Geoderma, 26, 267–286, 1981.

Meyerholt, J. and Zaehle, S.: The role of stoichiometric flexibility in modelling forest ecosystem responses to nitrogen fertilization, New Phytologist, pp. n/a–n/a, 2015.

Monteith, J. L. and Unsworth, M. H.: Principles of Environmental Physics (Fourth Edition), Academic Press, Boston, fourth edition edn., https://doi.org/https://doi.org/10.1016/B978-0-12-386910-4.00023-8, http://www.sciencedirect.com/science/article/pii/B9780123869104000238, 2013.

Mäkelä, A., Hari, P., Berninger, F., Hänninen, H., and Nikinmaa, E.: Acclimation of photosynthetic capacity in Scots pine to the annual cycle of temperature, Tree Physiology, 24, 369–376, https://doi.org/10.1093/treephys/24.4.369, http://dx.doi.org/10.1093/treephys/24.4.369, 2004.

Niinemets, Ü. and Tenhunen, J. D.: A model separating leaf structural and physiological effects on carbon gain along light gradients for the shade-tolerant species Acer saccharum, Plant, Cell and Environment, 20, 845–866, 1997.

Niinemets, Ü., Kull, O., and Tenhunen, J. D.: An analysis of light effects on foliar morphology, physiology, and light interception in temperate deciduous woody species of contrasting shade tolerance, Tree Physiology, 18, 681–696, https://doi.org/10.1093/treephys/18.10.681, http://dx.doi.org/10.1093/treephys/18.10.681, 1998.

Olander, L. P. and Vitousek, P. M.: Short-term controls over inorganic phosphorus during soil and ecosystem development, Soil Biology and Biochemistry, 37, 651–659, https://doi.org/10.1016/j.soilbio.2004.08.022, 2005.

Otto, J., Berveiller, D., Bréon, F.-M., Delpierre, N., Geppert, G., Granier, A., Jans, W., Knohl, A., Kuusk, A., Longdoz, B., and Others: Forest summer albedo is sensitive to species and thinning: how should we account for this in Earth system models?, Biogeosciences, 11, 2411–2427, https://goedoc.uni-goettingen.de/handle/1/10219, 2014.

Pal, S. K.: Phosphorus sorption-desorption characteristics of soils under different land use patterns of eastern India, Archives of Agronomy and Soil Science, 57, 365–376, https://doi.org/10.1080/03650341003605743, http://www.tandfonline.com/doi/abs/10.1080/03650341003605743, 2011.

Parton, W. J., Scurlock, J. M. O., Ojima, D. S., Gilmanov, T. G., Scholes, R. J., Schimmel, D. S., Kirchner, T., Menaut, J. C., Seastedt, T., Moya, E. G., Kamnalrut, A., and Kinyamario, J. I.: Observations and modelling of biomass and soil organic matter dynamics for the grassland biome worldwide, Global Biogeochemical Cycles, 7, 785–809, 1993.

Raddatz, T. J., Reick, C. H., Knorr, W., Kattge, J., Roeckner, E., Schnur, R., Schnitzler, K.-G., Wetzel, P., and Jungclaus, J.: Will the tropical land biosphere dominate the climate–carbon cycle feedback during the twenty-first century?, Climate Dynamics, 29, 565–574, https://doi.org/10.1007/s00382-007-0247-8, https://doi.org/10.1007/s00382-007-0247-8, 2007.

Robinson, D.: δ15N as an integrator of the nitrogen cycle, Trends in ecology & evolution, 16, 153–162, https://doi.org/10.1016/S0169-5347(00)02098-X, http://www.sciencedirect.com/science/article/pii/S016953470002098X, 2001.

Roeckner, E., Tompkins, A., Bäuml, G., Bonaventura, L., Brokopf, R., Esch, M., Giorgetta, M., Hagemann, S., Kirchner, I., Kornblueh, L., Manzini, E., Rhodin, E., Schlese, U., and Schulzweida, U.: The atmospheric general circulation model ECHAM5 - Part I: Model description, Tech. Rep. 349, Max Planck Institute for Meteorology, Hamburg, 2003.

Rogers, A., Medlyn, B. E., Dukes, J. S., Bonan, G. B., von Caemmerer, S., Dietze, M. C., Kattge, J., Leakey, A. D. B., Mercado, L. M., Niinemets, Ü., Prentice, I. C., Serbin, S. P., Sitch, S. A., Way, D. A., and Zaehle, S.: A roadmap for improving the representation of photosynthesis in Earth system models, New Phytologist, 213, 22–42, 2017.

Sakadevan, K. and Bavor, H. J.: Phosphate adsorption characteristics of soils, slags and zeolite to be used as substrates in constructed wetland systems, Water Research, 32, 393–399, https://doi.org/10.1016/S0043-1354(97)00271-6, 1998.

Sanyal, S. K., Chan, P. Y., and De Datta, S. K.: Phosphate Sorption-Desorption Behavior of Some Acidic Soils of South and Southeast Asia, Soil Science Society of America Journal, 57, 937–937, https://doi.org/10.2136/sssaj1993.03615995005700040011x, https://www.soils.org/publications/sssaj/abstracts/57/4/SS0570040937, 1993.

Sato, S. and Comerford, N. B.: Influence of soil pH on inorganic phosphorus sorption and desorption in a humid Brazilian Ultisol, Revista Brasileira de Ciencia do Solo, 29, 685–694, https://doi.org/10.1590/S0100-06832005000500004, 2005.

Saxton, K. E. and Rawls, W. J.: Soil Water Characteristic Estimates by Texture and Organic Matter for Hydrologic Solutions, Soil Science Society of America Journal, 70, 1569–10, 2006.

Shirvani, M., Khalili, B., Mohaghegh, P., Ghasemi, S., Arabzadegan, H., and Nourbakhsh, F.: Land-Use Conversion Effects on Phosphate Sorption Characteristics in Soils of Forest and Rangeland Sites from Zagros Area, Western Iran, Arid Land Research and Management, 24, 223–237, https://doi.org/10.1080/15324982.2010.487454, http://www.tandfonline.com/doi/abs/10.1080/15324982.2010.487454, 2010.

Singh, B. R., Krogstad, T., Shivay, Y. S., Shivakumar, B. G., and Bakkegard, M.: Phosphorus fractionation and sorption in P-enriched soils of Norway, Nutrient Cycling in Agroecosystems, 73, 245–256, https://doi.org/10.1007/s10705-005-2650-z, http://link.springer.com/10.1007/s10705-005-2650-z, 2005.

Singh, V., Dhillon, N. S., and Brar, B. S.: Influence of long-term use of fertilizers and farmyard manure on the adsorption-desorption behaviour and bioavailability of phosphorus in soils, Nutrient Cycling in Agroecosystems, 75, 67–78, https://doi.org/10.1007/s10705-006-9012-3, http://link.springer.com/10.1007/s10705-006-9012-3, 2006.

Sitch, S. A., Smith, B., Prentice, I. C., Arneth, A., Bondeau, A., Cramer, W., Kaplan, J. O., Levis, S., Lucht, W., Sykes, M. T., and Venevsky, S.: Evaluation of ecosystem dynamics, plant geography and terrestrial carbon cycling in the LPJ Dynamic Global Vegetation Model, Global Change Biology, 9, 161–185, 2003.

Spitters, C. J. T.: Separating the Diffuse and Direct Component of Global Radiation and Its Implications for Modeling Canopy Photosynthesis .2. Calculation of Canopy Photosynthesis, Agricultural and Forest Meteorology, 38, 231–242, 1986.

Sprugel, D. G., Ryan, M. G., Brooks, J. R., Vogt, K. A., and Martin, T. A.: Respiration from the Organ Level to the Stand, in: Resource Physiology of Conifers, edited by Smith, W. K. and Hinckley, T. M., pp. 255–299, Academic Press, San Diego, https://doi.org/10.1016/B978-0-08-092591-2.50013-3, http://www.sciencedirect.com/science/article/pii/B9780080925912500133, 1995.

Tazoe, Y., Noguchi, K. O., and Terachima, I.: Effects of growth light and nitrogen nutrition on the organization of the photosynthetic apparatus in leaves of a C4 plant, Amaranthus cruentus, Plant, Cell and Environment, 29, 691–700, 2006.

Villapando, R. R. and Graetz, D. a.: Phosphorus Sorption and Desorption Properties of the Spodic Horizon from Selected Florida Spodosols, Soil Science Society of America Journal, 65, 331–331, https://doi.org/10.2136/sssaj2001.652331x, 2001.

Wang, Y. P., Law, R. M., and Pak, B.: A global model of carbon, nitrogen and phosphorus cycles for the terrestrial biosphere, Biogeosciences, 7, 2261–2282, 2010.

White, M. A., Thornton, P. E., Running, S., and Nemani, R.: Parameterization and Sensitivity Analysis of the BIOME-BGC Terrestrial Ecosystem Model: Net Primary Production Controls, Earth Interactions, 4, 1–55, 2000.

Wisawapipat, W., Kheoruenromne, I., Suddhiprakarn, A., and Gilkes, R. J.: Phosphate sorption and desorption by Thai upland soils, Geoderma, 153, 408–415, https://doi.org/10.1016/j.geoderma.2009.09.005, http://linkinghub.elsevier.com/retrieve/pii/S0016706109002821, 2009.

Wullschleger, S. D.: Biochemical Limitations to Carbon Assimilation in C3 Plants—A Retrospective Analysis of the A/Ci Curves from 109 Species, Journal of experimental botany, 44, 907–920, https://doi.org/10.1093/jxb/44.5.907, https://academic.oup.com/jxb/article-abstract/44/5/907/503778, 1993.

Xu, D., Xu, J., Wu, J., and Muhammad, A.: Studies on the phosphorus sorption capacity of substrates used in constructed wetland systems, Chemosphere, 63, 344–352, https://doi.org/10.1016/j.chemosphere.2005.08.036, http://www.ncbi.nlm.nih.gov/pubmed/16242173, 2006.

Xu-Ri and Prentice, I. C.: Terrestrial nitrogen cycle simulation with a dynamic global vegetation model, Global Change Biology, 14, 1745–1764, 2008.

Yang, X., Thornton, P. E., Ricciuto, D. M., and Post, W. M.: The role of phosphorus dynamics in tropical forests – a modeling study using CLM-CNP, Biogeosciences, 11, 1667–1681, https://doi.org/10.5194/bg-11-1667-2014, https://www.biogeosciences.net/11/1667/2014/, 2014.

Zaehle, S. and Friend, A. D.: Carbon and nitrogen cycle dynamics in the O-CN land surface model: 1. Model description, site-scale evaluation, and sensitivity to parameter estimates, Global Biogeochemical Cycles, 24, GB 1005, 2010.

Zaehle, S., Friedlingstein, P., and Friend, A. D.: Terrestrial nitrogen feedbacks may accelerate future climate change, Geophysical Research Letters, 37, https://doi.org/10.1029/2009GL041345, https://agupubs.onlinelibrary.wiley.com/doi/abs/10.1029/2009GL041345, 2010.

Zaehle, S., Ciais, P., Friend, A. D., and Prieur, V.: Carbon benefits of anthropogenic reactive nitrogen offset by nitrous oxide emissions, Nature Geoscience, 4, 601–605, 2011.

Zafar, M., Tiecher, T., de Castro Lima, J. A., Schaefer, G. L., Santanna, M. A., and Dos Santos, D. R.: Phosphorus seasonal sorption-desorption kinetics in suspended sediment in response to land use and management in the Guapore catchment, Southern Brazil, Environ Monit Assess, 188, 643, https://doi.org/10.1007/s10661-016-5650-3, https://www.ncbi.nlm.nih.gov/pubmed/27796828, 2016.

Zanne, A., Lopez-Gonzalez, G., Coomes, D., Ilic, J., Jansen, S., Lewis, S., Miller, R., Swenson, N., Wiemann, M., and Chave, J.: Data from: Towards a worldwide wood economics spectrum, https://doi.org/doi:10.5061/dryad.234, https://doi.org/10.5061/dryad.234, 2009.

Zerihun, A., McKenzie, B. A., and Morton, J. D.: Photosynthate costs associated with the utilization of different nitrogen–forms: influence on the carbon balance of plants and shoot–root biomass partitioning, The New Phytologist, 138, 1–11, 1998.

Zhou, M. and Li, Y.: Phosphorus-Sorption Characteristics of Calcareous Soils and Limestone from the Southern Everglades and Adjacent Farmlands, Soil Science Society of America Journal, 65, 1404–1404, https://doi.org/10.2136/sssaj2001.6551404x, 2001.

Zou, P., Fu, J., and Cao, Z.: Chronosequence of paddy soils and phosphorus sorption-desorption properties, Journal of Soils and Sediments, 11, 249–259, https://doi.org/10.1007/s11368-010-0301-8, http://link.springer.com/10.1007/s11368-010-0301-8, 2011.